CFD analysis of performance and downstream vortices on a Savonius type vertical axis wind turbine.

Nathan Guignard

PONTIFICIA
UNIVERSIDAD
CATÓLICA
DEL PERÚ

INTRODUCTION

Since the turn of the century, the talk about the limited reserve of fossil fuels and the effects of their burning on our climate has become a major topic of the media. The evidence is staggering and as a consequence most of our world's countries have started an energy transition. The main goal is to get away from fossil fuels and use "renewable energies", so called because the resources are constantly renewed and compared to fossil fuels seem infinite. Energies such as solar, wind, biomass and geothermal are examples of such sources of renewables. Denmark is the current leader in wind generated electricity, California and Spain are showing how to harness the power of the Sun, and all those efforts to generate more with renewables has to be matched with the effort to make those solutions more efficient and more attractive to other countries who still view fossil fuels as the easy solution and keep on using them. With the knowledge available now renewables it feels for some that burning fossil fuels is a primitive solution. Nonetheless it should be the duty of engineers to enlarge and better that knowledge for everyone to use.

Now more specifically about wind energy. Humans have harvested the energy in the wind for more than 2000 years (the Persians used windmills around 200 B.C.) and with time our technology has improved. They have designed incredible new machines such as the Savonius and Darreus type turbines and their knowledge of fluid dynamics has permitted the implementation of new streamlined blades that harvest more energy from the wind. Albert Betz has shown that a maximum of 59% was the limit for the efficiency of a wind-turbine. They have been getting closer to this number with the years but there is still room for improvement on certain types of turbines. Vertical axis wind

turbines (or VAWTs) have always been considered not as suitable for energy production as horizontal type wind turbines. It is true because not all blades are exposed to the wind at all times (like in a horizontal axis wind turbine), but new studies have proved that streamlining the blades a certain way and adding a wing like thickness to them improved the overall efficiency of the turbine. Knowing that and considering that HAWTs are significantly cheaper to produce and maintain than HAWTS, it makes them a more viable solution notably for local decentralized production in isolated areas of the world.

That leads to Peru. Peru is a fast growing still yet a 3rd world country. Its potential for renewable energies production (especially wind energy) is tremendous, yet the great amount of gas and oil available in the underground and them coming at a cheap price does not encourage the government to subsidize renewables. It leaves Peru dependent on foreign investments to develop this sector and takes away a great opportunity to forego its energetical transition and get ahead of competition in South America. Some projects have surfaced notably in northern Peru, in the Trujillo region, but there are few compared to the mega industry of oil and gas.

This thesis paper has for goal to further the knowledge of wind turbines in the context of hoping to change Peru's view on their use and also for the world to use as a database for further research and other works.

NOMENCLATURE

Cp : Coefficient of power

TSR or λ : Tip Speed Ratio

ω : Angular frequency

S_v : Power spectral density

V_m : Quasi steady wind speed

V : Wind speed

v : Wind speed due to atmospheric turbulence

k : Shape coefficient

C : Scale coefficient

z : Height above ground level

z_{ref} : Height of reference

z_0 : Roughness

E_k : Kinetic energy

ρ : Air density

A : Cross section area

P_v : Power available in the wind

t_p or T_p : Time interval

α : Aspect ratio

β : Overlap ratio

H : Rotor height

D: Rotor diameter

e : Overlap between blades

a : Shaft diameter

d : Blade diameter

C_m : Torque on the blades

V_{rotor} : Edge speed of the rotor

$\dot{m}$: Mass flow rate

P : Power

Cr : Courant number

Re : Reynold's number

Δs : Height of the first cell

μ : Fluid dynamic viscosity

Y+ : Y+ criteria

Θ_{min}, Θ_{max} : Cell edge angles

A_i : Area vector of a face

f_i : Vector from centroid of one cell to centroid of an adjacent cell

ABSTRACT

The performance of a Vertical Axis Wind Turbine (VAWT) of Savonius type with constant cross-sections is examined through the use of quasi 2D flow predictions executed in ANSYS Fluent. The simulations are performed in a way that allows comparison with wind tunnel data presented in a related paper **[VIII]**, where this design was tested. This first design will be named D1SAV.

In addition, another turbine design with a NACA 0012 applied to the previous blade geometry is modelled. The new model is called D2NACA12. Such a shape has been examined before with the use of CFD but on less efficient base geometries **[IX]**.

Those two designs are analyzed at different values of tip speed ratio (TSR). This paper presents an analysis of Power Coefficient (Cp).

Finally, the downstream wake is observed through comparison of velocity profiles at various distances behind the Savonius. This last observation is made to obtain a "security distance" where another Savonius can be placed without it being affected by the first one.

REFERENCES

This thesis is based on the following papers, which will be referred to in the text by their Roman numerals.

[I] *Wind Turbine Control Systems: Principles, Modelling and Gain Scheduling Design*
Bianchi, F.D. ; de Battista, H. ; Mantz, R.J.
2007, XX, 208p., Hardcover
ISBN: 978-1-84628-492-2

[II] *Peru Renewable Readiness Assessment 2014*
© IRENA 2014

[III] *Computational Analysis of Flow around a Two-Bladed Savonius Rotor*
Bhaskar Jyoti Choudhury, Gaurav Saraf
ISESCO JOURNAL of Science and Technology Volume 10, Number 17, May 2014 (39-48)

[IV] *CFD and PIV investigation of unsteady flow through Savonius wind turbine*
Ivan Dobreva, Fawaz Massouha
Energy Procedia 6 (2011) (711–720)

[V] *An experimental study on improvement of Savonius rotor performance*
N.H. Mahmoud a, A.A. El-Haroun a,*, E. Wahba a, M.H. Nasef b
Alexandria Engineering Journal (2012) 51, (19–25)

[VI] *CFD COMPUTATION OF THE SAVONIUS ROTOR*
Krzysztof Rogowski, Ryszard Maroński
JOURNAL OF THEORETICALAND APPLIED MECHANICS
53, 1, pp. 37-45, Warsaw 2015

[VII] *Numerical investigation of conventional and modified Savonius wind turbines*
Konrad Kacprzak, Grzegorz Liskiewicz, Krzysztof Sobczak
Renewable Energy 60 (2013) (578-585)

[VIII] *Wind tunnel experiments of a newly developed two-bladed Savonius-style wind turbine*
Sukanta Roy, Ujjwal K. Saha
Applied Energy 137 (2015) (117–125)

[IX] *Enhancement of Savonius wind rotor aerodynamic performance: a computational study of new blade shapes and curtain systems*
Mariano Tartuferi, Valerio D'Alessandro, Sergio Montelpare, Renato Ricci
Energy 79 (2015) (371-384)

[X] *COMPARISON OF SOLUTION ALGORITHM FOR FLOW AROUND A SQUARE CYLINDER*
Y. Saito, T. Soma, R. Sagawa, Y. Matsushita, H. Aoki, M. Daikoku, M. Shirota and T. Inamura
Ninth International Conference on CFD in the Minerals and Process Industries
CSIRO, Melbourne, Australia, 10-12 December 2012

[XI] *PERU RENEWABLES READINESS ASSESSMENT 2014,*
IRENA.

[XII] http://www.engineeringtoolbox.com/air-altitude-density-volume-d_195.html

[XIII] *Censos nacionales 2007 :XI de poblacion y VI de vivienda*
INEI, UNFPA
2007

[XIV] Applied Computational Fluid Dynamics
André Bakker
http://www.bakker.org
© André Bakker (2002-2006) © Fluent Inc. (2002)

[XV] http://www.arc.vt.edu/ansys_help/flu_ug/flu_ug_mesh_quality.html

[XVI]
http://home.anadolu.edu.tr/~esuvaci/egitim/Fluid%20Dynamics%20Lecture%205.pdf

[XVII] US 1766765
US Patent Office
October 11, 1928
Serial Number 311 793

[XVIII] US 1697574
US Patent Office
August 13, 1925
Serial Number 49 985

[XIX] SolidWorks
http://www.solidworks.fr/

[XX] ANSYS Workbench
http://www.ansys.com/fr_fr

[XXI] Microsoft Excel
https://products.office.com/fr-fr/excel

[XXII] FindGraph
http://www.findgraph.com/

INDEX

CORPUS

Theoretical background

1. The wind and Peru

1.1. The wind

This section is devoted to the study of the patterns, strengths and measured values of wind and their effects on its interaction with turbines **[I]**

1.1.1. The Source of Winds

The wind is the movement of an air mass within the atmosphere mainly originated by temperature differences. The temperature gradients are caused by uneven solar heating. The equatorial region is heated more than the Polar Regions. Consequently, the warmer and lighter air from the equator rises to the outer layers of the atmosphere and moves towards the poles. This air is replaced by a return flow of cool air from the poles, this flow being located in the lower layers of the atmosphere. This air circulation is also affected by the Coriolis forces which originate from the rotation of the Earth. In fact, these forces deflect the upper flow eastward and the lower flow to the west. Actually, for latitudes greater than 30^{o}N and 30^{o}S westerly winds predominate due to the rotation of the Earth, the consequence being that the effects of differential heating decrease above these latitudes. Such large-scale air flows take place in all the atmosphere and constitute

the geostrophic winds. The lower layer of the atmosphere is known as surface layer and is defined by its height (100m). In this layer, winds are slowed down due to friction with the environment and obstacles altering their velocity but also their direction. Turbulent flows originate from that phenomenon, which causes wind speed variations with a great range of amplitudes and frequencies. In addition to that, the presence of seas and large water areas causes air masses circulation resembling in nature to the geostrophic winds. All these air movements are called local winds. The wind in a given location near the Earth's surface results from the combination of geostrophic and local winds. It depends then on the following factors: the geographic location, the climate, the height above ground level, the roughness of the terrain and the obstacles in the immediate environment. These are the winds the wind turbines interact with. A way of characterizing these surface winds is by their kinetic energy distribution in the frequency domain, which is called Van Der Hoven spectrum. Figure 1.1 shows such a spectrum. Note that the figure shows the power spectral density SV multiplied with the angular frequency ω. Although we can spot differences, the spectra evaluated in different sites follow a similar pattern. Independently of the location, the spectrum exhibits two peaks approximately at 0.01 cycles/h (4-days cycles) and 50 cycles/h (1 min cycles), which are separated by an energy gap between periods of 10 min and 2 h. The low frequency side of the spectrum is linked to the geostrophic winds whereas the high frequency side is associated with the turbulence due to local winds.

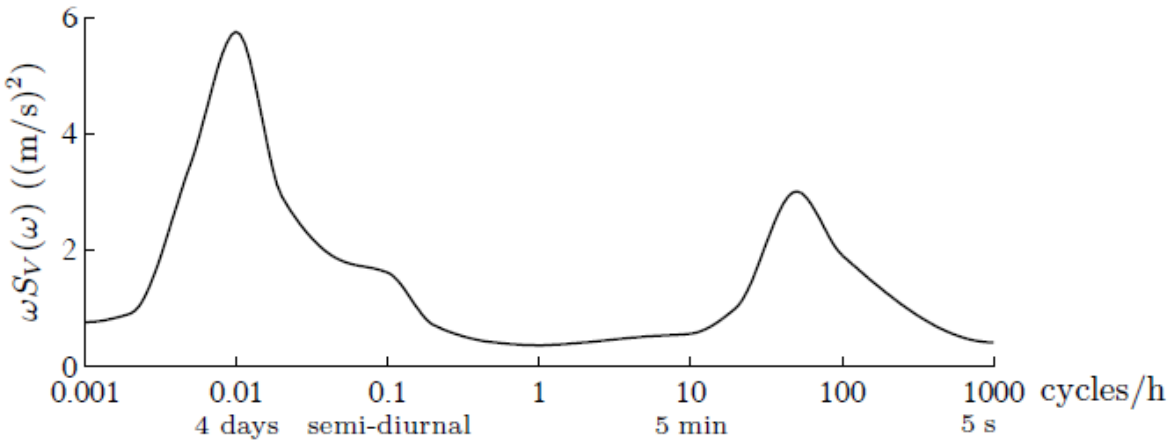

Fig. 1.1. Typical Van Der Hoven spectrum **[I]**

The concentration of energy around two separate frequencies allows us to split the original wind speed signal V into two components,

$$V = V_m + v \tag{1.0}$$

where the quasi-steady wind speed (called mean wind speed) V_m is calculated as the average of the instantaneous speed over an interval t_p:

$$V_m = \frac{1}{t_p}\int_{t_0-t_p/2}^{t_0+t_p/2} V(t)dt \tag{1.1}$$

Usually, the average period is chosen to be within the energy gap, more precisely around 10 min to 20 min. When it is done, the macro meteorological changes in wind speed appear as slight changes in the mean wind speed, and the term *v* shows the atmospheric turbulences.

1.1.2. Mean Wind Speed

The economic viability of a wind energy project is directed by the knowledge of the quasi steady mean wind speed on the site. This information is also essential in order to maximize efficiency and durability. The probability distribution of the mean wind speed is predicted from measurements surveyed over several years. All these data are usually arranged in a histogram. The wind distribution obtained experimentally can be approximated by a Weibull distribution, such as that shown in Figure 1.2. The Weibull distribution is given by **[I]**:

$$p(V_m) = \frac{k}{C}\left(\frac{V_m}{C}\right)^{k-1} e^{-\left(\frac{V_m}{C}\right)^k} \quad (1.3)$$

where k is the shape coefficient and C the scale coefficient. Those two coefficients are adjusted to match the wind data at a particular location.

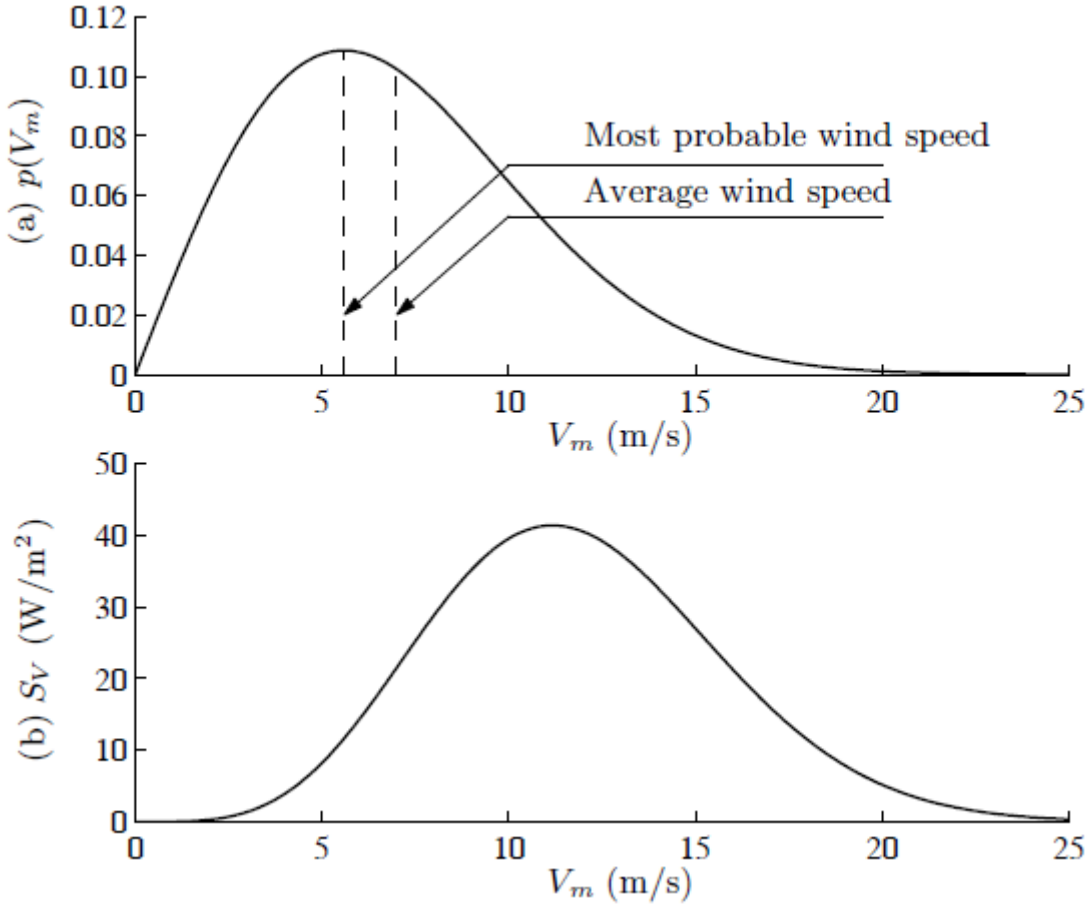

Figure 1.2: Weibull probability distribution of (a) mean wind speeds and (b) power density vs. wind speed **[I]**

The Weibull probability function shows that large mean wind speeds are rare and unlike them moderate winds are more common. In the particular case of Figure 1.2, the most probable mean wind speed is approximately 5.5 m/s whereas the average wind speed is 7 m/s. Mean wind speed is also function of altitude. The ground, even in the absence of obstacles, induces friction forces that slow the wind down in the lower layers. This effect, called wind shear, is more appreciable as height decreases and has important

impact on wind turbine operation. Various mathematical models have been created to describe this phenomenon. One of them is called the Prandtl logarithmic law **[I]**:

$$\frac{V_m(z)}{V_m(zref)} = \frac{\ln(\frac{z}{z_0})}{\ln(\frac{z_{ref}}{z_0})} \tag{1.4}$$

where z is the height above ground level, z_{ref} is the height of reference (typically 10 m) and z_0 is the roughness. Values for roughness are listed in Table 2.1. We can use a different empirical formula to describe the effect of the terrain on the wind speed gradient is this exponential law **[I]**:

$$V_m(z) = V_m(z_{ref})\left(\frac{z}{z_{ref}}\right)^{\propto} \tag{1.5}$$

where the surface roughness exponent alpha is also a function of the terrain. Values of this exponent are presented in the last column of Table 1.3

Type of surface	z_0 (mm)	α
sand	0.2 to 0.3	0.10
mown grass	1 to 10	0.13
high grass	40 to 100	0.19
suburb	1000 to 2000	0.32

Table 1.3. Typical values of roughness length z_0 and roughness exponent α for different types of surface.

1.2. Wind energy in Peru

1.2.1. Role of the government

Despite Peru's immense reserve of fossil fuels their government and business partners have taken steps towards the implementation of wind power in the country. As the RRA of 2014 **[XII]** shows 987 GigaWattsHour over two years have been supplied to the country but Peru still ranks near the bottom of the South American chart for wind power installed up to 2014. 148 total MegaWatts were installed by the end of 2014 which ranks 8th among South American nations (see Annex V). Peru's capital: Lima, having hosted the 20th World Climate Change Conference (COP 20) in December 2014 it showed the increased will of the government to go through its energetical transition and transfer to more renewables.

1.2.2. Localisation of main sites

Peru has a very wide range of topography. From desertic pacific coast to the inland tropical jungle of the Amazon and passing through the mountain range of the Andes (reaching summits above 6000m), all landscapes are represented. A brief look at the weather records tells us that the strongest winds are present along the coast and in some locations in the Andes. The former block most of the winds and in result the amazon is a more quiet zone. Another factor to be aware of is altitude: going from sea level to 1500m elevation there is almost a 20% drop in air density for a constant temperature **[XII]**. That means a significant drop in electricity production because there is less air to push on the blades. For this reason most of the production sites are located

on the coastal area. This is also where most of the population is living (Lima represents almost a third of the country's total population). Moreover there are more big cities on the coastline than in the mountains (4 out the top 5 including Lima) **[XIII]** which means than the demand is greater on site. This decentralization in the mountain and tropical jungle zone suits better a local production at small scale (with home installed turbines or off grid equipment in some cases). In all zones, a different solution should be implemented and that is what will highlighted on later in this paper.

2. Fluid mechanics equations:

The following paragraphs will cover the mechanics of Wind Turbines and what equations can be used best to describe their behavior **[I]**.

2.1. Energy in the wind:

The kinetic energy (Ek) available in a fluid flow per unit volume is:

$$Ek = \frac{1}{2}\rho V^2 \qquad (1.6)$$

, where ρ is the density of the fluid. For a stream flowing through an area of cross section A the flow rate is AV. In consequence, the power available in the wind going through this area A with a velocity V is:

$$Pv = \frac{1}{2}\rho A V^3 \qquad (1.7)$$

The energy available in the wind is calculated by integrating (1.7) during a time interval T_p.

Usually a duration of one year is used:

$$Average\ Energy = \frac{1}{2}\rho A \int_0^{Tp} V^3 dt \qquad (1.8)$$

It could be tempting to use the most probable wind speed or the average wind speed from the Weibull distribution (Figure 1.2) and then calculate the average energy in the wind. Doing so the wind resource would greatly underestimated. This is because high velocity winds contain much more energy than low velocity wind, this thanks to the power being related to speed at the third power Figure 1.2 shows the power density, that is how energy is distributed with speed. This graph is obtained by combining the Weibull probability distribution of the wind speed with the power available at a different wind speeds. As a consequence, the shape of the previous Weibull curve changes. We can observe that most of the wind energy is supplied by wind with speeds above average. In Figure 1.2, the average energy corresponds to a wind speed of 11.2 m/s.

3. Wind turbines characteristics

3.1. Horizontal Axis Wind Turbine (VAWT)

Wind turbines are mechanical devices specifically designed to harvest part of the kinetic energy of the wind and convert it into useful mechanical energy. Several designs have been devised throughout the centuries. Most of them include a rotor that turns round propelled by lift or drag forces due to the incoming wind. Depending on the orientation of the rotor axis, wind turbines are classified into two families: vertical-axis and horizontal-axis wind turbines (respectively VAWT and HAWT). The most efficient VAWT is the Darrieus rotor illustrated in Figure 1.11. The best feature for VAWTs is that the generator and transmission devices are located at the base of the device which is at

ground level. In addition to that, they are able to capture the wind from any direction without the need to be oriented towards the wind. However, these advantages are counteracted by a reduced efficiency since the blades on the rotor are not exposed to the wind force at all times (unlike HAWTs). Furthermore, despite having the generator and transmission at ground level, maintenance is not simple since it usually requires rotor removal. This is a feature that can be worked around through intelligent coupling between the rotor and the generator. In addition, these rotors are supported by cables taking up large land extensions. By these reasons the use of vertical-axis wind turbines in mass energy production is rare.

Nowadays, almost all wind turbines connected to the grid possess horizontal-axis with two or three blades. The rotor is located at the top of a tower where the winds have more energy (less ground friction) and are less turbulent. The gearbox and the generator are assembled inside the nacelle on top of the tower. There is also a yaw mechanism that turns the rotor and nacelle towards the wind. While operating, the rotor is yawed to face the incoming wind so the turbine can capture as much energy as possible. This yaw mechanism is simple when used in low power applications but it becomes one of the more complicated devices in high power wind turbines. Finally, the power electronics are arranged at ground level. Only horizontal-axis wind turbines are treated in this book.

3.2. Savonius type VAWT

The Savonius wind turbine was invented by Sigurd Johannes Savonius in 1922. Some similar wind turbines were invented prior to that date but none was as advanced as the Savonius. Two patents were filed: US1697574 **[XVIII]** in 1925 and US1766765 **[XVII]** filed in 1928.

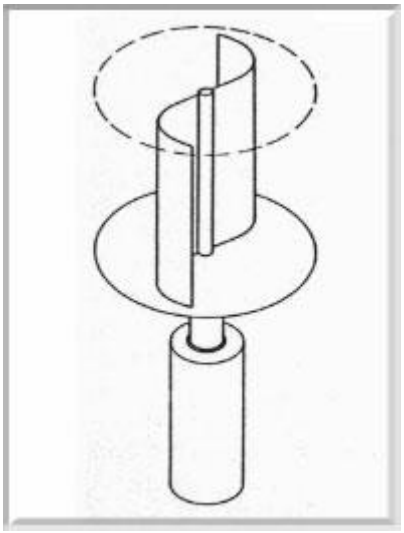

Figure 1.4: Savonius simple design

The Savonius design resides in the fact that one side of the blade has a higher drag coefficient going with the going than fighting against it (as seen in figure 1.5)

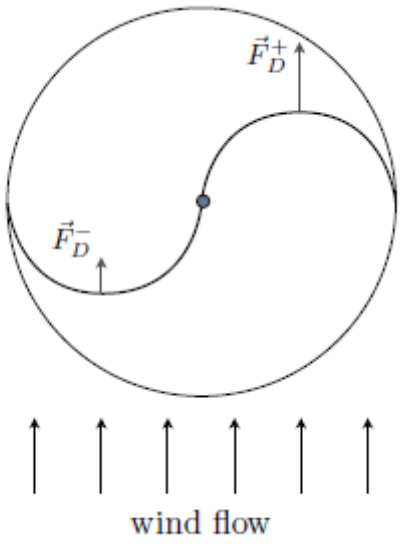

Figure 1.5: Savonius basic functionality

As said above the Savonius rotor is a drag based wind turbine: which uses means that the drag forces are prominent over the lift forces on the rotor's blades.

The design of Savonius has evolved over the years and improvements have been made. Savonius with more than two blades have been developed in order to have a more constant torque applied to the central shaft. Another solution for that is to have multiple levels of Savonius on top of each other with an offset angle (see figure 1.6)

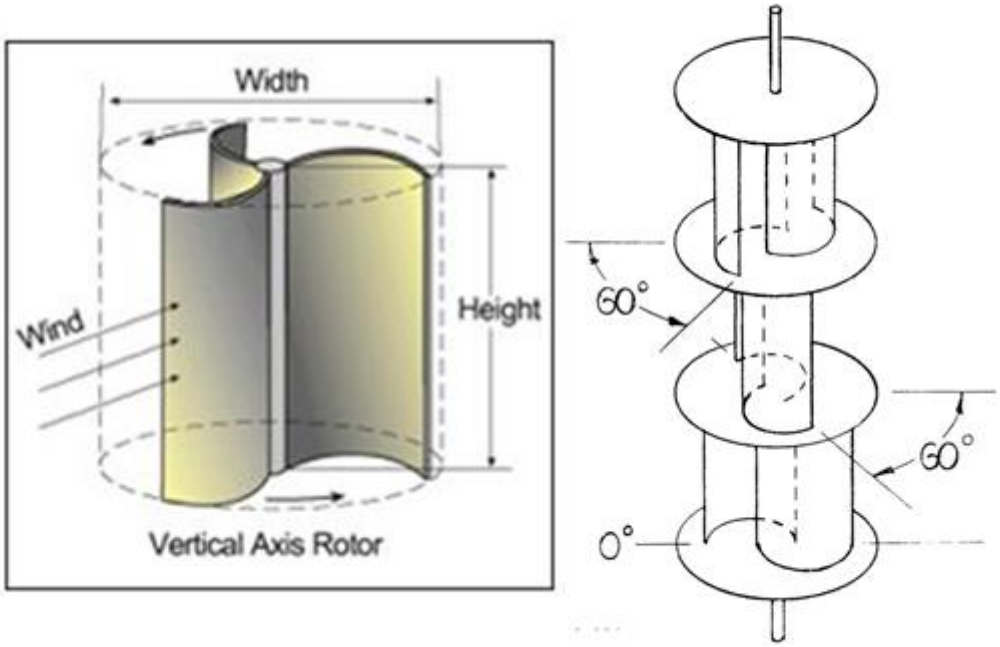

Figure 1.6: three blade Savonius and three stage Savonius

Another improvement was the work on an overlap between the blades. This feature works best when used with two bladed Savonius. It has for purpose to redirect the air flow pushing one blade onto the other and by doing so increasing the torque applied on the shaft and therefore the efficiency of the Savonius.

The figure below shows the effect of the overlap:

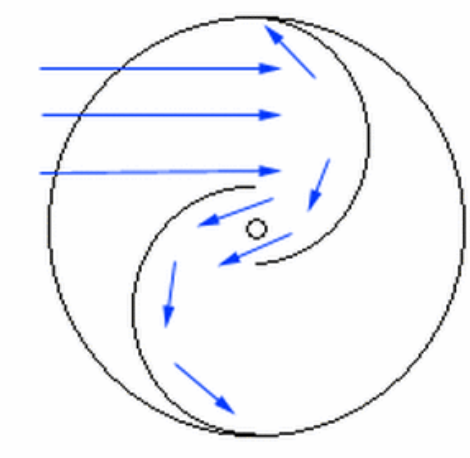

Figure 1.7: Effect of the overlap on a Savonius

It was also proven that the geometrical ratios also have an effect on the performance of the Savonius rotor. The aspect ratio $\propto$ and overlap ratio β are the most commonly used **[V]**.

$$\alpha = \frac{H}{D} \quad and \ \beta = \frac{e-a}{d} \tag{1.9}$$

Where H is the rotor height, D the rotor diameter, e the overlap between the blades, a the diameter of the shaft and d the blade diameter (as seen in figure 1.8).

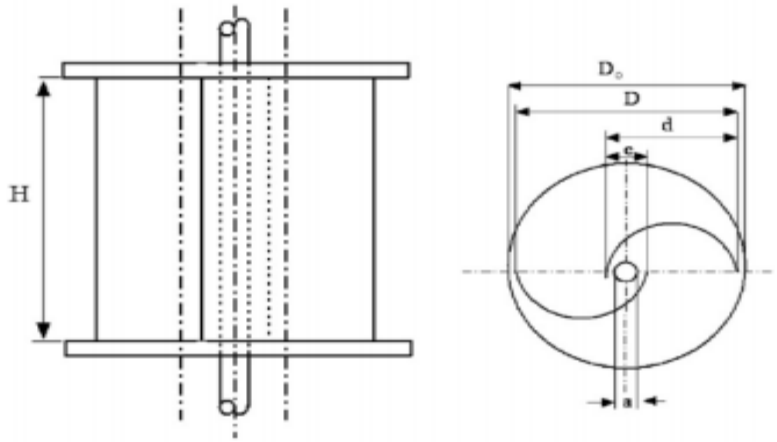

Figure 1.8: Geometrical features of a Savonius rotor

Finally the addition of end plates also increases the efficiency of the rotor. It prevents the air flow to escape above or under the blades and increases efficiency. Those end plates have a slightly greater diameter than the blades **[V].**

3.3. C_p and TSR

What ultimately interests engineers is efficiency. If they can find a way to get more energy out of a process without significantly increasing the cost, engineers will improve that process.

An efficiency is typically described as the ratio of power that is used over the power initially available. For example, in an electric motor the efficiency would be the mechanical power that the motor provides in relation to the electrical power that it drains from the grid. For wind turbines it is the same thing: the power applied to the shaft of the rotor related to the power available in the wind (see section I.2.1).

$$Cp = \frac{C_m.\omega}{\frac{1}{2}A\rho V^3} \qquad (1.10)$$

Where C_p is the power coefficient, C_m is the average torque on the rotor and ω is the angular velocity of the rotor.

C_p is usually graphed in function the Tip Speed Ratio (TSR or λ). This value is the ratio between the velocity of the rotor at the tip of the blade and the wind velocity.

$$TSR = \frac{Vrotor}{Vwind} \qquad (1.11)$$

The figure below shows a typical C_p versus TSR graph.

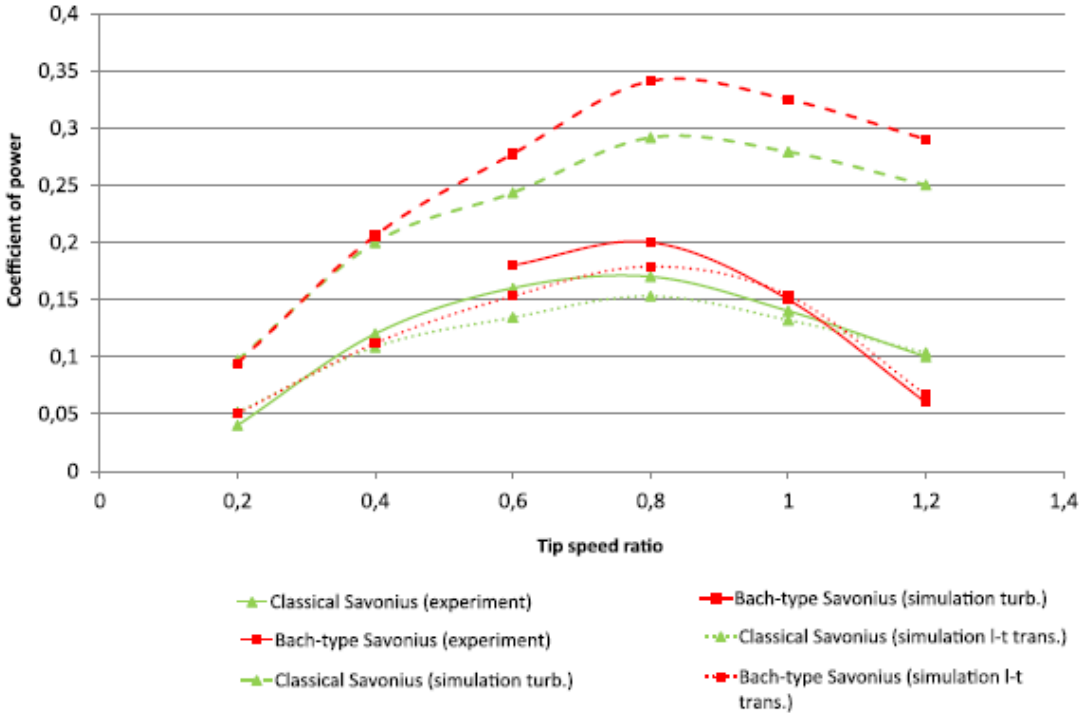

Figure 1.9: C_p =f(TSR) for different Savonius designs, experimental and CFD simulations.

As it is seen in Figure 1.9, a specific wind turbine design has a value of TSR for which the efficiency C_p is at a maximum. Therefore it is interesting to modify that TSR in order to always produce at maximum C_p. That can be achieved by slowing down the rotor using a braking system if the TSR is higher than the one needed. In the opposite case there is nothing to do as it would be foolish to give a "push" to the rotor which is supposed to provide power. This TSR regulation can be achieved coupling the braking system with simple electronic devices using the meteorological data measured in live. The efficiency of this regulation system depends on its core design but mainly on the frequency with which it corrects the TSR.

3.4. Betz limit

The Betz limit is the term we use to describe the maximum efficiency that a wind turbine can attain **[I]**. It was proved in 1919 by German scientist Alfred Betz. It can be re proved by the actuator disc method described below.

3.4.1. Actuator Disc Model

In order to calculate the maximum theoretical efficiency of a rotor (in this example for a HAWT), the rotor will be imagined to be replaced by a disc that harvests energy from the fluid flow going through it. After passing through the rotor the flow will come back to a steady state but with a reduced velocity.

Assumptions

1. The rotor does not have a central hub. The rotor is considered ideal and possesses an infinite number of blades which have no drag. Any resulting drag would only lower this idealized value.

2. The flow into and out of the rotor has a direction parallel to its axis. This is a control volume analysis, and to construct a solution the control volume must contain all flows going in and out. If that flow is not accounted for the conservation equations will be violated. The fluid is incompressible, its density remains constant, and there is no heat transfer.

4. The thrust over the disc or rotor area is considered uniform.

Application of conservation of mass (continuity equation)

The conservation of mass equation is applied to this control volume, the mass flow rate (the mass of fluid flowing per unit time) is given by:

$$\dot{m} = \rho A_1 v_1 = \rho S v = \rho A_2 v_2 \quad (1.12)$$

where v_1 being the speed before entering the rotor and v_2 the speed downstream of the rotor, and v is the speed at the fluid power device. ρ is the fluid density, and the area exposed to the flow of the turbine is given by the value S. The force applied to the rotor by the wind can be written as:

$$F = ma = m\frac{dv}{dt}\ \dot{m}\,\Delta v$$

$$F = \rho S v(v_1 - v_2) \quad (1.13)$$

Power and work

The work done by this force can be written incrementally as:

$$dE = F\,.\,dx \quad (1.14)$$

and the power (rate of work done) of the wind is:

$$P = \frac{dE}{dt} = F\,.\frac{dx}{dt} = F\,.\,v \quad (1.15)$$

Now the force F is substituted as seen above into the power equation:

$$P = \rho\,.\,S\,.\,v^2\,.\,(v_1 - v_2) \quad (1.16)$$

However, power can be computed another way, using the kinetic energy. Applying the conservation of energy equation to our control volume shows:

$$P = \frac{\Delta E}{\Delta t} = \frac{1}{2} . \dot{m} . (v_1^2 - v_2^2) \qquad (1.17)$$

Looking again at the continuity equation, mass flow rate is substituted for and the result is:

$$P = \frac{1}{2} . \rho . S . v . (v_1^2 - v_2^2) \qquad (1.18)$$

Both of these expressions for power are valid, one was found by derivation of the incremental work done and the other by the conservation of energy. Equating these two expression:

$$P = \frac{1}{2} . \rho . S . v . (v_1^2 - v_2^2) = \rho . S . v^2 . (v_1 - v_2) \qquad (1.19)$$

Examining the two expressions this can be infered:

$$v = \frac{1}{2} . (v_1 + v_2) \qquad (1.20)$$

The velocity at the rotor may then be selected as the average of upstream and downstream velocity of the flow.

Betz' law and coefficient of performance

Returning to the previous expression of power based on kinetic energy:

$$\dot{E} = \frac{1}{2} . \dot{m} . (v_1^2 - v_2^2) = \frac{1}{2} . \rho . S . v . (v_1^2 - v_2^2) = \frac{1}{4} . \rho . S . v . (v_1^2 - v_2^2) . (v_1 + v_2)$$

$$= \frac{1}{4} . \rho . S . v_1^3 . (1 - \left(\frac{v_2}{v_1}\right)^2 + \left(\frac{v_2}{v_1}\right) - \left(\frac{v_2}{v_1}\right)^3) \qquad (1.21)$$

By differentiating the kinetic energy with respect to v_2/v_1 for a specific fluid velocity v_1 and a given area S we can find the maximum or minimum value for kinetic energy. The result is that E reaches maximum value when $v_2/v_1 = 1/3$

Substituting this value results in:

$$Pmax = \frac{16}{27} . \frac{1}{2} . \rho . S . v_1^3 \qquad (1.22)$$

The power obtainable from a cylinder of fluid that has a cross sectional area S and speed v_1 is:

$$P = Cp . \frac{1}{2} . \rho . S . v_1^3 \qquad (1.23)$$

The reference power for the Betz efficiency calculation is the power in a moving fluid flow in a cylinder with a cross section S and speed v_1:

$$Pwind = \frac{1}{2} . \rho . S . v_1^3 \qquad (1.24)$$

Cp has then a maximum value of 16/27 or 59.3% (see graph below)

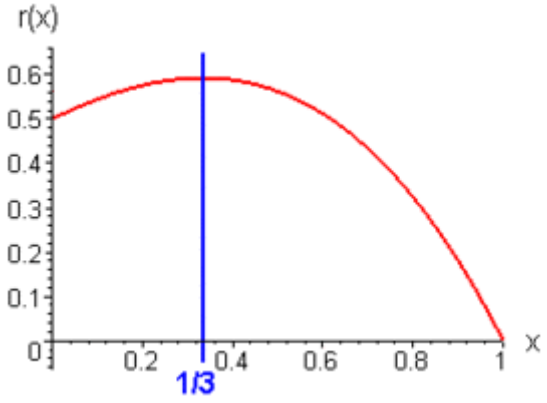

Figure 1.10: $dE/dt = f(v_2/v_1)$

Every design of wind turbine has its own Cp values for different TSRs as you can see in Figure 1.11.

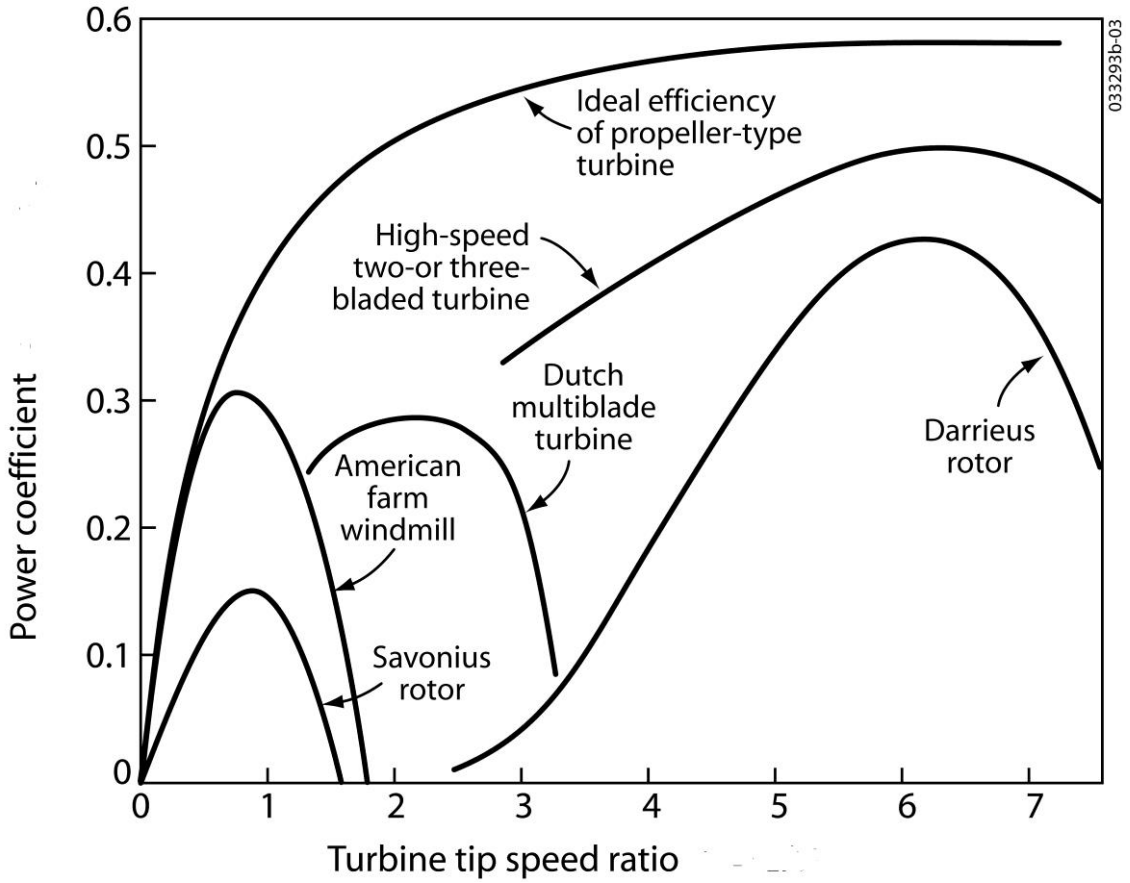

Figure 1.11: Power coefficients for different designs

As seen in Figure 1.11 the Savonius rotor is among the very low efficiency designs for wind turbines but it remains a design that has more upside since the scientific community has not conducted as much research on Savonius rotors as they have on other designs.

4. Justification

The reason why we study a Savonius VAWT, despite it being less efficient that a regular Horizontal Axis Wind Turbine (HAWT), is that: they are much cheaper to produce than HAWTs, they do not have to be oriented towards the wind like a HAWT, the electricity generator does not need to be placed in the nacelle, they do not need a starting mechanism (like a Darrieus for example) and if their efficiency can be approved significantly it will become economically interesting to use them in electricity production.

Moreover, the Savonius does not need high wind speeds to be efficient which means that it suits most of the locations in the world and its simple yet robust design makes it a perfect candidate for electricity generation in isolated or off grid environments. Finally this work is a direct continuation of a previous publication that specifies that CFD analysis is the next step in the research on this matter **[VIII]**.

II. CFD Simulation

In this part all the thoughts and steps necessary to construct a simulating environment for the Savonius VAWT will be reviewed as well as the way the results are recorded and interpreted.

1. Simulation protocol

1.1. Methodology

The figure below shows the protocol followed to conduct our ANSYS Fluent CFD simulation and the paragraph below explains it in more detail.

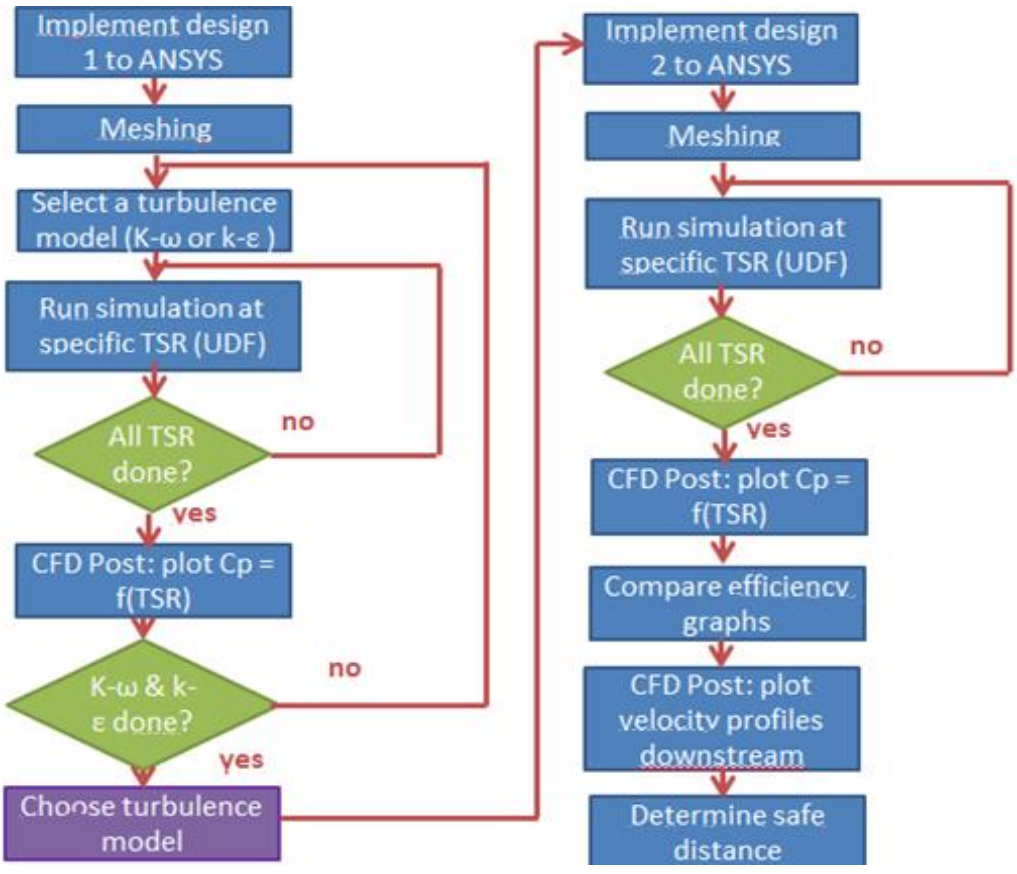

Figure 2.1: methodology of the ANSYS CFD simulation

The main goal of this study is: through the CFD modeling and simulating, to evaluate the efficiency (C_p) of two different blade designs (D1SAV and D2NACA12) at one Reynold's number. One design is directly inspired from a previous study **[I]** and it is expected to validate our CFD model through comparison of the CFD results obtained with the experimental results from this study. After modeling the two designs, having them included in ANSYS Workbench and completed the meshing process the ANSYS Fluent simulation is carried on.

The turbine is set to rotate at a known angular velocity while being subject to a constant wind velocity. This angular velocity is changed in every simulation since it is run with Tip Speed Ratios. For the D1SAV, two turbulence models are tested (k-ε realizable and k-ω SST) and the most accurate one is used in further simulations.

The D2NACA12 is tested in the exact same conditions (with the correct turbulence model). The torque on the turbine's blades is measured and knowing its angular velocity the calculation of its power output is possible and therefore its efficiency. The efficiencies of both designs are compared.

The third and final part of the case is the study of the downstream vortices after the wind turbine or more specifically when do they dissipate and the flow goes back to inlet conditions. This will tell where in space another turbine could be placed and therefore how a power plant can be optimized.

1.2. Expectations

The study's expected results are the following:

Design D1SAV: - the two turbulence models should show results close to reality, the closest one should be chosen as the reference model for the rest of the study.

Design D2NACA12: - the efficiency of the second design should be higher than the first design, according to **[IX]**.

For both designs, it should be determined where the vortices dissipate and the medium comes back to an "undisturbed" state.

2. Geometry

The topic of this paragraph is the geometry design of the simulation environment and the different models of wind turbines studied.

2.1. 2-dimension geometry

First of all, a choice needs to me made between a 2 dimensional or a 3 dimensional simulation. Two paths can be taken: being as true to reality as possible (3D) or simplifying the system in order to shorten the calculations and reach the expected results faster (2D).

Throughout literature there have been both 3D and 2D simulations. However considering that this study is to be carried throughout a 6 month period and that the computer power available is limited, the 2D simulation is the chosen option.

2.2. First design

The first blade design tested is directly inspired from an already used design. We will name it D1SAV. It was implemented and wind tunnel tested by Sukanta Roy and Ujjwal K. Saha from the Department of Mechanical Engineering at the Indian Institute of Technology Guwahati **[VIII]**.

Below is the diagram used to recreate their design:

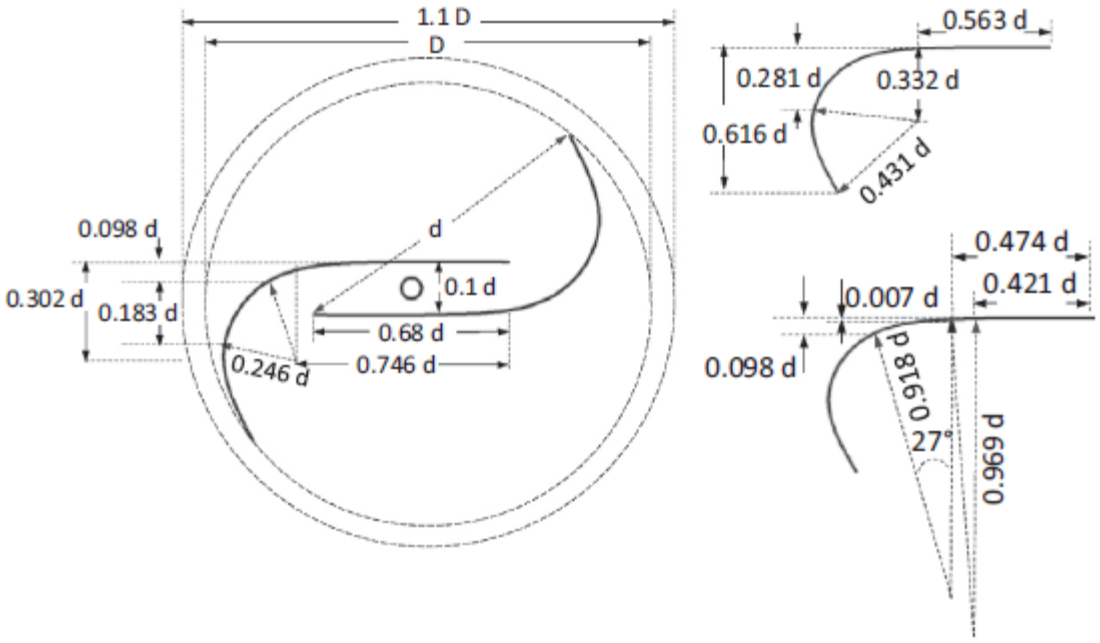

Figure 2.2: Diagram of the D1SAV dimensions **[VIII]**

The value of d we used in this paper is 108 millimeters and the thickness of the blade is constant at 0,63 millimeters. This value is to be considered later in this document.

2.3. Second design

The second design, named D2NACA12, is a hybrid based on the D1SAV design. The difference between the two is that the blade thickness is not constant at 0.63 millimeters but a NACA0012 thickness is implemented using the D1SAV as the mean line (see Appendix NN)

The NACA0012 is a profile commonly used in aerospace engineering to design wing profiles. It being a symmetrical profile (the underneath and upper thickness are the same) the two thickness values (Y+ for the upper and Y- for the underneath) shown in the table Appendix I are identical apart from their sign. Those said thicknesses and the mean abscises are expressed in a percentage, this percentage is the ratio between the value sought and the total chord length. For example:

$$X_{Camber} = X_{Camber}(\%) * Total\ Chord\ length \tag{2.1}$$

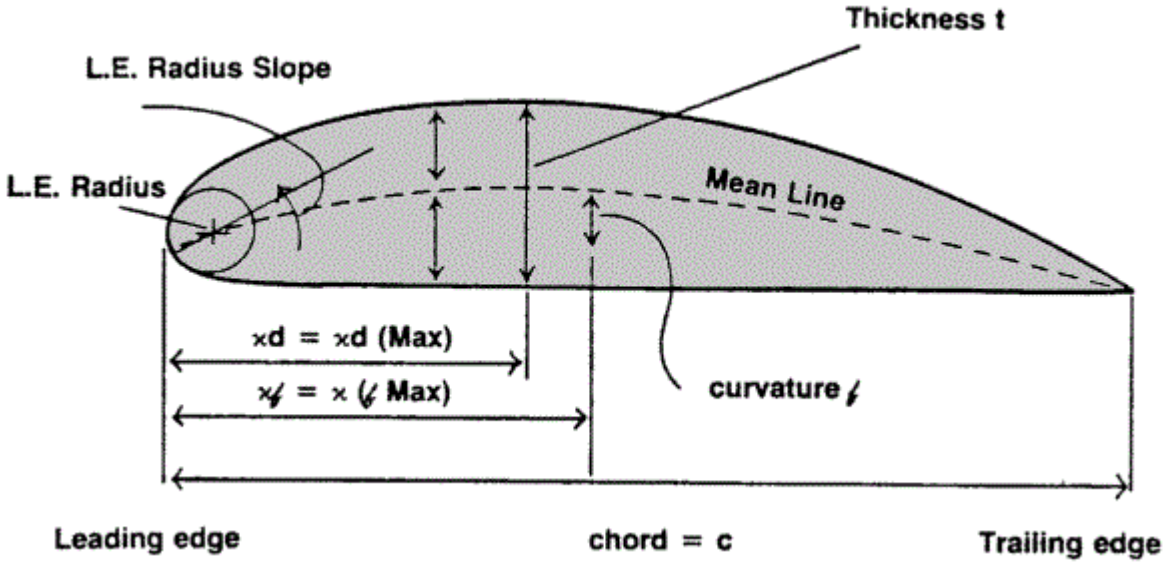

Fig 2.3. Method to generate a NACA Profile

This added thickness is proved to enhance the efficiency of a Savonius VAWT **[IX]** by using the pressure difference caused by the wing-like tip of the profile. This feature has been tested on another base Savonius blade **[IX]** and one of the goals of this study is to prove it still is true for this new geometry (D2NACA12).

Figure 2.4: Solidworks view of one D2NACA12 blade **[XIX]**

2.4. Topology of the studied area

After the two blade geometries have been created using SolidWorks **[XIX]** , an simulating environment needs to be constructed. Typically, in an experimental study a big enough wind tunnel for the model is used so the tested turbine fits. Also the airflow around the Savonius must not affect the flow near the boundaries of the tunnel, again a question of size between the model and the environment. A finite elements simulation is subject to the same problematic with the addition of the environment being small enough for calculation time purposes. Since the work is a 2D simulation, this has to do with the width of the simulating environment.

While spinning in the fluid, the Savonius rotor may cause vortices to form and will separate and continue their path downstream until their energy dissipates and the flow returns to a steady state. In this study one of the interesting variables is the distance after which those vortices dissipate. That means the minimal distance downstream the turbine after which the flow returns to its original steady state. If this distance is known

another Savonius can be placed downstream without its performance being affected by the previous turbine. This is very important in the eventuality of multiple Savonius being installed, like in a plant. This conditions the overall length of the simulating environment.

As said earlier, the characteristic dimension of the geometry d was chosen at 108 millimeters which makes the overall diameter of the Savonius at 170 millimeters for the D1SAV and 173 millimeters for the D2NACA12. The simulation environment is inspired from multiple previous studies **[III][IV][VI][VII]**; all of them agree that there has to be at least two zones in the environment: one includes the Savonius and one is the stationary zone that makes up the rest of the environment. The former has to be bigger than the Savonius itself. This has to do with this zone often being subjected to mesh movemement or remeshing due to movement of the Savonius. In this case it is set at 0.2 meters in diameter which contains easily either of the designs, being at a diameter of 0,17m (0,173m for D2NACA12). The width of the environment is also chosen at 1 meter which is 5 times the diameter of the Savonius zone. The reason why having a wide "tunnel" is for the boundaries not to have any effect on the Savonius rotor. If they are far enough, they will not affect the velocity profile entering the turbine and they will not affect the vortices created by it either. A third zone is also added: called the wake zone; for meshing purposes.

Below is a diagram showing the 3 different zones:

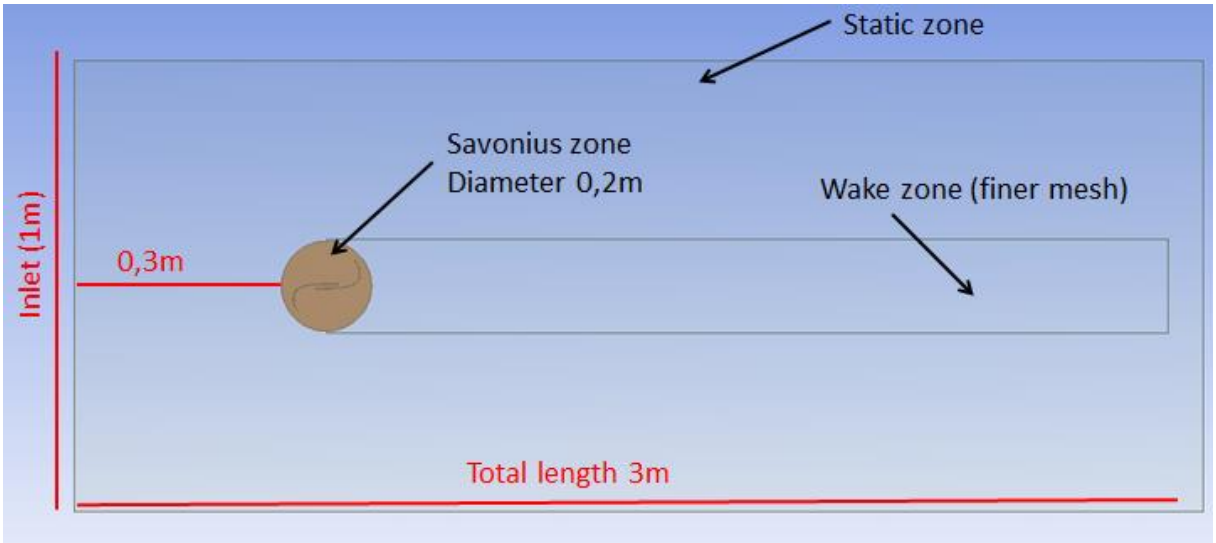

Figure 2.5: Simulation environment (ANSYS Design Modeler) **[XX]**

The overall length is calculated taking into account the velocity of the fluid and the shortest simulation time (see paragraph II.4.6) so the formation and dissipation of the vortices can be observed in the simulation environment even in the shortest conditions.

$$Distance\ covered\ by\ the\ fluid = V_{fluid} * Simulation\ time \quad (2.1)$$

The shortest simulation time is 1,351 seconds and the fluid velocity is constant through all simulations at 5,16 meters/second. This gives a 6,9 meters distance covered by the fluid (minimum). It was decided to leave the length of our environment at 3 meters in order not to have an environment too big and that will generate more computation time. Plus the first results showed signs that the vortex dissipation was happening inside the environment.

3. Meshing

In this paragraph the characteristics of the mesh will be discussed

3.1. Sizing of the different zones

First of it was decided that a triangular mesh was more suited for the simulation. The great variation in size of the cells (particularly around the Savonius zone and the blades) gives better mesh quality statistics with triangles rather than rectangles/squares. It also helps on the interface area.

Meshing is a crucial part of any CFD simulation. It will determine the precision with which the calculations are carried in space. The shape and size of the cells have to be selected adequately knowing the movements that the different mesh zones are subject to, the velocity of the fluids that go through it, the time step and the mathematical scheme used. One way to include two of those is the Courant number **[X]**:

$$Cr = \frac{Flow\ velocity * Time\ step}{cell\ size} \quad (2.2)$$

Since the model is to be verified (compared it to experimental results) at only one value of Reynold's number, there is one flow velocity. Reynolds 6.10^4 means a velocity of 5,16 meters/second in these conditions.

The time step chosen is 1millisecond, or an iteration time of 1 millisecond. Since the Savonius rotor rotates at TSRs going from 0,2 to 1,2, the turbine will spin between 11 and 73 rad/s which means that in 1millisecond (or one iteration)the turbine will cover between 0,17% and 1,16% of a complete revolution. That means a minimum of 85 iterations per revolution. A higher time step (5 millisecond or 10 millisecond) would have given less precision on the data collected and neither would it have given a good resolution on the rotational movement of the Savonius.

Considering those two factors and the fact that Courant numbers close to 1 (under 5 for most cases) are recommended a cell size can be chosen. With a cell size of 3 millimeters, the Courant number is 1.72 which satisfies the criteria **[X]**.

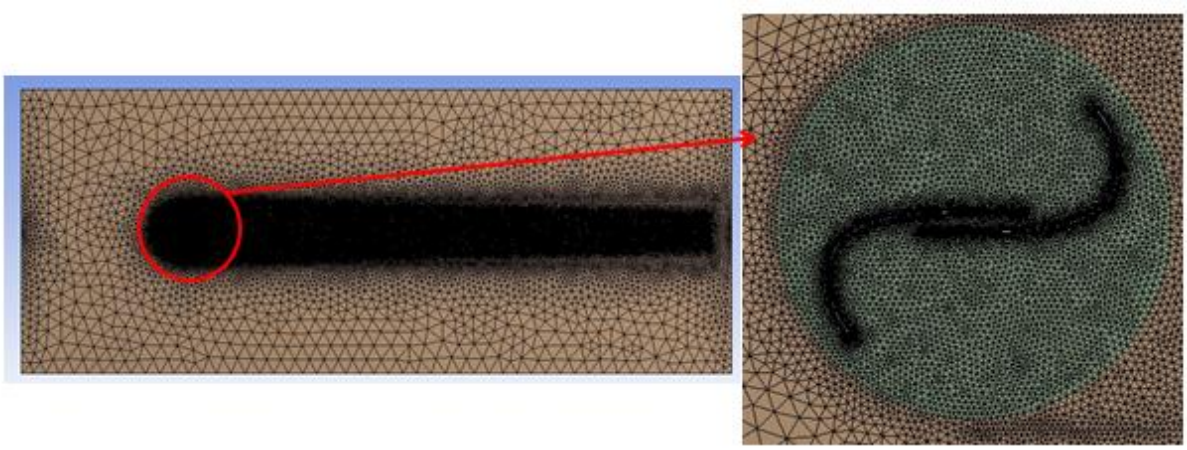

Figure 2.6: ANSYS Mesher view of the overall mesh sized mesh around the Savonius **[XX]**

This calculation is done for the Savonius zone only, because of it being the most critical area of computation. On the wake the size is chosen to be bigger: 4 mm. This is done for computation time purposes, the medium being a much greater area and not needing such precise calculations a less refined mesh is used.

3.2. Inflation on the blades

The Savonius are the only solid part of the simulation environment that is solid. In this particular case aluminum is the material used, it being the default material in the solver and also the most commonly used for building such turbines. It offers great mechanical resistance and weight for a relatively low price.

As shown in Figure 2.7, for every solid present in a fluid flow there is a gradient of velocity at its boundaries. This phenomenon is called the boundary layer effect.

It is illustrated in the figure below:

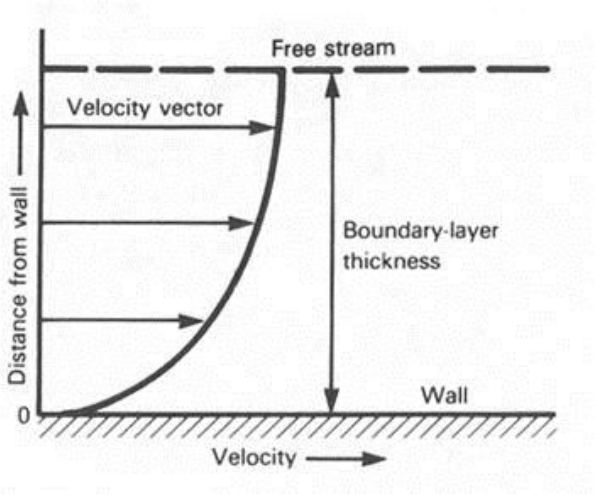

Fig 2.7: Boundary layer on a solid wall

For these reasons, it is an obligation to refine the mesh on the blades so the boundary layer effect can be taken into account (energy loss due to friction, velocity loss…). Now the size of this layer needs to be determined so it can be refined just enough and save precious computation time. For that the y^+ criteria is used:

$$\Delta s = \frac{\mu * y^+}{\rho * V} \tag{2.3}$$

Where:

Δs : Height of the first cell (m)

μ : Fluid dynamic viscosity (kg/(m.s))

y^+ : Y^+ criteria

ρ : Fluid density (kg/m^3)

V : Fluid flow velocity

In previous studies the y^+ criteria was taken approximatively at value of 1. Following this value which gives a first cell height of 0,26 millimeters or $2{,}6.10^{-4}$ meters.

As you can see in the figure below we respect this criteria with a margin. We have implemented a 7 layer inflation with a growing rate of 1,2 and a total thickness adjusted so the first cell respects the y+ criteria.

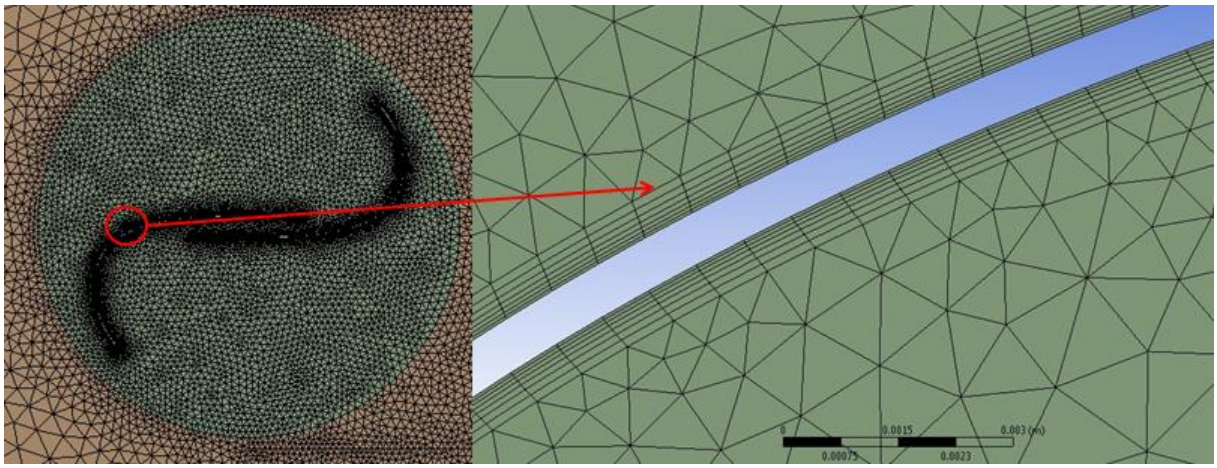

Figure 2.8: ANSYS Mesher view of the inflation on the blades **[XX]**

3.3. Mesh statistics

For the two designs the mesh statistics are the following **[XIV][XV]**:

3.3.1. Number of nodes

The number of cell joints in the mesh.

3.3.2. - Skewness

Skewness is characteristic of the cell, a low skewness is needed for good computation and convergence.

There are two methods for determining skewness:

1) Based on the equilateral volume:

$$Skewness = \frac{optimal\ cell\ size - cell\ size}{optimal\ cell\ size} \quad (2.4)$$

- Applies only to triangular and tetrahedral cells.
- Default method for triangles and tetrahedrons

2) Based on the deviation from a normalized equilateral angle:

$$Skewness\ (for\ a\ triangle) = \max\left[\frac{\theta max - 60}{60}, \frac{60 - \theta min}{60}\right] \quad (2.5)$$

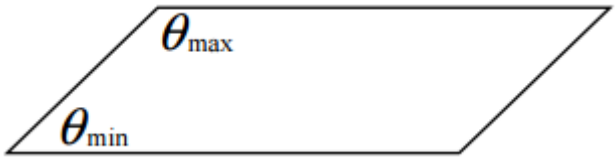

Figure 2.9: Angles on a parallelogram-like cell.

- Applies to all cell and face shapes.
- Always used for prisms and pyramids.

3.3.3. Aspect ratio

Aspect ratio is ratio of longest edge length to shortest edge length. A value equal to 1 is ideal for an equilateral triangle or a square.

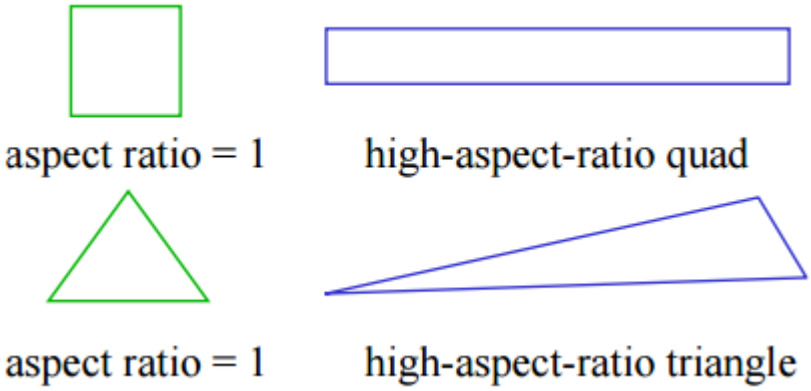

Figure 2.10: Graphical explanation of aspect ratio:

3.3.4. Orthogonal quality

In order to determine the orthogonal quality of a given cell, the following quantities are calculated for each face:

- the normalized dot product of the area vector of a face (A_i) and a vector from the centroid of the cell to the centroid of that face (f_i):

$$\frac{\vec{A}_i \cdot \vec{f}_i}{|\vec{A}_i \| \vec{f}_i|} \tag{2.6}$$

- the normalized dot product of the area vector of a face (A_i) and a vector from the centroid of the cell to the centroid of the adjacent cell that shares that face (c_i):

$$\frac{\vec{A}_i \cdot \vec{c}_i}{|\vec{A}_i \| \vec{c}_i|} \tag{2.7}$$

The minimum value that results from calculating the previous equations for all of faces is then defined as the orthogonal quality for the cell. Therefore, the worst cells will have an orthogonal quality closer to 0 and the best cells will have an orthogonal quality closer to 1.

Below is the recap of mesh statistics for both designs:

	D1SAV		D2NACA12	
# nodes	68799		262296	
# elements	130136		129003	
skewness	tri: 81 over 0.4	quadri: 1029 over 0.4	tri: 64 over 0.4	quadri: 248 over 0.4
aspect ratio	tri: all under 4	quadri: 3455 over 10	tri: all under 4	quadri: 2520 over 10
orthogonal quality	tri: 558 under 0.8	quadri: 494 under 0.8	tri: 421 under 0.8	quadri: 410 under 0..8

Figure 2.11: Mesh statistics for designs D1SAV and D2NACA12

The strong difference in the number of nodes for the two designs is due to the difference in surface subject to inflation and smaller cells. For the D2NACA12 design the edges of the Savonius that are subject to sizing and inflation are greater than in the D1SAV.

4. Fluent solver setup

This paragraph will cover all the information regarding the Solver (Fluent 16.0 in this case) and all additional features added to it. All screenshots of Fluent explaining what come in this paragraph can be found in Appendix VI

4.1. Transient and turbulence

A test simulation with a non-moving rotor has shown that at this value of Reynold's number, the flow around the Savonius is non stationary, therefore fully turbulent. Vortices form at the tips and then separate before dissipating in the wake. This factor as well as the geometry being in motion around the fluid, our simulation will be run under the transient option.

The time step has already been discussed earlier in this paper.

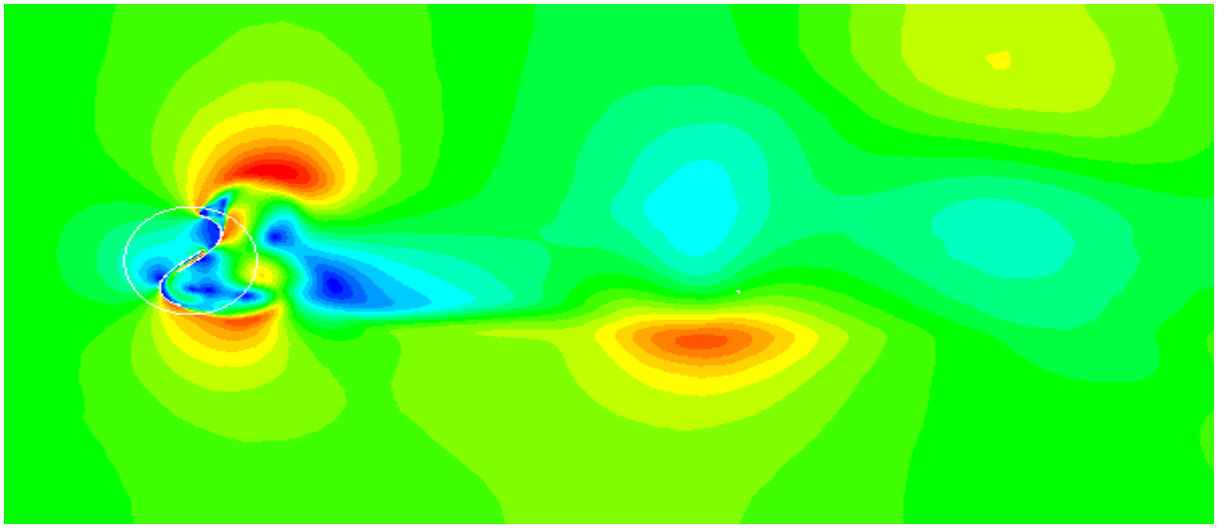

Figure 2.12: Example of velocity in Standard frame at a particular time step **[XX]**

4.2. Boundary conditions

The conditions applied to them are the following (see figure 2.12):

Inlet: Velocity 5.16 m/s (see the UDF explained in the next paragraph). This value will remain constant during all our simulation since the Reynold's number is kept constant at 6.10^4.

$$V = \frac{Re.\mu}{\rho.d} \tag{2.8}$$

ρ being the density of the air (1.225 kg/m^3 in our case), d the characteristic dimension of the system (here the diameter of the Savonius 0.17m), μ the dynamic viscosity of the air ($1.79.10^{-5}$ kg/(m.s) here) and Re being the Reynold's number.

Outlet: Pressure 0 Pa

Walls: set as wall with shear stress of 0 Pa (also known as free surface)

Interface: set as interface with mesh matching on both sides (cell size and nodes coincide). That means the fluid will go through it without being disturbed even though the Savonius area will be subject to a certain rotational speed.

Savonius zone: set as moving mesh with a rotational speed depending on the TSR evaluated in the calculation, see table below:

	omega	rad/s	TSR					
			0.2	0.4	0.6	0.8	1	1.2
	reynolds	speed						
D1SAV	6.00E+04	5.16	12.17	24.35	36.52	48.69	60.87	73.04
D2NACA12	6.00E+04	5.16	11.94	23.88	35.82	47.77	59.71	71.65

Figure 2.13: Angular velocity in function of TSR for D1SAV and D2NACA12

The setting will be modified with a UDF in the next paragraph.

Figure 2.14: Boundary conditions of the simulation environment, ANSYS Mesher **[XX]**

The detailed settings are shown by pictures of the Fluent solver in appendix VI.

4.3. UDF (User Defined Functions) and moving mesh

UDFs or User Defined Functions are available to Fluent users for them to add some features to the existing options of the software. The possibilities are great: you can program different behaviors of flow or a special movement of a solid.

In our case the simulation could not start the simulation directly with an inlet velocity of 5.16meters/second and the established angular velocity of the Savonius. So the flow was eased into the environment by introducing a linear increase in velocity at the inlet and a linear increase in angular velocity of the Savonius. For that we wrote two UDFs that allowed us to have this linear velocity increase (see Figure 2.15) of the Savonius Angular velocity and also a linear increase of the inlet flow speed (see appendix IV).

The linear increase is set as it is shown in the figure below:

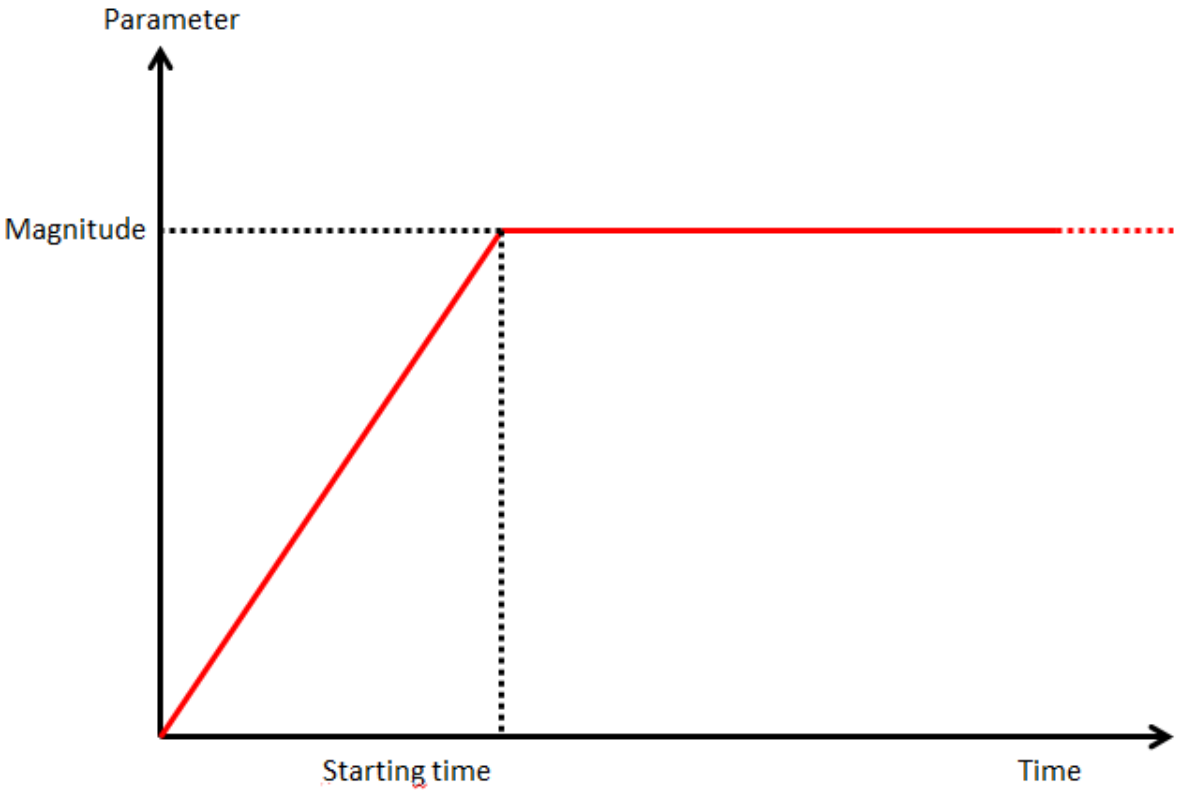

Figure 2.15: Linear increase model

The inlet velocity magnitude is set to 5.16 meters/second, as it was explained in the previous paragraph. The rotational speed magnitude is function of the TSR as shown in the previous paragraph as well.

The starting period is obviously not to take into account in the final results but it helps to have a smooth transition to standard conditions, as it would be in an experiment with the wind picking up from 0 m/s to the desired speed.

4.4. Turbulence model

Going through scientific literature and researching for this paper, CFD dynamic studies of Savonius VAWTs have been found to help in this study **[X][III][IV][VI][VII]**.

. All of them present similarities and they also differ greatly in some other areas. One of them is the turbulence model used in the simulation. In the papers researched there was about a 50/50 split between k-ω SST and k-ε realizable and sometimes there is no clear justification of its use in the publication.

The k-ε turbulence model is the most common model used in CFD to simulate mean flow characteristics for turbulent flow conditions. It is composed of two transport equations which give a general description of turbulence. It is an improvement of the original mixing-length model.

The first transported variable determines the energy in the turbulence and is called turbulent kinetic energy (k).

The second transported variable is the turbulent dissipation (ε) that determines the rate of dissipation of the turbulent kinetic energy.

The k-ω based model accounts for turbulence by two partial differential equations for two variables, k and ω, with the first variable being the turbulence kinetic energy (k) while the second (ω) is the specific rate of dissipation (of the turbulence kinetic energy k). The SST (Shear Stress Transport) specification gives accurate results with shear stress in high pressure gradient areas (typically walls).

As a consequence it was decided to run the simulation with the two turbulence models but only with the first geometry. This will allow the validation of one turbulent model, the one that shows results closer to reality than the other. It obviously increases

the number of simulation (going from 12 to 18) but it is necessary in the thorough study of this problem.

4.5. Mathematical scheme

As for the turbulence model, the mathematical scheme used in solving the fluid mechanics equations of the simulation differs in its use in research papers. The SIMPLE, PISO scheme are all used in CFD dynamic Savonius simulations.

Those mathematical schemes have one thing in common: they all are based on the continuity and momentum equation of Navier-Stokes that are shown below (the details are on Appendix VII) **[XVI]**.

Continuity equation:

$$\nabla.(\rho u) = 0 \qquad (2.9)$$

Momentum equation:

$$\frac{\partial \rho u}{\partial t} + \nabla.(\rho u u) = -\nabla p + \nabla(\mu \nabla u) \qquad (2.10)$$

For this study the SIMPLE scheme will be run. It has been shown that this scheme **[X]** is more precise than the SMAC (which is a more efficient PISO) at higher Courant numbers (above 1).

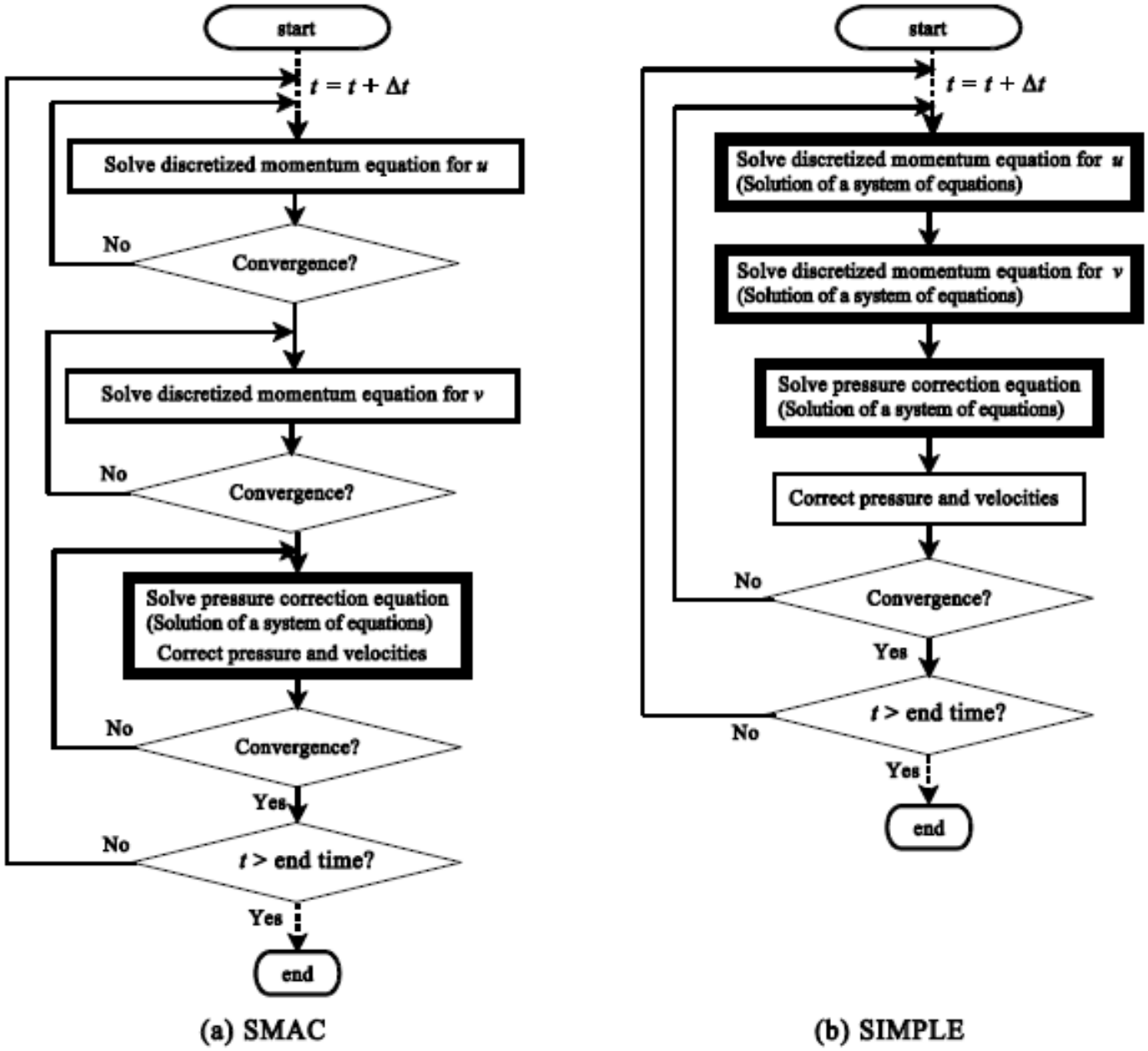

Figure 2.16: Difference between SMAC and SIMPLE scheme **[X]**

4.6. Time of simulation and time step

It was said in paragraph II.4.4 and Appendix IV: the UDFs are set so there is a 1 second starting time before the boundary conditions wanted are attained. After this period the system will stabilize and attain a periodical state. The inlet velocity and rotational speed of the Savonius will be reached and the data can be measured (see II.5 Processing). Knowing the rotational speed of the Savonius the time needed to complete 4 revolutions after the starting time of 1 second can be determined. It was decided that 4 rotations was enough to witness the periodical regime being instated. The table below shows the different rotational speeds for every TSR and the computation times associated:

	computation time	s	TSR					
		-	0.2	0.4	0.6	0.8	1	1.2
D1SAV	reynolds	speed						
D2NACA12	6.00E+04	5.16	3.065	2.032	1.688	1.516	1.413	1.344
	6.00E+04	5.16	3.105	2.052	1.702	1.526	1.421	1.351

Figure 2.16: Angular velocity for different TSRs and two designs

After these 4 revolutions, it can be verified on the Fluent torque monitor that periodic state is reached (see paragraph II.4.7). After that the simulation is run for the equivalent of 2 more revolutions. During those two revolutions, the data will be saved and is to be exploited later.

The time step has already been discussed in paragraph II.3.1 and is set to 1millisecond. In order to get the number of time steps needed, the computational time is divided by the time step length.

Example:

$$Computational\ time = 3.36\ s \qquad Time\ step = 1\ ms$$

$$Number\ of\ time\ steps = \frac{3.36\ s}{1\ ms} = 3360 \qquad (2.11)$$

The number of iterations per time step is kept at 20 iteration/time step as a standard value of Fluent.

4.7. Monitoring

The post processing will be done through the use of CFD Post but some monitoring in Fluent is used to assure that the periodic regime is reached. Below is a screen view of the monitoring of the torque around the Savonius blades. We can observe the starting period of 1 second and then the periodic regime. The latter data will be exploited in CFD-Post.

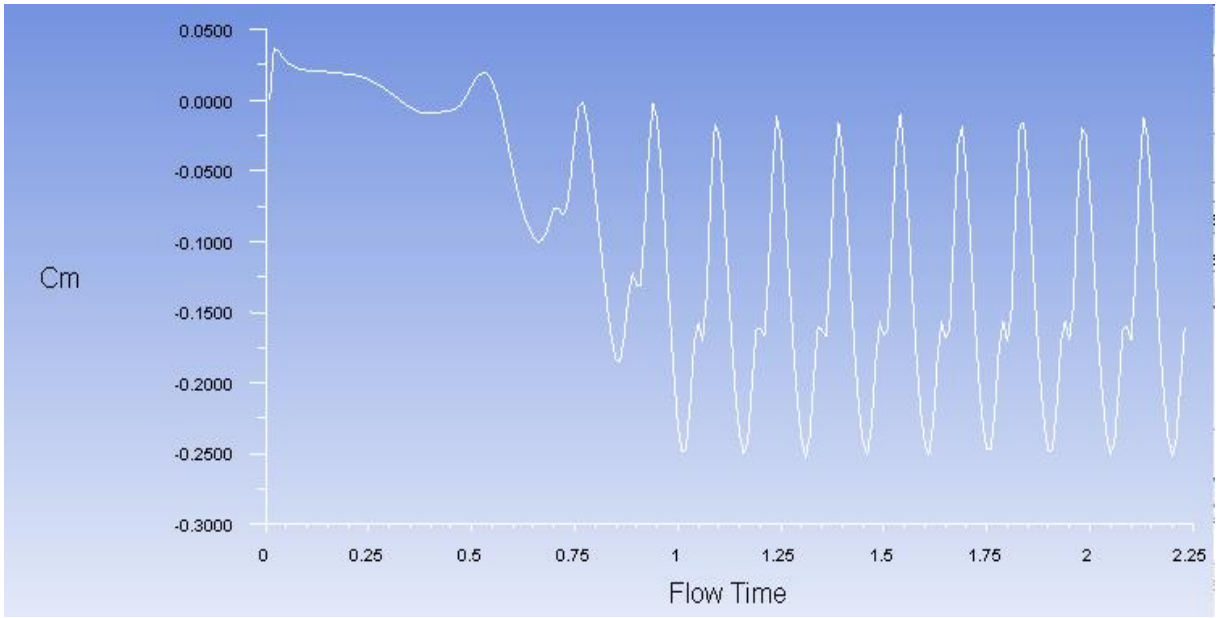

Figure 2.17: Monitoring the torque in ANSYS Fluent **[XX]**

5. Post processing

In this paragraph all the process of data extracting and processing using Fluent and CFD-Post will be explained:

5.1. Torque in function of time

One of the goals of this simulation is to evaluate the efficiency (Cp) of different Savonius rotors at various TSR and at one wind speed (by consequence one Reynold's number).

In order to calculate Cp, the average torque on the blades (C_m), the rotational speed of said blades (ω), the wind velocity (V) and also the air density (ρ) and the area covered by the blades(A) are needed.

$$Cp = \frac{C_m * \omega}{\frac{1}{2} * A * \rho * V^3} \qquad (2.12)$$

All those values except the torque on the blades are constant one in a periodic regime. It is logical then that the value extracted from CFD-Post is the average torque applied to the Savonius blades. After creating a new variable and plotting it against time through the chart viewer (Figure 2.18), the data was extracted to Microsoft Excel and the average torque was evaluated (by calculating the average over two full periods, see Appendix III). After the average torque is calculated, the coefficient of power (C_p) is also calculated using equation 2.12.

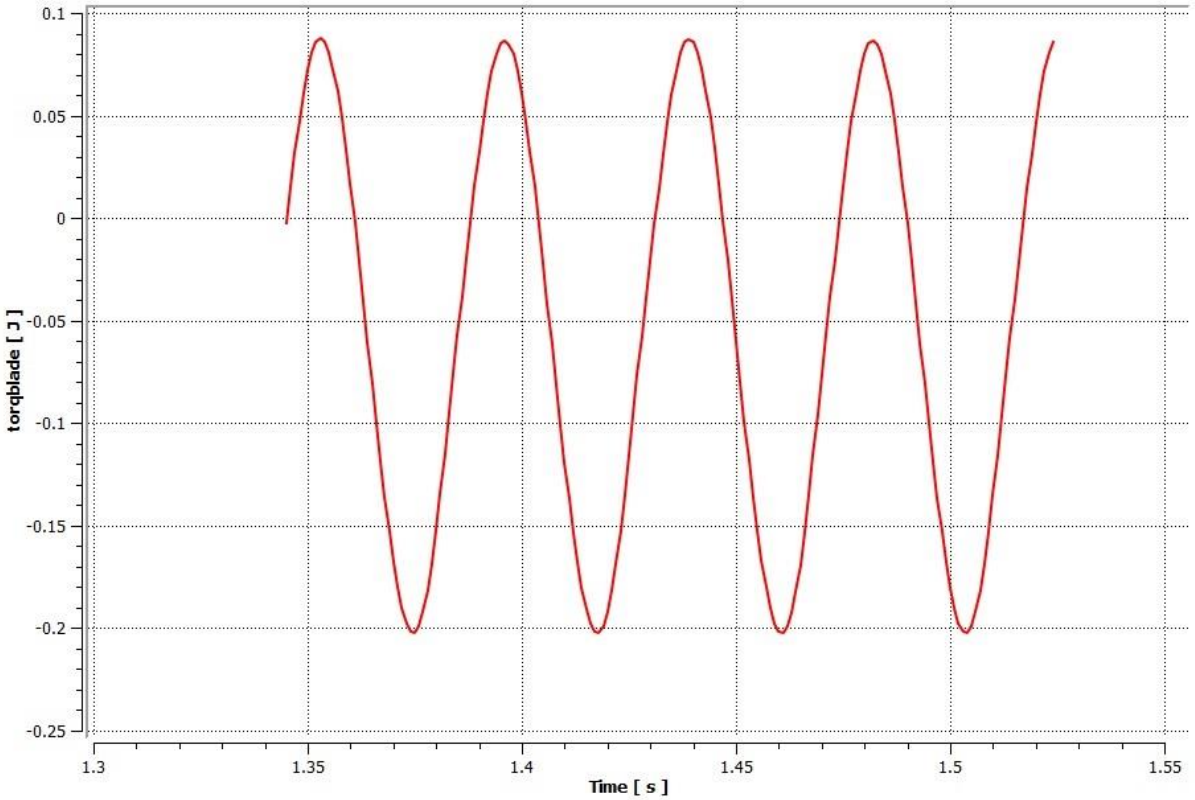

Figure 2.18: Torque in function of time for D1SAV at TSR 1.2 (k-ε), ANSYS CFD-Post **[XX]**

5.2. Evaluation of downstream vortices

The other goal of this project is to evaluate the downstream vortices produced by the movement of the Savonius in the airflow. "Evaluating the vortices" means to evaluate where those vortices dissipate and the flow returns to its original state (inlet). For this the velocity profiles along the wake of the Savonius are plotted and compared with the inlet velocity profile through time. Probe lines are set up along the wake (each at 0.5m from one another starting 0.5m downstream from the Savonius) and the velocity is probed in the direction of the wind along those lines and compared with a reference value (the inlet velocity profile).

The figures below show the probe lines and the velocity profiles graphs:

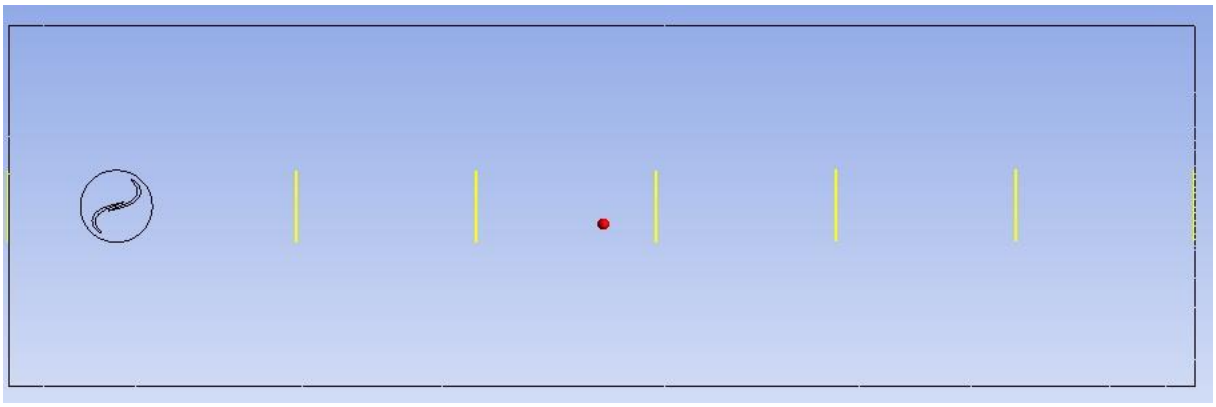

Figure 2.19: Probe lines along the wake of the Savonius, ANSYS CFD-Post **[XX]**

The reference value (inlet velocity) is the black line, the progression following the stream mirrors the rainbow colors:

Color	Distance from Savonius (m)
Purple	0.5
Blue	1
Dark green	1.5
Bright green	2
Orange	2.5
Red	3

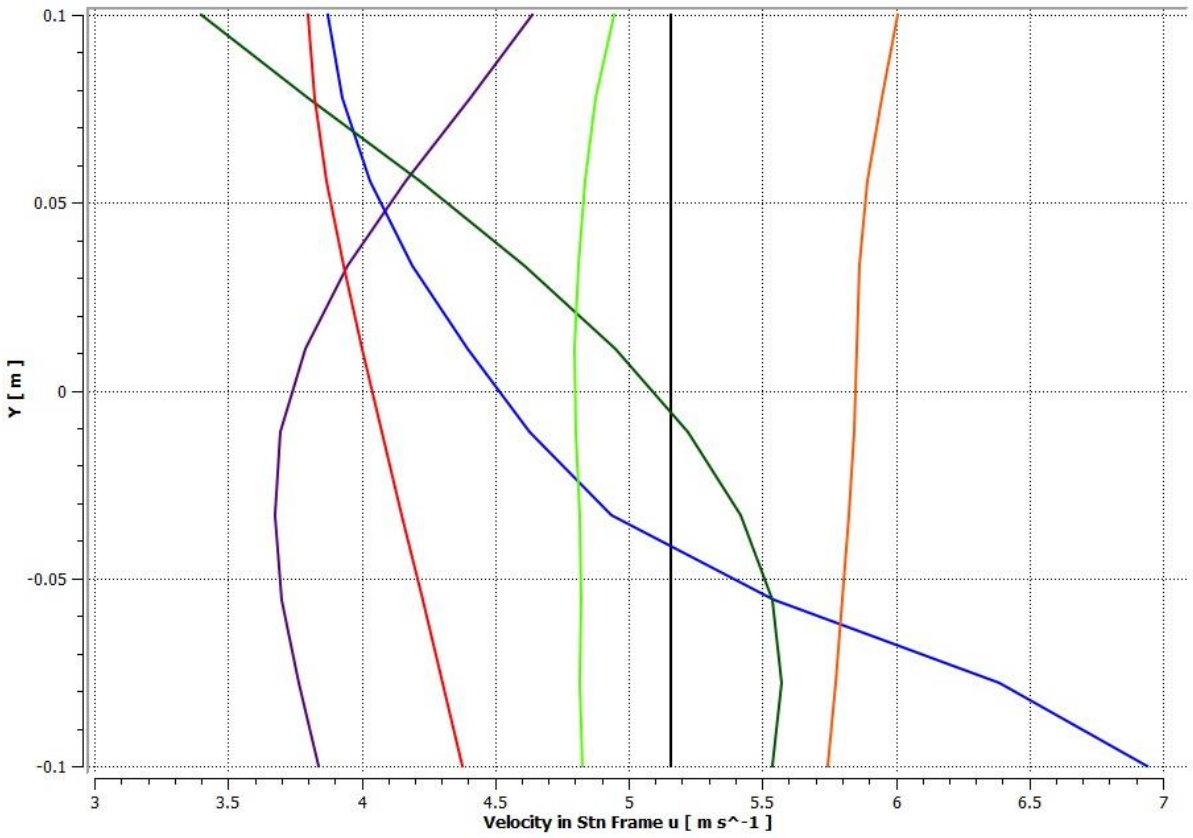

Figure 2.20: Velocity profiles for D2NACA12 at TSR 0.2 (k-ε) at T= 4.158s, ANSYS CFD-Post **[XX]**

III. Results

1. Turbulence model comparison for D1SAV

While testing the two different designs through our CFD simulation, the torque applied on the blades is evaluated over time. It is done for two different turbulence models and six different values of TSR ranging from 0.2 to 1.2 as explained in paragraph II.1.1.

The screenshot below shows a display of that torque over time:

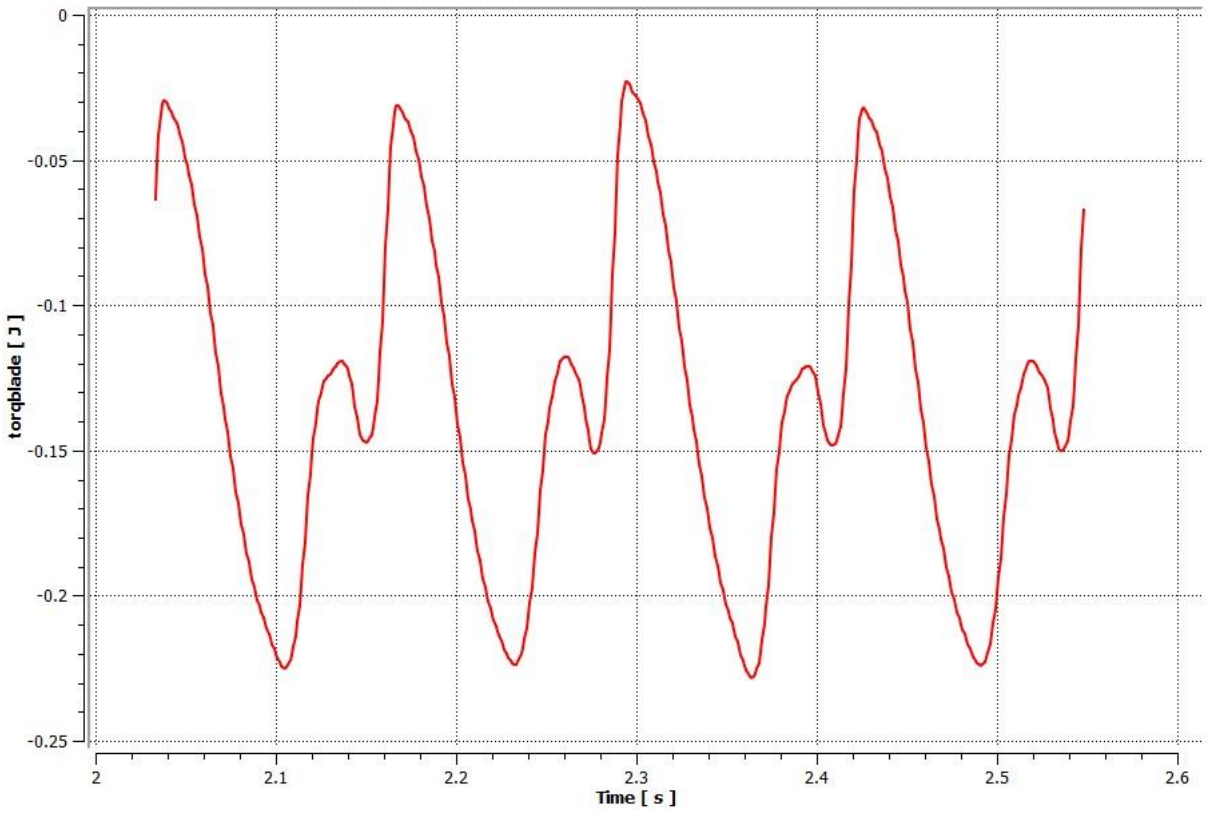

Figure 3.1: Torque on the blades vs time (k-ω) for D1SAV at TSR 0.6, ANSYS CFD-Post **[XX]**

This data is exported to Microsoft Excel for treatment. The average torque applied to the blades is then calculated over multiple revolutions. The different values of torque in function of TSR and turbulence models are shown in appendix II:

In appendix II the calculated rotational speed of the Savonius for every TSR (with the two designs) can be seen, with that the Cp for every TSR was evaluated

Those values are plotted on a Cp = f(TSR) graph and compared to the experimental values found by Sukanta Roy and Ujjwal K. Saha **[VIII]**. Those experimental values were plotted using a software named FindGraph **[XXII]**. This free software is used to extract the data from an image of a graph. This data can be used in an Excel spreadsheet for example. The following figure shows the 3 graphs:

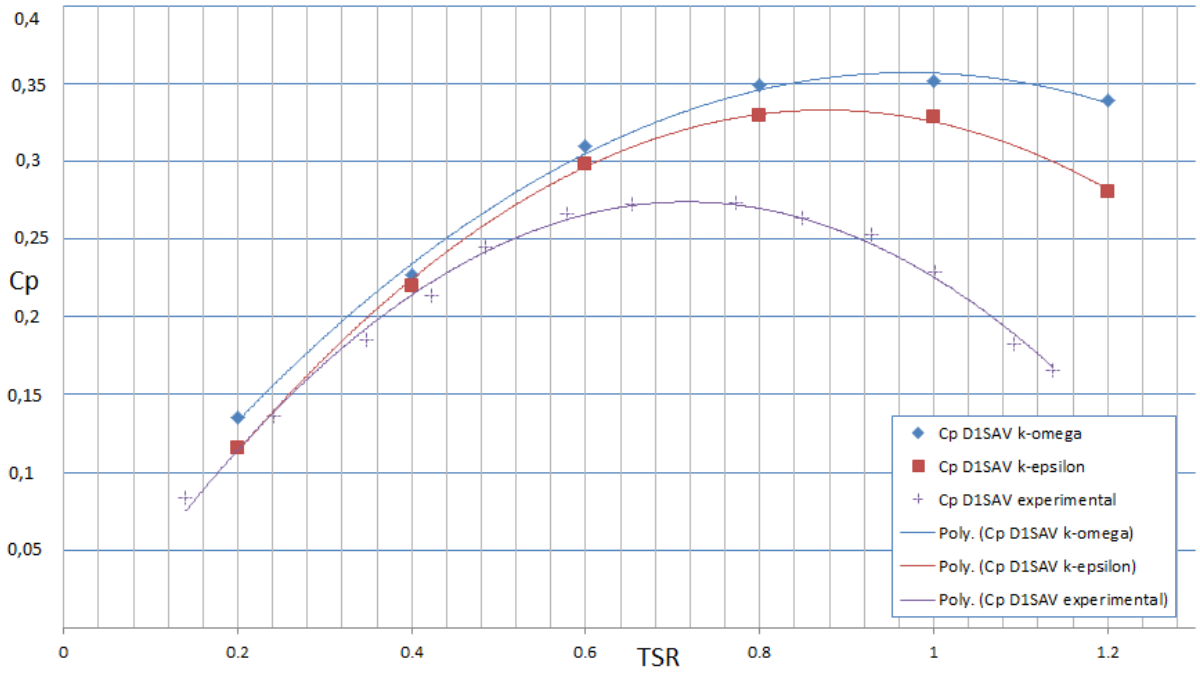

Figure 3.2: C_p comparison for different turbulence models with experimental reference, Microsoft Excel **[XXI]**

It can be observed that the results of Cp are overestimated for TSRs greater than 1 and very close to reality for low TSRs. Usually 2D CFD results overestimate values of CP because the turbulent effects that take place by the end plates are not taken into account. What can also be pointed out is that the maximum value of C_p for this Reynold's number is for a TSR around 0.7 experimentally but a TSR around 0.9 for our CFD simulation. This means that our model represents what really happens when evaluating the efficiency of a Savonius rotor but not to the extent of replacing physical testing with pure CFD analysis. This model is close but does not mimic reality enough for it to stand on itself.

However it can be noted that one turbulence model approaches reality closer than the other. The k-ε realizable shows more promising results than the k-ω SST. In order to compare the two different designs with the exact same simulation environment and set up we will continue forward with the k-ε realizable.

TSR	0.2	0.4	0.6	0.8	1	1.2
experimental	0.114	0.214	0.266	0.270	0.226	0.134
k-omega	0.135	0.227	0.310	0.349	0.352	0.339
error omega (%)	18.1	6.0	16.6	29.3	56.0	153.7
k-epsilon	0.116	0.220	0.299	0.330	0.380	0.281
error epsilon (%)	1.4	2.7	12.4	22.3	68.4	110.3

Figure 3.3: percentage error for the different turbulence models.

2. Design comparison

In this paragraph, the efficiencies of the two different designs (D1SAV and D2NACA12) will be compared as well as the downstream vortices for those designs.

2.1. Coefficient of power

After choosing k-ε realizable as a solver, the simulation was run again with the same conditions. The UDFs for angular velocity are adjusted, because the diameter of the D2NACA12 is slightly larger than the D1SAV, so the TSRs tested are the same. Obviously the mesh was redone since the Savonius geometry was changed.

The figure below shows the two different graphs:

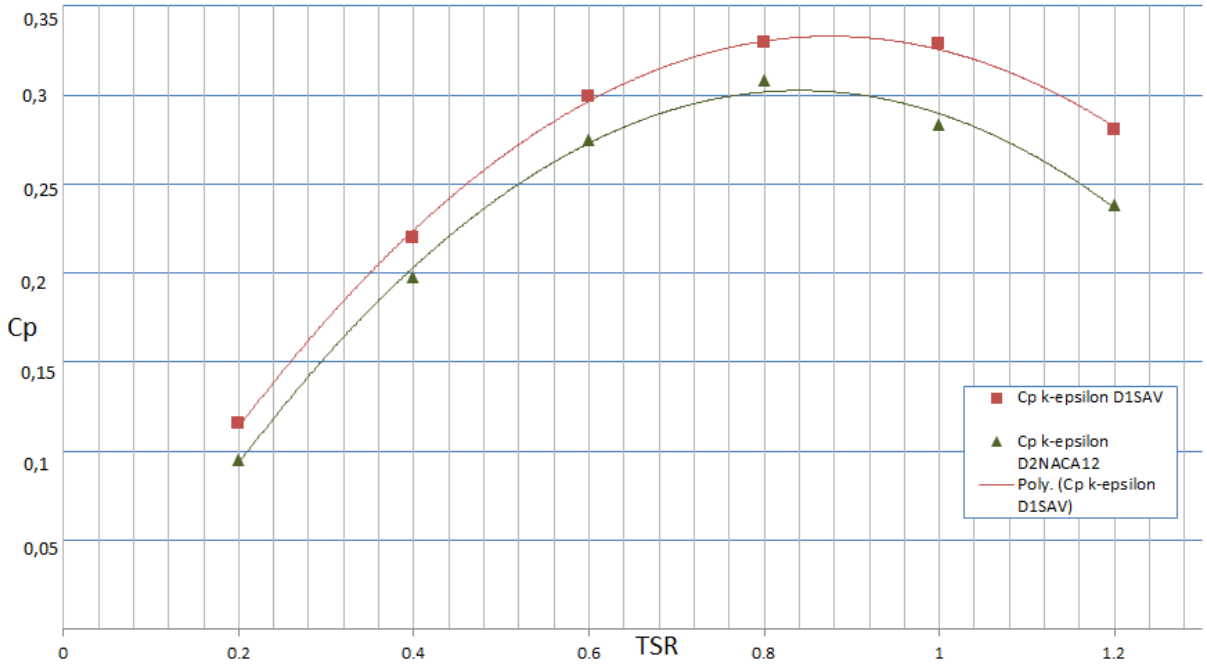

Figure 3.4: C_p vs TSR for D1SAV and D2NACA12, Microsoft Excel **[XXI]**

A lower efficiency is observed for the D2NACA12 design which comes into contradiction with the study redacted by M. Tartuferi **[IX]** which tells that the addition of a NACA0012 thickness improves the C_p for a same base geometry. It seems that the pressure differential inducing a lift force on the blade is not a factor that improves the efficiency. On the other hand, the drop off can be explained by the fact that the areas on either side

of the Savonius blade is not the same with D2NACA12 (as it was for D1SAV). The figure below explains this difference.

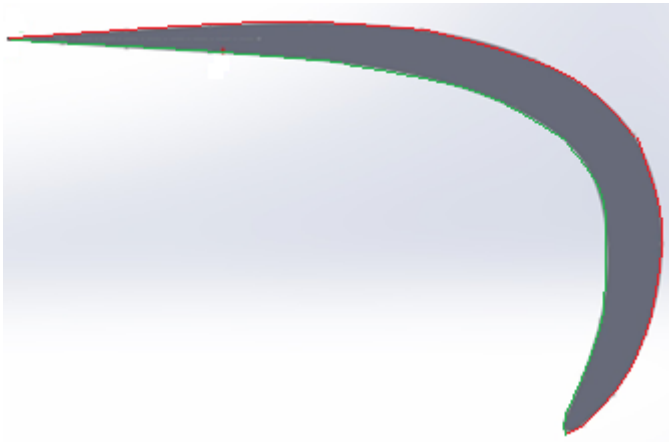

Figure 3.5: area differential between front (green) and back (red) face of a D2NACA12 blade, SolidWorks view **[XIX]**

It can be observed that the red area is greater than the green area in Figure 3.5. The back face (in red) is the one that contributes to slowing down the Savonius rotor and the front one (in green is the one that is responsible for catching the wind flow and pushing it forward. As a consequence the negative drag is greater and the positive drag and therefore the efficiency decreases.

2.2. Downstream vortices

To evaluate if a vortex is dissipated, eye test is not sufficient. A quantitative criteria needs to be implemented that defines whether or not the vortices have dissipated or not. Kinetic energy inside the vortex can be used but that would mean tracking the vortices through the mesh and powerful calculations to evaluate their kinetic energy. It was decided that the use velocity profiles in the flow original direction (the one set at the inlet) was the best option. When the flow comes back to a steady state it would mean that the velocity profile would come back to a straight line like in the inlet (black line in

the graphs) and that equals vortex dissipation. There was one study **[VII]** that used a monitoring point method to determine the frequency of the vortices. The velocity profile method was found to be better suited to the information sought.

Since there was no precedent of a likely method used it was decided that a 15% variation from the original wind speed was acceptable to say that the vortex was dissipated. This gives us a range, knowing the inlet velocity is 5.16m/s, of [4,39 ; 5,93]m/s.

It was clearly noticed after a couple graphs that the first probe lines were never going to fit the criteria. It was then decided to focus on the last three (distance 2m, 2,5m and 3m). Note that the lines have a length of 0.2m which is the width of the Savonius zone. They are shown respectively in blue green and red in Figure 3.6.

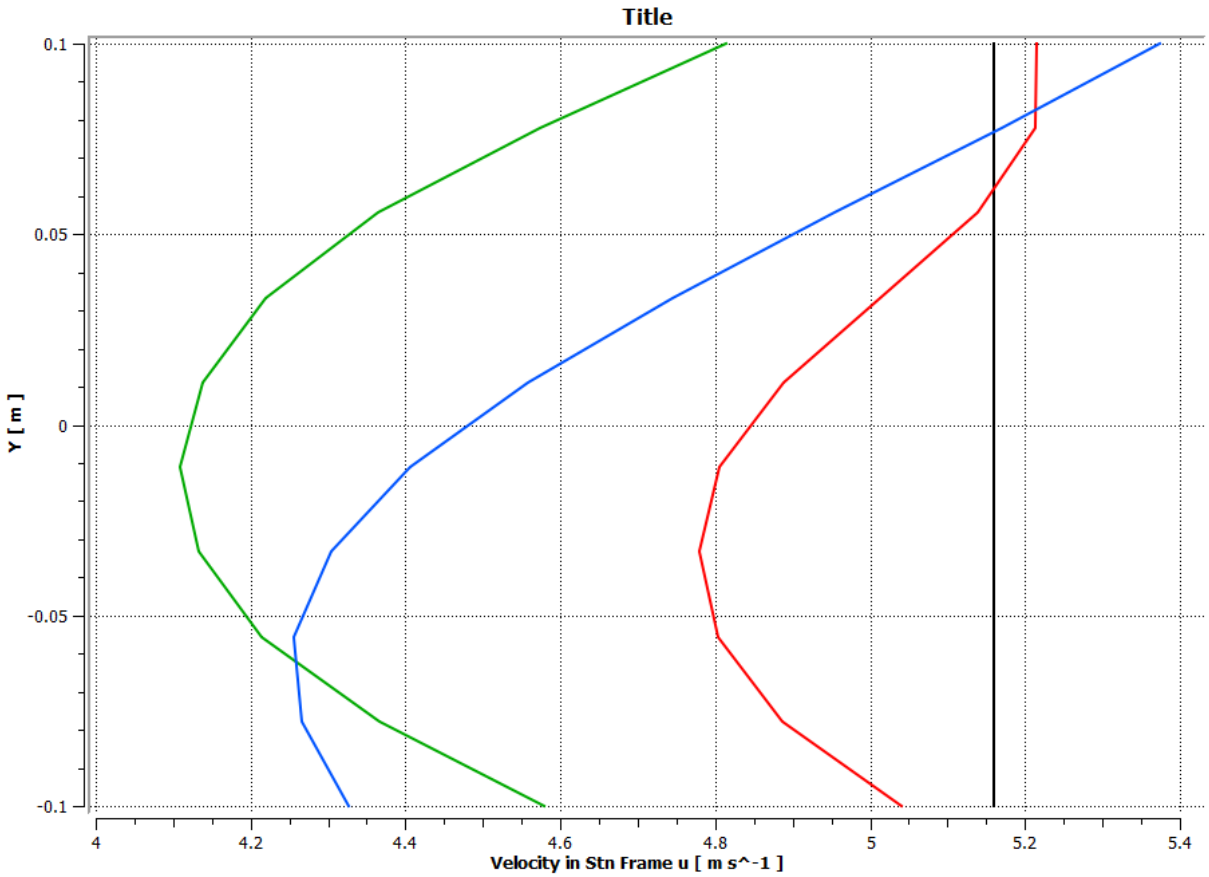

Figure 3.6: Velocity profiles with D1SAV at TSR 1.2 (k-ε) at T=1.5s, ANSYS CFD-Post **[XX]**

Those profiles were graphed for the two designs (both tested with k-ε Realizable) at all TSR and for each TSR at 100ms intervals. The quantity of time steps being high it was too time costly to graph at every time step. For time step chosen we then answered by yes or no if at that probe line the velocity profile fit the ±15% criteria. The results for every TSR are shown in the table below:

	D1SAV		criteria -15%			
TSR	0.2	0.4	0.6	0.8	1	1.2
probe 1 (blue)	no	no	no	no	no	no
probe 2 (green)	no	no	no	no	yes	no
probe 3 (red)	no	no	no	yes	yes	yes

	D2NACA12		criteria -15%			
TSR	0.2	0.4	0.6	0.8	1	1.2
probe 1 (blue)	no	no	no	no	no	no
probe 2 (green)	no	no	no	no	no	no
probe 3 (red)	no	no	no	no	yes	yes

Figure 3.7: Vortex re-establishment criteria for both designs.

The D2NACA12 does not show improvement in terms of generating vortices. The velocity profiles generated are more disturbed with the D2NACA12 than with the D1SAV.

Usually while producing electricity the goal is to maximize C_p. It can be done by monitoring the TSR and adjusting it to where the efficiency is at a maximum. This means that the TSR where the Savonius will be used is above 0.7. This means that if you want to place another Savonius downstream the first one the "safe distance" or minimum distance where to place it will be at 3 meters for both designs.

If you want to have a more accurate reading on the vortices (±10, 5% or complete reestablishing of the flow) it will be needed to create a larger simulating environment.

CONCLUSION

During this project a 2D simulating environment for a vertical axis wind turbine was created from scratch. It was done by considering what turbine technology was to be studied, what variable were to be measured and extracted from the simulation, what were the requirements in dimensions, meshing, turbulence models and mathematical scheme. It was also conceived so it could host further calculations and could be used in different projects with similar characteristics. The model was partially validated by comparing the efficiency with experimental results. A turbulence analysis was then conducted but there are still improvements to be made by expanding the simulation environment (more input parameters, size of the simulation environment…).

This simulation may be used for further studies (other types of VAWTs or other Savonius designs). Although in this paper only one Reynold's number was considered (so one wind speed) which is not representative of the full spectrum of meteorological conditions, it was already a step forward in a better understanding of Savonius HAWTs of this particular design. Increasing the amount of simulation runs can be the object of a future study. Also physical testing needs to be conducted on the D2NACA12 in order to confirm the results found in this study.

ACKNOWLEDGEMENTS

In order to complete this research project Nathan Guignard received help from various persons and he would like to thank them in this paragraph:

Luis Chirinos and Vincent Caillé for signing the double degree agreement between ECAM Lyon and PUCP and always being supportive of Nathan during his stay in Lima.

Alex Arnaldo Pachas and ESSS Peru who have helped him greatly with the use of ANSYS Fluent

Nathan’s parents and close friends who were always here when he needed them.

APPENDICES

I- NACA 0012 profile

X_Camber(%)	Y+ (%)		X_Camber(%)	Y- (%)
0	0		0	0
0.0005839	0.0042603		0.0005839	-0.0042603
0.0023342	0.0084289		0.0023342	-0.0084289
0.0052468	0.0125011		0.0052468	-0.0125011
0.0093149	0.0164706		0.0093149	-0.0164706
0.0145291	0.02033		0.0145291	-0.02033
0.0208771	0.0240706		0.0208771	-0.0240706
0.0283441	0.0276827		0.0283441	-0.0276827
0.0369127	0.0311559		0.0369127	-0.0311559
0.0465628	0.0344792		0.0465628	-0.0344792
0.057272	0.0376414		0.057272	-0.0376414
0.0690152	0.040631		0.0690152	-0.040631
0.0817649	0.0434371		0.0817649	-0.0434371
0.0954915	0.0460489		0.0954915	-0.0460489
0.1101628	0.0484567		0.1101628	-0.0484567
0.1257446	0.0506513		0.1257446	-0.0506513
0.1422005	0.0526251		0.1422005	-0.0526251
0.1594921	0.0543715		0.1594921	-0.0543715
0.1775789	0.0558856		0.1775789	-0.0558856
0.1964187	0.057164		0.1964187	-0.057164
0.2159676	0.0582048		0.2159676	-0.0582048
0.2361799	0.0590081		0.2361799	-0.0590081
0.2570083	0.0595755		0.2570083	-0.0595755
0.2784042	0.0599102		0.2784042	-0.0599102
0.3003177	0.0600172		0.3003177	-0.0600172
0.3226976	0.0599028		0.3226976	-0.0599028
0.3454915	0.0595747		0.3454915	-0.0595747
0.3686463	0.0590419		0.3686463	-0.0590419
0.3921079	0.0583145		0.3921079	-0.0583145
0.4158215	0.0574033		0.4158215	-0.0574033
0.4397317	0.05632		0.4397317	-0.05632
0.4637826	0.0550769		0.4637826	-0.0550769
0.4879181	0.0536866		0.4879181	-0.0536866
0.5120819	0.052162		0.5120819	-0.052162

0.5362174	0.0505161		0.5362174	-0.0505161
0.5602683	0.0487619		0.5602683	-0.0487619
0.5841786	0.0469124		0.5841786	-0.0469124
0.6078921	0.0449802		0.6078921	-0.0449802
0.6313537	0.0429778		0.6313537	-0.0429778
0.6545085	0.0409174		0.6545085	-0.0409174
0.6773025	0.0388109		0.6773025	-0.0388109
0.6996823	0.03667		0.6996823	-0.03667
0.7215958	0.0345058		0.7215958	-0.0345058
0.7429917	0.0323294		0.7429917	-0.0323294
0.7638202	0.0301515		0.7638202	-0.0301515
0.7840324	0.0279828		0.7840324	-0.0279828
0.8035813	0.0258337		0.8035813	-0.0258337
0.8224211	0.0237142		0.8224211	-0.0237142
0.8405079	0.0216347		0.8405079	-0.0216347
0.8577995	0.0196051		0.8577995	-0.0196051
0.8742554	0.0176353		0.8742554	-0.0176353
0.8898372	0.0157351		0.8898372	-0.0157351
0.9045085	0.0139143		0.9045085	-0.0139143
0.9182351	0.0121823		0.9182351	-0.0121823
0.9309849	0.0105485		0.9309849	-0.0105485
0.942728	0.0090217		0.942728	-0.0090217
0.9534372	0.0076108		0.9534372	-0.0076108
0.9630873	0.0063238		0.9630873	-0.0063238
0.9716559	0.0051685		0.9716559	-0.0051685
0.9791229	0.0041519		0.9791229	-0.0041519
0.9854709	0.0032804		0.9854709	-0.0032804
0.990685	0.0025595		0.990685	-0.0025595
0.9947532	0.0019938		0.9947532	-0.0019938
0.9976658	0.001587		0.9976658	-0.001587
0.9994161	0.0013419		0.9994161	-0.0013419
1	0.00126		1	-0.00126

II- Excel spreadsheet of results

Overall view of the numerical results. The Excel file can be attached for better comprehension **[XXI]**.

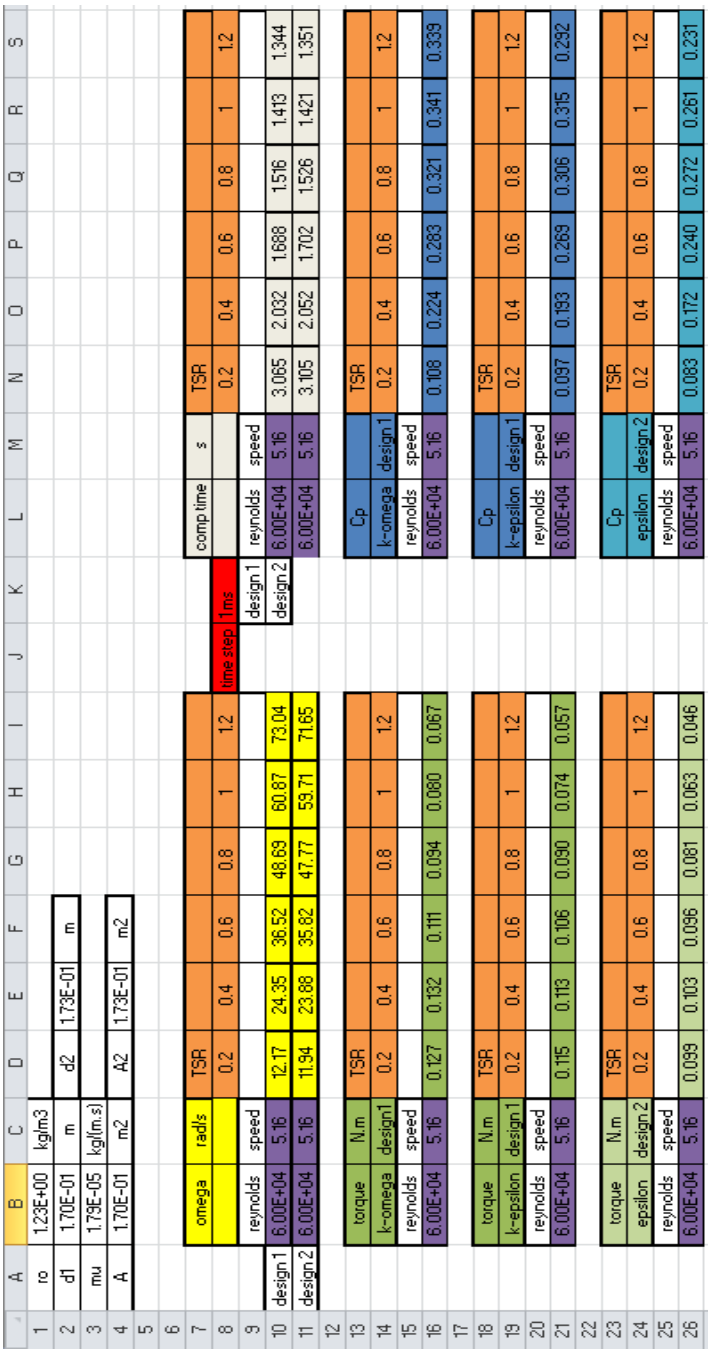

	A	B	C	D	E	F	G	H	I
1	ro	1.23E+00	kg/m3						
2	d1	1.70E-01	m	d2	1.73E-01	m			
3	mu	1.79E-05	kg/(m.s)						
4	A	1.70E-01	m2	A2	1.73E-01	m2			
5									
6									
7		omega	rad/s	TSR					
8				0.2	0.4	0.6	0.8	1	1.2
9		reynolds	speed						
10	design 1	6.00E+04	5.16	12.17	24.35	36.52	48.69	60.87	73.04
11	design 2	6.00E+04	5.16	11.94	23.88	35.82	47.77	59.71	71.65
12									
13		torque	N.m	TSR					
14		k-omega	design1	0.2	0.4	0.6	0.8	1	1.2
15		reynolds	speed						
16		6.00E+04	5.16	0.127	0.132	0.111	0.094	0.080	0.067
17									
18		torque	N.m	TSR					
19		k-epsilon	design1	0.2	0.4	0.6	0.8	1	1.2
20		reynolds	speed						
21		6.00E+04	5.16	0.115	0.113	0.106	0.090	0.074	0.057
22									
23		torque	N.m	TSR					
24		epsilon	design 2	0.2	0.4	0.6	0.8	1	1.2
25		reynolds	speed						
26		6.00E+04	5.16	0.099	0.103	0.096	0.081	0.063	0.046

	J	K	L	M	N	O	P	Q	R	S
7			comp time	s	TSR					
8	time step	1 ms			0.2	0.4	0.6	0.8	1	1.2
9		design 1	reynolds	speed						
10		design 2	6.00E+04	5.16	3.065	2.032	1.688	1.516	1.413	1.344
11			6.00E+04	5.16	3.105	2.052	1.702	1.526	1.421	1.351
13			Cp		TSR					
14			k-omega	design 1	0.2	0.4	0.6	0.8	1	1.2
15			reynolds	speed						
16			6.00E+04	5.16	0.108	0.224	0.283	0.321	0.341	0.339
18			Cp		TSR					
19			k-epsilon	design 1	0.2	0.4	0.6	0.8	1	1.2
20			reynolds	speed						
21			6.00E+04	5.16	0.097	0.193	0.269	0.306	0.315	0.292
23			Cp		TSR					
24			epsilon	design 2	0.2	0.4	0.6	0.8	1	1.2
25			reynolds	speed						
26			6.00E+04	5.16	0.083	0.172	0.240	0.272	0.261	0.231

III- EXCEL view of torque data

The whole spreadsheet is composed of too much data to be shown in this annex. The Excel file can be attached for better comprehension **[XXI]**.

TSR 0.2		TSR 0.4		TSR 0.6		TSR 0.8		TSR 1.0		TSR 1.2	
average torque (J)	1.59E-01	average torque (J)	1.34E-01	average torque (J)	1.22E-01	average torque (J)	1.03E-01	average torque (J)	8.28E-02	average torque (J)	6.19E-02
[Data]		[Data]		[Data]		[Data]		[Data]		[Data]	
Time [s]	torqblade [J]	Time [s]	torqblade [J]	Time [s]	torqblade [J]	Time [s]	torqblade [J]	Time [s]	torqblade [J]	Time [s]	torqblade [J]
3.07E+00	-2.56E-01	2.03E+00	-6.36E-02	1.69E+00	-4.67E-02	1.52E+00	-2.50E-02	1.41E+00	-9.86E-03	1.35E+00	-1.57E-02
3.07E+00	-2.56E-01	2.03E+00	-5.16E-02	1.69E+00	-4.60E-02	1.52E+00	-1.80E-02	1.41E+00	1.30E-03	1.35E+00	1.55E-03
3.07E+00	-2.54E-01	2.04E+00	-4.17E-02	1.69E+00	-4.59E-02	1.52E+00	-1.14E-02	1.42E+00	1.12E-02	1.35E+00	1.81E-02
3.07E+00	-2.52E-01	2.04E+00	-3.47E-02	1.69E+00	-4.61E-02	1.52E+00	-5.83E-03	1.42E+00	2.03E-02	1.35E+00	3.35E-02
3.07E+00	-2.49E-01	2.04E+00	-3.09E-02	1.69E+00	-4.64E-02	1.52E+00	-1.51E-03	1.42E+00	2.75E-02	1.35E+00	4.78E-02
3.07E+00	-2.46E-01	2.04E+00	-2.95E-02	1.69E+00	-4.60E-02	1.52E+00	2.04E-03	1.42E+00	3.25E-02	1.35E+00	5.96E-02
3.07E+00	-2.41E-01	2.04E+00	-2.98E-02	1.70E+00	-4.46E-02	1.52E+00	4.32E-03	1.42E+00	3.56E-02	1.35E+00	6.87E-02
3.07E+00	-2.36E-01	2.04E+00	-3.10E-02	1.70E+00	-4.19E-02	1.52E+00	5.98E-03	1.42E+00	3.67E-02	1.35E+00	7.49E-02
3.07E+00	-2.31E-01	2.04E+00	-3.24E-02	1.70E+00	-3.82E-02	1.52E+00	6.45E-03	1.42E+00	3.60E-02	1.35E+00	7.77E-02
3.08E+00	-2.24E-01	2.04E+00	-3.36E-02	1.70E+00	-3.37E-02	1.53E+00	6.07E-03	1.42E+00	3.37E-02	1.35E+00	7.68E-02
3.08E+00	-2.17E-01	2.04E+00	-3.48E-02	1.70E+00	-2.92E-02	1.53E+00	4.76E-03	1.42E+00	3.01E-02	1.36E+00	7.27E-02
3.08E+00	-2.09E-01	2.04E+00	-3.59E-02	1.70E+00	-2.51E-02	1.53E+00	1.87E-03	1.42E+00	2.50E-02	1.36E+00	6.58E-02
3.08E+00	-2.01E-01	2.05E+00	-3.73E-02	1.70E+00	-2.25E-02	1.53E+00	-1.91E-03	1.43E+00	1.83E-02	1.36E+00	5.60E-02
3.08E+00	-1.93E-01	2.05E+00	-3.89E-02	1.70E+00	-2.18E-02	1.53E+00	-7.02E-03	1.43E+00	1.01E-02	1.36E+00	4.36E-02
3.08E+00	-1.84E-01	2.05E+00	-4.10E-02	1.70E+00	-2.34E-02	1.53E+00	-1.32E-02	1.43E+00	3.36E-04	1.36E+00	2.90E-02
3.08E+00	-1.76E-01	2.05E+00	-4.35E-02	1.70E+00	-2.72E-02	1.53E+00	-2.01E-02	1.43E+00	-1.09E-02	1.36E+00	1.24E-02
3.08E+00	-1.69E-01	2.05E+00	-4.63E-02	1.71E+00	-3.28E-02	1.53E+00	-2.84E-02	1.43E+00	-2.32E-02	1.36E+00	-5.65E-03
3.08E+00	-1.62E-01	2.05E+00	-4.91E-02	1.71E+00	-3.99E-02	1.53E+00	-3.75E-02	1.43E+00	-3.66E-02	1.36E+00	-2.48E-02
3.08E+00	-1.56E-01	2.05E+00	-5.20E-02	1.71E+00	-4.78E-02	1.53E+00	-4.73E-02	1.43E+00	-5.08E-02	1.36E+00	-4.43E-02
3.09E+00	-1.52E-01	2.05E+00	-5.51E-02	1.71E+00	-5.59E-02	1.54E+00	-5.80E-02	1.43E+00	-6.56E-02	1.36E+00	-6.41E-02
3.09E+00	-1.50E-01	2.05E+00	-5.83E-02	1.71E+00	-6.42E-02	1.54E+00	-6.90E-02	1.43E+00	-8.07E-02	1.37E+00	-8.38E-02
3.09E+00	-1.48E-01	2.05E+00	-6.17E-02	1.71E+00	-7.23E-02	1.54E+00	-8.04E-02	1.43E+00	-9.59E-02	1.37E+00	-1.03E-01
3.09E+00	-1.48E-01	2.06E+00	-6.53E-02	1.71E+00	-8.04E-02	1.54E+00	-9.20E-02	1.44E+00	-1.11E-01	1.37E+00	-1.22E-01
3.09E+00	-1.49E-01	2.06E+00	-6.89E-02	1.71E+00	-8.84E-02	1.54E+00	-1.04E-01	1.44E+00	-1.26E-01	1.37E+00	-1.40E-01
3.09E+00	-1.51E-01	2.06E+00	-7.27E-02	1.71E+00	-9.63E-02	1.54E+00	-1.15E-01	1.44E+00	-1.41E-01	1.37E+00	-1.57E-01
3.09E+00	-1.53E-01	2.06E+00	-7.66E-02	1.71E+00	-1.04E-01	1.54E+00	-1.27E-01	1.44E+00	-1.54E-01	1.37E+00	-1.72E-01
3.09E+00	-1.56E-01	2.06E+00	-8.07E-02	1.72E+00	-1.11E-01	1.54E+00	-1.38E-01	1.44E+00	-1.67E-01	1.37E+00	-1.85E-01
3.09E+00	-1.59E-01	2.06E+00	-8.49E-02	1.72E+00	-1.19E-01	1.54E+00	-1.49E-01	1.44E+00	-1.79E-01	1.37E+00	-1.95E-01
3.09E+00	-1.61E-01	2.06E+00	-8.91E-02	1.72E+00	-1.26E-01	1.54E+00	-1.59E-01	1.44E+00	-1.89E-01	1.37E+00	-2.03E-01
3.10E+00	-1.63E-01	2.06E+00	-9.35E-02	1.72E+00	-1.33E-01	1.55E+00	-1.68E-01	1.44E+00	-1.97E-01	1.37E+00	-2.06E-01
3.10E+00	-1.64E-01	2.06E+00	-9.79E-02	1.72E+00	-1.40E-01	1.55E+00	-1.76E-01	1.44E+00	-2.03E-01	1.38E+00	-2.06E-01
3.10E+00	-1.64E-01	2.06E+00	-1.02E-01	1.72E+00	-1.46E-01	1.55E+00	-1.84E-01	1.45E+00	-2.07E-01	1.38E+00	-2.02E-01
3.10E+00	-1.63E-01	2.07E+00	-1.07E-01	1.72E+00	-1.52E-01	1.55E+00	-1.90E-01	1.45E+00	-2.09E-01	1.38E+00	-1.95E-01
3.10E+00	-1.64E-01	2.06E+00	-1.02E-01	1.72E+00	-1.46E-01	1.55E+00	-1.84E-01	1.45E+00	-2.07E-01	1.38E+00	-2.02E-01
3.10E+00	-1.63E-01	2.07E+00	-1.07E-01	1.72E+00	-1.52E-01	1.55E+00	-1.90E-01	1.45E+00	-2.09E-01	1.38E+00	-1.95E-01
3.10E+00	-1.61E-01	2.07E+00	-1.12E-01	1.72E+00	-1.58E-01	1.55E+00	-1.96E-01	1.45E+00	-2.07E-01	1.38E+00	-1.85E-01
3.10E+00	-1.59E-01	2.07E+00	-1.16E-01	1.72E+00	-1.63E-01	1.55E+00	-2.00E-01	1.45E+00	-2.04E-01	1.38E+00	-1.72E-01
3.10E+00	-1.58E-01	2.07E+00	-1.21E-01	1.72E+00	-1.69E-01	1.55E+00	-2.03E-01	1.45E+00	-1.99E-01	1.38E+00	-1.57E-01
3.10E+00	-1.56E-01	2.07E+00	-1.26E-01	1.73E+00	-1.74E-01	1.55E+00	-2.05E-01	1.45E+00	-1.92E-01	1.38E+00	-1.40E-01
3.10E+00	-1.56E-01	2.07E+00	-1.30E-01	1.73E+00	-1.78E-01	1.55E+00	-2.06E-01	1.45E+00	-1.83E-01	1.38E+00	-1.22E-01
3.10E+00	-1.56E-01	2.07E+00	-1.35E-01	1.73E+00	-1.83E-01	1.55E+00	-2.05E-01	1.45E+00	-1.74E-01	1.38E+00	-1.03E-01
3.11E+00	-1.58E-01	2.07E+00	-1.39E-01	1.73E+00	-1.87E-01	1.56E+00	-2.04E-01	1.45E+00	-1.64E-01	1.38E+00	-8.54E-02
3.11E+00	-1.63E-01	2.07E+00	-1.44E-01	1.73E+00	-1.91E-01	1.56E+00	-2.02E-01	1.45E+00	-1.54E-01	1.38E+00	-6.73E-02
3.11E+00	-1.70E-01	2.07E+00	-1.48E-01	1.73E+00	-1.94E-01	1.56E+00	-2.00E-01	1.46E+00	-1.43E-01	1.39E+00	-5.00E-02
3.11E+00	-1.79E-01	2.08E+00	-1.52E-01	1.73E+00	-1.97E-01	1.56E+00	-1.98E-01	1.46E+00	-1.33E-01	1.39E+00	-3.26E-02
3.11E+00	-1.90E-01	2.08E+00	-1.56E-01	1.73E+00	-2.00E-01	1.56E+00	-1.95E-01	1.46E+00	-1.21E-01	1.39E+00	-1.54E-02
3.11E+00	-2.01E-01	2.08E+00	-1.60E-01	1.73E+00	-2.02E-01	1.56E+00	-1.92E-01	1.46E+00	-1.10E-01	1.39E+00	1.76E-03
3.11E+00	-2.08E-01	2.08E+00	-1.64E-01	1.73E+00	-2.04E-01	1.56E+00	-1.88E-01	1.46E+00	-9.71E-02	1.39E+00	1.86E-02
3.11E+00	-2.12E-01	2.08E+00	-1.68E-01	1.74E+00	-2.06E-01	1.56E+00	-1.83E-01	1.46E+00	-8.42E-02	1.39E+00	3.42E-02
3.11E+00	-2.11E-01	2.08E+00	-1.72E-01	1.74E+00	-2.07E-01	1.56E+00	-1.78E-01	1.46E+00	-7.10E-02	1.39E+00	4.80E-02
3.11E+00	-2.08E-01	2.08E+00	-1.75E-01	1.74E+00	-2.09E-01	1.57E+00	-1.72E-01	1.46E+00	-5.75E-02	1.39E+00	5.95E-02
3.12E+00	-2.02E-01	2.08E+00	-1.79E-01	1.74E+00	-2.10E-01	1.57E+00	-1.66E-01	1.46E+00	-4.37E-02	1.39E+00	6.87E-02
3.12E+00	-1.94E-01	2.08E+00	-1.82E-01	1.74E+00	-2.10E-01	1.57E+00	-1.59E-01	1.46E+00	-2.99E-02	1.39E+00	7.45E-02
3.12E+00	-1.85E-01	2.08E+00	-1.85E-01	1.74E+00	-2.11E-01	1.57E+00	-1.51E-01	1.47E+00	-1.72E-02	1.40E+00	7.69E-02
3.12E+00	-1.75E-01	2.09E+00	-1.88E-01	1.74E+00	-2.11E-01	1.57E+00	-1.43E-01	1.47E+00	-5.55E-03	1.40E+00	7.61E-02
3.12E+00	-1.65E-01	2.09E+00	-1.91E-01	1.74E+00	-2.11E-01	1.57E+00	-1.34E-01	1.47E+00	4.97E-03	1.40E+00	7.21E-02
3.12E+00	-1.57E-01	2.09E+00	-1.94E-01	1.74E+00	-2.10E-01	1.57E+00	-1.25E-01	1.47E+00	1.46E-02	1.40E+00	6.48E-02
3.12E+00	-1.51E-01	2.09E+00	-1.97E-01	1.74E+00	-2.09E-01	1.57E+00	-1.15E-01	1.47E+00	2.26E-02	1.40E+00	5.50E-02
3.12E+00	-1.47E-01	2.09E+00	-1.99E-01	1.75E+00	-2.08E-01	1.57E+00	-1.04E-01	1.47E+00	2.89E-02	1.40E+00	4.25E-02
3.12E+00	-1.44E-01	2.09E+00	-2.02E-01	1.75E+00	-2.06E-01	1.57E+00	-9.37E-02	1.47E+00	3.31E-02	1.40E+00	2.80E-02
3.12E+00	-1.44E-01	2.09E+00	-2.04E-01	1.75E+00	-2.04E-01	1.58E+00	-8.26E-02	1.47E+00	3.53E-02	1.40E+00	1.14E-02
3.13E+00	-1.45E-01	2.09E+00	-2.06E-01	1.75E+00	-2.02E-01	1.58E+00	-7.20E-02	1.47E+00	3.58E-02	1.40E+00	-6.64E-03
3.13E+00	-1.47E-01	2.09E+00	-2.08E-01	1.75E+00	-1.99E-01	1.58E+00	-6.18E-02	1.47E+00	3.47E-02	1.40E+00	-2.56E-02

3.13E+00	-1.49E-01	2.09E+00	-2.10E-01	1.75E+00	-1.95E-01	1.58E+00	-5.24E-02	1.48E+00	3.18E-02	1.41E+00	-4.52E-02
3.13E+00	-1.50E-01	2.10E+00	-2.11E-01	1.75E+00	-1.90E-01	1.58E+00	-4.41E-02	1.48E+00	2.73E-02	1.41E+00	-6.49E-02
3.13E+00	-1.52E-01	2.10E+00	-2.13E-01	1.75E+00	-1.85E-01	1.58E+00	-3.62E-02	1.48E+00	2.14E-02	1.41E+00	-8.45E-02
3.13E+00	-1.53E-01	2.10E+00	-2.15E-01	1.75E+00	-1.79E-01	1.58E+00	-2.92E-02	1.48E+00	1.42E-02	1.41E+00	-1.04E-01
3.13E+00	-1.54E-01	2.10E+00	-2.17E-01	1.75E+00	-1.72E-01	1.58E+00	-2.25E-02	1.48E+00	5.57E-03	1.41E+00	-1.23E-01
3.13E+00	-1.54E-01	2.10E+00	-2.18E-01	1.76E+00	-1.63E-01	1.58E+00	-1.58E-02	1.48E+00	-4.60E-03	1.41E+00	-1.41E-01
3.13E+00	-1.54E-01	2.10E+00	-2.20E-01	1.76E+00	-1.54E-01	1.58E+00	-9.82E-03	1.48E+00	-1.62E-02	1.41E+00	-1.57E-01
3.13E+00	-1.55E-01	2.10E+00	-2.22E-01	1.76E+00	-1.44E-01	1.59E+00	-4.85E-03	1.48E+00	-2.88E-02	1.41E+00	-1.72E-01
3.13E+00	-1.55E-01	2.10E+00	-2.23E-01	1.76E+00	-1.33E-01	1.59E+00	-9.57E-04	1.48E+00	-4.25E-02	1.41E+00	-1.85E-01
3.14E+00	-1.55E-01	2.10E+00	-2.24E-01	1.76E+00	-1.23E-01	1.59E+00	2.44E-03	1.48E+00	-5.68E-02	1.41E+00	-1.95E-01
3.14E+00	-1.55E-01	2.10E+00	-2.25E-01	1.76E+00	-1.13E-01	1.59E+00	4.54E-03	1.49E+00	-7.16E-02	1.42E+00	-2.02E-01
3.14E+00	-1.56E-01	2.11E+00	-2.25E-01	1.76E+00	-1.03E-01	1.59E+00	5.65E-03	1.49E+00	-8.66E-02	1.42E+00	-2.06E-01
3.14E+00	-1.56E-01	2.11E+00	-2.25E-01	1.76E+00	-9.46E-02	1.59E+00	5.94E-03	1.49E+00	-1.02E-01	1.42E+00	-2.06E-01
3.14E+00	-1.57E-01	2.11E+00	-2.24E-01	1.76E+00	-8.73E-02	1.59E+00	4.88E-03	1.49E+00	-1.17E-01	1.42E+00	-2.02E-01
3.14E+00	-1.59E-01	2.11E+00	-2.22E-01	1.76E+00	-8.12E-02	1.59E+00	2.97E-03	1.49E+00	-1.32E-01	1.42E+00	-1.95E-01
3.14E+00	-1.61E-01	2.11E+00	-2.21E-01	1.76E+00	-7.60E-02	1.59E+00	-3.35E-04	1.49E+00	-1.46E-01	1.42E+00	-1.85E-01
3.14E+00	-1.63E-01	2.11E+00	-2.18E-01	1.77E+00	-7.16E-02	1.59E+00	-4.77E-03	1.49E+00	-1.59E-01	1.42E+00	-1.72E-01
3.14E+00	-1.65E-01	2.11E+00	-2.14E-01	1.77E+00	-6.80E-02	1.60E+00	-1.00E-02	1.49E+00	-1.72E-01	1.42E+00	-1.57E-01
3.14E+00	-1.68E-01	2.11E+00	-2.09E-01	1.77E+00	-6.48E-02	1.60E+00	-1.66E-02	1.49E+00	-1.83E-01	1.42E+00	-1.40E-01
3.15E+00	-1.71E-01	2.11E+00	-2.04E-01	1.77E+00	-6.16E-02	1.60E+00	-2.41E-02	1.49E+00	-1.92E-01	1.42E+00	-1.22E-01
3.15E+00	-1.74E-01	2.11E+00	-1.97E-01	1.77E+00	-5.86E-02	1.60E+00	-3.25E-02	1.50E+00	-2.00E-01	1.43E+00	-1.04E-01
3.15E+00	-1.77E-01	2.12E+00	-1.90E-01	1.77E+00	-5.55E-02	1.60E+00	-4.20E-02	1.50E+00	-2.05E-01	1.43E+00	-8.58E-02
3.15E+00	-1.81E-01	2.12E+00	-1.82E-01	1.77E+00	-5.21E-02	1.60E+00	-5.21E-02	1.50E+00	-2.08E-01	1.43E+00	-6.81E-02
3.15E+00	-1.84E-01	2.12E+00	-1.74E-01	1.77E+00	-4.90E-02	1.60E+00	-6.28E-02	1.50E+00	-2.08E-01	1.43E+00	-5.04E-02
3.15E+00	-1.88E-01	2.12E+00	-1.66E-01	1.77E+00	-4.62E-02	1.60E+00	-7.41E-02	1.50E+00	-2.06E-01	1.43E+00	-3.32E-02
3.15E+00	-1.92E-01	2.12E+00	-1.58E-01	1.77E+00	-4.41E-02	1.60E+00	-8.55E-02	1.50E+00	-2.02E-01	1.43E+00	-1.59E-02
3.15E+00	-1.95E-01	2.12E+00	-1.52E-01	1.78E+00	-4.27E-02	1.60E+00	-9.73E-02	1.50E+00	-1.95E-01	1.43E+00	1.07E-03
3.15E+00	-1.99E-01	2.12E+00	-1.46E-01	1.78E+00	-4.19E-02	1.61E+00	-1.09E-01	1.50E+00	-1.88E-01	1.43E+00	1.76E-02
3.15E+00	-2.02E-01	2.12E+00	-1.41E-01	1.78E+00	-4.15E-02	1.61E+00	-1.21E-01	1.50E+00	-1.79E-01	1.43E+00	3.33E-02
3.16E+00	-2.06E-01	2.12E+00	-1.36E-01	1.78E+00	-4.15E-02	1.61E+00	-1.32E-01	1.50E+00	-1.70E-01	1.43E+00	4.74E-02
3.16E+00	-2.09E-01	2.12E+00	-1.33E-01	1.78E+00	-4.17E-02	1.61E+00	-1.43E-01	1.51E+00	-1.59E-01	1.44E+00	5.93E-02
3.16E+00	-2.12E-01	2.13E+00	-1.30E-01	1.78E+00	-4.23E-02	1.61E+00	-1.54E-01	1.51E+00	-1.49E-01	1.44E+00	6.86E-02
3.16E+00	-2.15E-01	2.13E+00	-1.28E-01	1.78E+00	-4.28E-02	1.61E+00	-1.63E-01	1.51E+00	-1.39E-01	1.44E+00	7.48E-02
3.16E+00	-2.17E-01	2.13E+00	-1.26E-01	1.78E+00	-4.28E-02	1.61E+00	-1.72E-01	1.51E+00	-1.28E-01	1.44E+00	7.76E-02
3.16E+00	-2.19E-01	2.13E+00	-1.25E-01	1.78E+00	-4.19E-02	1.61E+00	-1.80E-01	1.51E+00	-1.16E-01	1.44E+00	7.69E-02
3.16E+00	-2.21E-01	2.13E+00	-1.24E-01	1.78E+00	-4.08E-02	1.61E+00	-1.87E-01	1.51E+00	-1.05E-01	1.44E+00	7.29E-02
3.16E+00	-2.22E-01	2.13E+00	-1.24E-01	1.79E+00	-3.93E-02	1.61E+00	-1.93E-01	1.51E+00	-9.22E-02	1.44E+00	6.61E-02
3.16E+00	-2.24E-01	2.13E+00	-1.23E-01	1.79E+00	-3.77E-02	1.62E+00	-1.98E-01	1.51E+00	-7.95E-02	1.44E+00	5.63E-02
3.16E+00	-2.25E-01	2.13E+00	-1.22E-01	1.79E+00	-3.63E-02	1.62E+00	-2.02E-01	1.51E+00	-6.60E-02	1.44E+00	4.40E-02
3.17E+00	-2.25E-01	2.13E+00	-1.21E-01	1.79E+00	-3.54E-02	1.62E+00	-2.04E-01	1.51E+00	-5.25E-02	1.45E+00	2.94E-02
3.17E+00	-2.26E-01	2.13E+00	-1.20E-01	1.79E+00	-3.59E-02	1.62E+00	-2.05E-01	1.51E+00	-3.89E-02	1.45E+00	1.28E-02
3.17E+00	-2.26E-01	2.13E+00	-1.20E-01	1.79E+00	-3.77E-02	1.62E+00	-2.06E-01	1.52E+00	-2.53E-02	1.45E+00	-5.17E-03
3.17E+00	-2.26E-01	2.14E+00	-1.19E-01	1.79E+00	-4.12E-02	1.62E+00	-2.05E-01	1.52E+00	-1.24E-02	1.45E+00	-2.43E-02
3.17E+00	-2.26E-01	2.14E+00	-1.19E-01	1.79E+00	-4.63E-02	1.62E+00	-2.03E-01	1.52E+00	-1.07E-03	1.45E+00	-4.38E-02
3.17E+00	-2.25E-01	2.14E+00	-1.20E-01	1.79E+00	-5.30E-02	1.62E+00	-2.01E-01	1.52E+00	9.21E-03	1.45E+00	-6.36E-02
3.17E+00	-2.25E-01	2.14E+00	-1.21E-01	1.79E+00	-6.08E-02	1.62E+00	-1.99E-01	1.52E+00	1.85E-02	1.45E+00	-8.34E-02
3.17E+00	-2.24E-01	2.14E+00	-1.22E-01	1.80E+00	-6.94E-02	1.62E+00	-1.96E-01	1.52E+00	2.62E-02	1.45E+00	-1.03E-01
3.17E+00	-2.23E-01	2.14E+00	-1.24E-01	1.80E+00	-7.79E-02	1.63E+00	-1.93E-01	1.52E+00	3.17E-02	1.45E+00	-1.22E-01
3.17E+00	-2.22E-01	2.14E+00	-1.27E-01	1.80E+00	-8.64E-02	1.63E+00	-1.89E-01	1.52E+00	3.52E-02	1.45E+00	-1.40E-01
3.18E+00	-2.21E-01	2.14E+00	-1.31E-01	1.80E+00	-9.49E-02	1.63E+00	-1.85E-01	1.52E+00	3.67E-02	1.46E+00	-1.56E-01
3.18E+00	-2.19E-01	2.14E+00	-1.35E-01	1.80E+00	-1.03E-01	1.63E+00	-1.80E-01	1.52E+00	3.64E-02	1.46E+00	-1.72E-01
3.18E+00	-2.17E-01	2.14E+00	-1.39E-01	1.80E+00	-1.11E-01	1.63E+00	-1.74E-01	1.53E+00	3.44E-02	1.46E+00	-1.85E-01
3.18E+00	-2.15E-01	2.15E+00	-1.42E-01	1.80E+00	-1.19E-01	1.63E+00	-1.68E-01	1.53E+00	3.11E-02	1.46E+00	-1.95E-01
3.18E+00	-2.12E-01	2.15E+00	-1.45E-01	1.80E+00	-1.27E-01	1.63E+00	-1.62E-01	1.53E+00	2.64E-02	1.46E+00	-2.03E-01
3.18E+00	-2.09E-01	2.15E+00	-1.46E-01	1.80E+00	-1.34E-01	1.63E+00	-1.54E-01	1.53E+00	2.00E-02	1.46E+00	-2.06E-01
3.18E+00	-2.06E-01	2.15E+00	-1.47E-01	1.80E+00	-1.41E-01	1.63E+00	-1.47E-01	1.53E+00	1.21E-02	1.46E+00	-2.06E-01
3.18E+00	-2.02E-01	2.15E+00	-1.47E-01	1.81E+00	-1.48E-01	1.63E+00	-1.38E-01	1.53E+00	2.66E-03	1.46E+00	-2.03E-01
3.18E+00	-1.98E-01	2.15E+00	-1.47E-01	1.81E+00	-1.54E-01	1.63E+00	-1.29E-01	1.53E+00	-8.23E-03	1.46E+00	-1.96E-01
3.18E+00	-1.94E-01	2.15E+00	-1.46E-01	1.81E+00	-1.60E-01	1.64E+00	-1.20E-01	1.53E+00	-2.03E-02	1.46E+00	-1.85E-01
3.19E+00	-1.89E-01	2.15E+00	-1.45E-01	1.81E+00	-1.66E-01	1.64E+00	-1.10E-01	1.53E+00	-3.35E-02	1.47E+00	-1.73E-01
3.19E+00	-1.85E-01	2.15E+00	-1.42E-01	1.81E+00	-1.72E-01	1.64E+00	-9.94E-02	1.53E+00	-4.76E-02	1.47E+00	-1.58E-01
3.19E+00	-1.80E-01	2.15E+00	-1.38E-01	1.81E+00	-1.77E-01	1.64E+00	-8.80E-02	1.54E+00	-6.22E-02	1.47E+00	-1.41E-01
3.19E+00	-1.76E-01	2.16E+00	-1.33E-01	1.81E+00	-1.82E-01	1.64E+00	-7.67E-02	1.54E+00	-7.73E-02	1.47E+00	-1.23E-01
3.19E+00	-1.71E-01	2.16E+00	-1.26E-01	1.81E+00	-1.87E-01	1.64E+00	-6.60E-02	1.54E+00	-9.25E-02	1.47E+00	-1.04E-01
3.19E+00	-1.67E-01	2.16E+00	-1.17E-01	1.81E+00	-1.91E-01	1.64E+00	-5.62E-02	1.54E+00	-1.08E-01	1.47E+00	-8.59E-02
3.19E+00	-1.62E-01	2.16E+00	-1.06E-01	1.82E+00	-1.95E-01	1.64E+00	-4.73E-02	1.54E+00	-1.23E-01	1.47E+00	-6.77E-02
3.19E+00	-1.58E-01	2.16E+00	-9.33E-02	1.82E+00	-1.99E-01	1.64E+00	-3.94E-02	1.54E+00	-1.37E-01	1.47E+00	-5.03E-02
3.19E+00	-1.54E-01	2.16E+00	-8.03E-02	1.82E+00	-2.02E-01	1.64E+00	-3.20E-02	1.54E+00	-1.51E-01	1.47E+00	-3.30E-02
3.19E+00	-1.50E-01	2.16E+00	-6.73E-02	1.82E+00	-2.04E-01	1.65E+00	-2.53E-02	1.54E+00	-1.64E-01	1.47E+00	-1.58E-02
3.20E+00	-1.47E-01	2.16E+00	-5.56E-02	1.82E+00	-2.07E-01	1.65E+00	-1.82E-02	1.54E+00	-1.76E-01	1.48E+00	1.58E-03
3.20E+00	-1.43E-01	2.16E+00	-4.58E-02	1.82E+00	-2.09E-01	1.65E+00	-1.17E-02	1.54E+00	-1.87E-01	1.48E+00	1.84E-02
3.20E+00	-1.41E-01	2.16E+00	-3.84E-02	1.82E+00	-2.10E-01	1.65E+00	-6.02E-03	1.55E+00	-1.95E-01	1.48E+00	3.38E-02
3.20E+00	-1.38E-01	2.17E+00	-3.37E-02	1.82E+00	-2.12E-01	1.65E+00	-1.68E-03	1.55E+00	-2.02E-01	1.48E+00	4.77E-02
3.20E+00	-1.35E-01	2.17E+00	-3.14E-02	1.82E+00	-2.13E-01	1.65E+00	1.94E-03	1.55E+00	-2.06E-01	1.48E+00	5.93E-02
3.20E+00	-1.33E-01	2.17E+00	-3.12E-02	1.82E+00	-2.13E-01	1.65E+00	4.26E-03	1.55E+00	-2.08E-01	1.48E+00	6.86E-02
3.20E+00	-1.31E-01	2.17E+00	-3.22E-02	1.83E+00	-2.14E-01	1.65E+00	5.98E-03	1.55E+00	-2.08E-01	1.48E+00	7.44E-02
3.20E+00	-1.29E-01	2.17E+00	-3.35E-02	1.83E+00	-2.14E-01	1.65E+00	6.39E-03	1.55E+00	-2.05E-01	1.48E+00	7.69E-02
3.20E+00	-1.27E-01	2.17E+00	-3.49E-02	1.83E+00	-2.14E-01	1.65E+00	6.14E-03	1.55E+00	-2.00E-01	1.48E+00	7.62E-02
3.20E+00	-1.26E-01	2.17E+00	-3.60E-02	1.83E+00	-2.14E-01	1.66E+00	4.86E-03	1.55E+00	-1.93E-01	1.48E+00	7.23E-02
3.21E+00	-1.24E-01	2.17E+00	-3.70E-02	1.83E+00	-2.13E-01	1.66E+00	1.99E-03	1.55E+00	-1.85E-01	1.49E+00	6.50E-02
3.21E+00	-1.23E-01	2.17E+00	-3.84E-02	1.83E+00	-2.12E-01	1.66E+00	-1.68E-03	1.55E+00	-1.76E-01	1.49E+00	5.52E-02
3.21E+00	-1.22E-01	2.17E+00	-3.99E-02	1.83E+00	-2.10E-01	1.66E+00	-6.79E-03	1.56E+00	-1.66E-01	1.49E+00	4.28E-02
3.21E+00	-1.21E-01	2.18E+00	-4.19E-02	1.83E+00	-2.08E-01	1.66E+00	-1.29E-02	1.56E+00	-1.56E-01	1.49E+00	2.84E-02
3.21E+00	-1.20E-01	2.18E+00	-4.42E-02	1.83E+00	-2.06E-01	1.66E+00	-1.98E-02	1.56E+00	-1.45E-01	1.49E+00	1.19E-02
3.21E+00	-1.20E-01	2.18E+00	-4.67E-02	1.83E+00	-2.03E-01	1.66E+00	-2.81E-02	1.56E+00	-1.35E-01	1.49E+00	-6.21E-03
3.21E+00	-1.20E-01	2.18E+00	-4.96E-02	1.84E+00	-1.99E-01	1.66E+00	-3.70E-02	1.56E+00	-1.24E-01	1.49E+00	-2.52E-02
3.21E+00	-1.20E-01	2.18E+00	-5.27E-02	1.84E+00	-1.95E-01	1.66E+00	-4.68E-02	1.56E+00	-1.12E-01	1.49E+00	-4.47E-02
3.21E+00	-1.20E-01	2.18E+00	-5.58E-02	1.84E+00	-1.90E-01	1.66E+00	-5.75E-02	1.56E+00	-9.99E-02	1.49E+00	-6.44E-02
3.21E+00	-1.20E-01	2.18E+00	-5.91E-02	1.84E+00	-1.84E-01	1.67E+00	-6.84E-02	1.56E+00	-8.69E-02	1.49E+00	-8.40E-02
3.22E+00	-1.20E-01	2.18E+00	-6.24E-02	1.84E+00	-1.77E-01	1.67E+00	-7.98E-02	1.56E+00	-7.39E-02	1.50E+00	-1.03E-01
3.22E+00	-1.21E-01	2.18E+00	-6.60E-02	1.84E+00	-1.69E-01	1.67E+00	-9.15E-02	1.57E+00	-6.04E-02	1.50E+00	-1.22E-01
3.22E+00	-1.21E-01	2.18E+00	-6.98E-02	1.84E+00	-1.60E-01	1.67E+00	-1.03E-01	1.57E+00	-4.67E-02	1.50E+00	-1.40E-01
3.22E+00	-1.22E-01	2.19E+00	-7.37E-02	1.84E+00	-1.50E-01	1.67E+00	-1.15E-01	1.57E+00	-3.28E-02	1.50E+00	-1.57E-01
3.22E+00	-1.23E-01	2.19E+00	-7.76E-02	1.84E+00	-1.40E-01	1.67E+00	-1.26E-01	1.57E+00	-1.96E-02	1.50E+00	-1.72E-01
3.22E+00	-1.23E-01	2.19E+00	-8.16E-02	1.84E+00	-1.30E-01	1.67E+00	-1.37E-01	1.57E+00	-8.13E-03	1.50E+00	-1.85E-01
3.22E+00	-1.24E-01	2.19E+00	-8.59E-02	1.85E+00	-1.20E-01	1.67E+00	-1.48E-01	1.57E+00	2.94E-03	1.50E+00	-1.95E-01
3.22E+00	-1.25E-01	2.19E+00	-9.02E-02	1.85E+00	-1.11E-01	1.67E+00	-1.58E-01	1.57E+00	1.25E-02	1.50E+00	-2.02E-01
3.22E+00	-1.26E-01	2.19E+00	-9.46E-02	1.85E+00	-1.03E-01	1.67E+00	-1.68E-01	1.57E+00	2.10E-02	1.50E+00	-2.06E-01
3.22E+00	-1.27E-01	2.19E+00	-9.91E-02	1.85E+00	-9.51E-02	1.68E+00	-1.76E-01	1.57E+00	2.78E-02	1.50E+00	-2.06E-01
3.23E+00	-1.29E-01	2.19E+00	-1.04E-01	1.85E+00	-8.85E-02	1.68E+00	-1.84E-01	1.57E+00	3.24E-02	1.51E+00	-2.02E-01
3.23E+00	-1.31E-01	2.19E+00	-1.08E-01	1.85E+00	-8.26E-02	1.68E+00	-1.90E-01	1.58E+00	3.51E-02	1.51E+00	-1.95E-01
3.23E+00	-1.33E-01	2.19E+00	-1.13E-01	1.85E+00	-7.75E-02	1.68E+00	-1.95E-01	1.58E+00	3.60E-02	1.51E+00	-1.85E-01
3.23E+00	-1.36E-01	2.20E+00	-1.18E-01	1.85E+00	-7.31E-02	1.68E+00	-2.00E-01	1.58E+00	3.52E-02	1.51E+00	-1.72E-01
3.23E+00	-1.40E-01	2.20E+00	-1.22E-01	1.85E+00	-6.95E-02	1.68E+00	-2.03E-01	1.58E+00	3.26E-02	1.51E+00	-1.57E-01
3.23E+00	-1.43E-01	2.20E+00	-1.27E-01	1.85E+00	-6.64E-02	1.68E+00	-2.05E-01	1.58E+00	2.86E-02	1.51E+00	-1.41E-01
3.23E+00	-1.47E-01	2.20E+00	-1.32E-01	1.86E+00	-6.39E-02	1.68E+00	-2.06E-01	1.58E+00	2.29E-02	1.51E+00	-1.23E-01
3.23E+00	-1.51E-01	2.20E+00	-1.36E-01	1.86E+00	-6.12E-02	1.68E+00	-2.05E-01	1.58E+00	1.59E-02	1.51E+00	-1.05E-01
3.23E+00	-1.55E-01	2.20E+00	-1.41E-01	1.86E+00	-5.80E-02	1.68E+00	-2.04E-01	1.58E+00	7.59E-03	1.51E+00	-8.62E-02
3.23E+00	-1.58E-01	2.20E+00	-1.45E-01	1.86E+00	-5.43E-02	1.69E+00	-2.02E-01	1.58E+00	-2.26E-03	1.51E+00	-6.84E-02
3.24E+00	-1.62E-01	2.20E+00	-1.50E-01	1.86E+00	-5.10E-02	1.69E+00	-2.00E-01	1.58E+00	-1.36E-02	1.51E+00	-5.09E-02

The data taken into account for the average torque is the one highlighted in yellow. It includes the torque data for periods of the signal. Only TSRs 1.0 and 1.2 are fully displayed because the spreadsheet would take too much space to fill this appendix.

IV- UDFs for inlet velocity and rotational speed of Savonius

Inlet velocity UDF:

```
#include "udf.h"

#define V_MAG 5.16
#define tarranq 1.0

DEFINE_PROFILE(inlet_u, ft, var)
{
        real flow_time;
        face_t f; /* Face index has its own type */
        flow_time = CURRENT_TIME; /* Special Fluent macro */
        begin_f_loop(f,ft) /* Fluent has special face loop macros too */
        {
                if (flow_time<=tarranq)
                        F_PROFILE(f,ft,var) = V_MAG*(flow_time/tarranq);
                else
                        F_PROFILE(f,ft,var) = V_MAG;
        }
        end_f_loop(f,ft)
}
```

Rotational speed UDF: in this case W_MAG is the angular velocity for D1SAV at TSR=1.2

```
#include "udf.h"

#define W_MAG 73.04
#define tarranq 1.0

DEFINE_ZONE_MOTION(velrot,omega,axis,origin,velocity,time,dtime)
{
        real flow_time;
        flow_time = CURRENT_TIME;
        if (flow_time<=tarranq)
        {
                *omega = -W_MAG*(flow_time/tarranq);
        }
        else
        {
                *omega = -W_MAG;
        }
        return;
}
```

V- Wind power installed worldwide 2013-2014

GLOBAL INSTALLED WIND POWER CAPACITY (MW) – REGIONAL DISTRIBUTION

		End 2013	New 2014	Total (End 2014)
AFRICA & MIDDLE EAST	Morocco	487	300	787
	South Africa	10	560	570
	Egypt	550	60	610
	Tunisia	245	-	245
	Ethiopia	171	-	171
	Cape Verde	24	-	24
	Other [1]	115	14	129
	Total	**1,602**	**934**	**2,535**
ASIA	PR China	91,413	23,196	114,609
	India	20,150	2,315	22,465
	Japan	2,669	130	2,789
	Taiwan	614	18	633
	South Korea	561	47	609
	Thailand	223	-	223
	Pakistan	106	150	256
	Philippines	66	150	216
	Other [2]	167	-	167
	Total	**115,968**	**26,007**	**141,964**
EUROPE	Germany	34,250	5,279	39,165
	Spain	22,959	28	22,987
	UK	10,711	1,736	12,440
	France	8,243	1,042	9,285
	Italy	8,558	108	8,663
	Sweden	4,382	1,050	5,425
	Portugal*	4,730	184	4,914
	Denmark	4,807	105	4,883
	Poland	3,390	444	3,834
	Turkey	2,958	804	3,763
	Romania	2,600	354	2,954
	Netherlands	2,671	141	2,805
	Ireland	2,049	222	2,272
	Austria	1,684	411	2,095
	Greece	1,866	114	1,980
	Rest of Europe [3]	5,715	835	6,543
	Total Europe of which EU-28 [4]	**121,573** 117,384	**12,858** 11,829	**134,007** 128,790
LATIN AMERICA & CARIBBEAN	Brazil**	3,466	2,472	5,939
	Chile	331	506	836
	Uruguay	59	405	464
	Argentina	218	53	271
	Costa Rica	148	50	198
	Nicaragua	146	40	186
	Honduras	102	50	152
	Peru	2	146	148
	Carribean [5]	250	-	250
	Others [6]	55	28	83
	Total	**4,777**	**3,749**	**8,526**
NORTH AMERICA	USA	61,110	4,854	65,879
	Canada	7,823	1,871	9,694
	Mexico	1,917	634	2,551
	Total	**70,850**	**7,359**	**78,124**
PACIFIC REGION	Australia	3,239	567	3,806
	New Zealand	623	-	623
	Pacific Islands	12	-	12
	Total	**3,874**	**567**	**4,441**
	World total	**318,644**	**51,473**	**369,597**

Source: GWEC

1 Algeria, Iran, Israel, Jordan, Kenya, Libya, Nigeria
2 Bangladesh, Mongolia, Sri Lanka, Vietnam
3 Bulgaria, Cyprus, Czech Republic, Estonia, Finland, Faroe Islands, FYROM, Hungary, Iceland, Latvia, Liechtenstein, Lithuania, Luxembourg, Malta,Norway, Romania, Russia, Switzerland, Slovakia, Slovenia, Ukraine
4 Austria, Belgium, Bulgaria, Cyprus, Croatia, Czech Republic, Denmark, Estonia, Finland, France, Germany, Greece, Hungary, Ireland, Italy, Latvia, Lithuania, Luxembourg, Malta, Netherlands, Poland, Portugal, Romania, Slovakia, Slovenia, Spain, Sweden, UK
5 Caribbean: Aruba, Bonaire, Curacao, Cuba, Dominica, Guadalupe, Jamaica, Martinica, Granada, St. Kitts and Nevis
6 Bolivia, Colombia, Ecuador, Venezuela

Note:
Project decommissioning of approximately 523 MW and rounding affect the final sums
*** Provisional figure**
**** Projects fully commissioned, grid connection pending in some cases**

VI- Fluent solver views

The next images are the complete windows from ANSYS Fluent. The settings used in the study are those shown in the following images. The windows follow the order of the arborescence seen on the left hand of the first image **[XX]**.

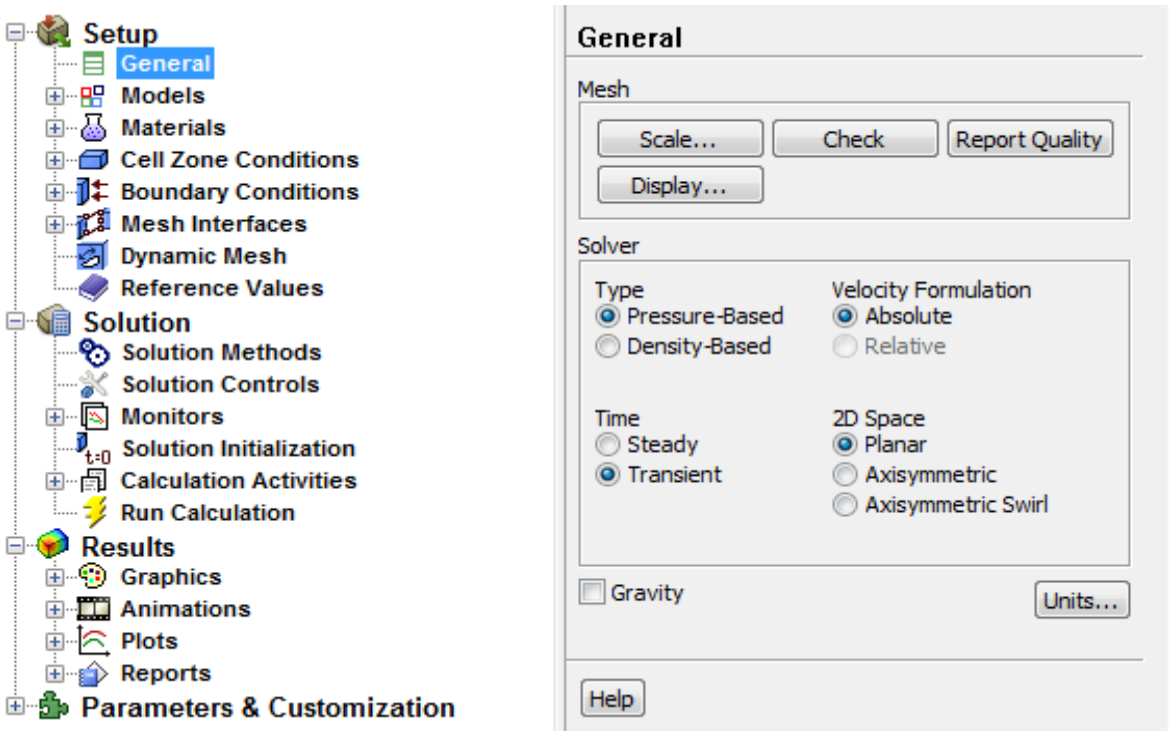

General Settings

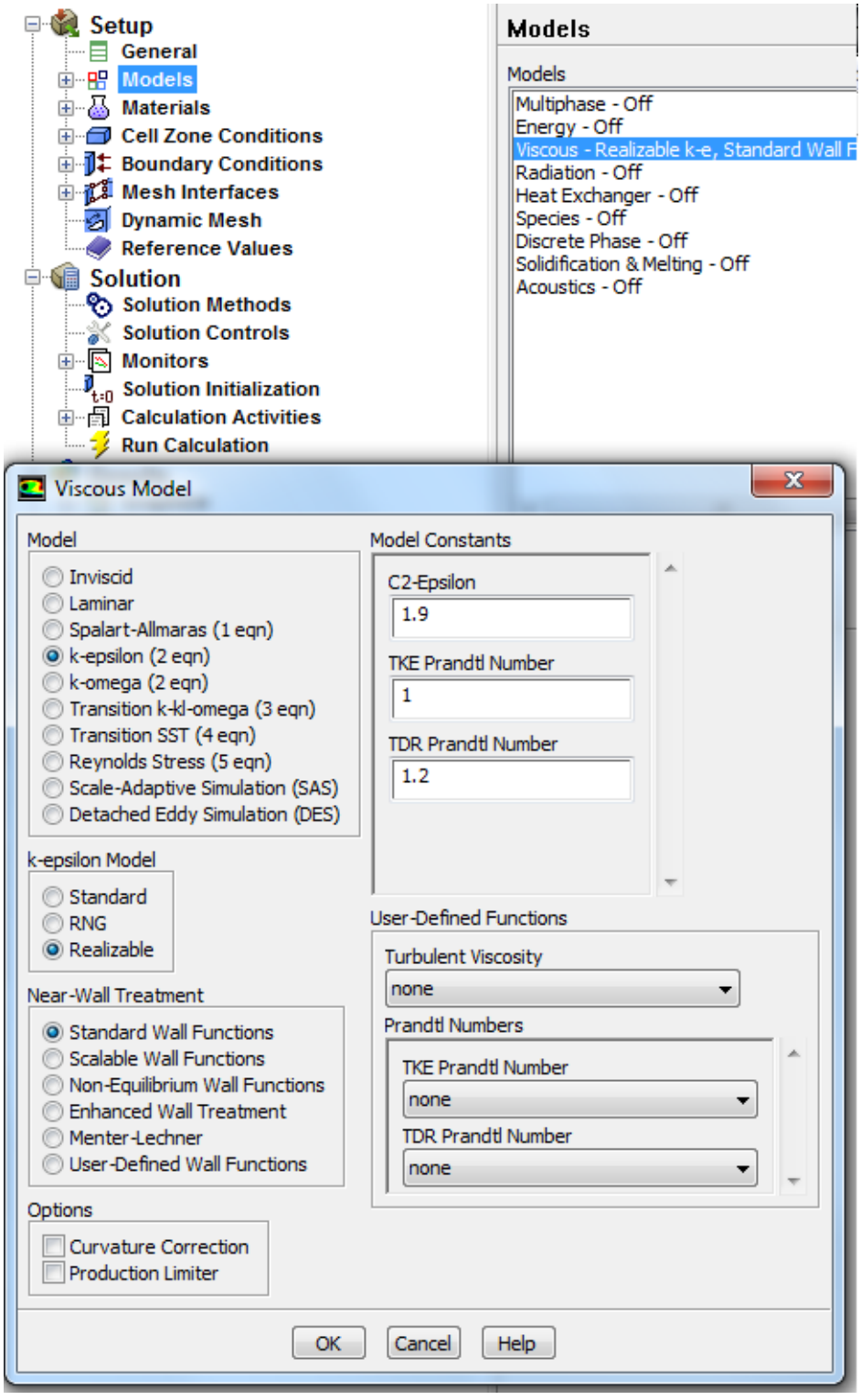

Models Settings

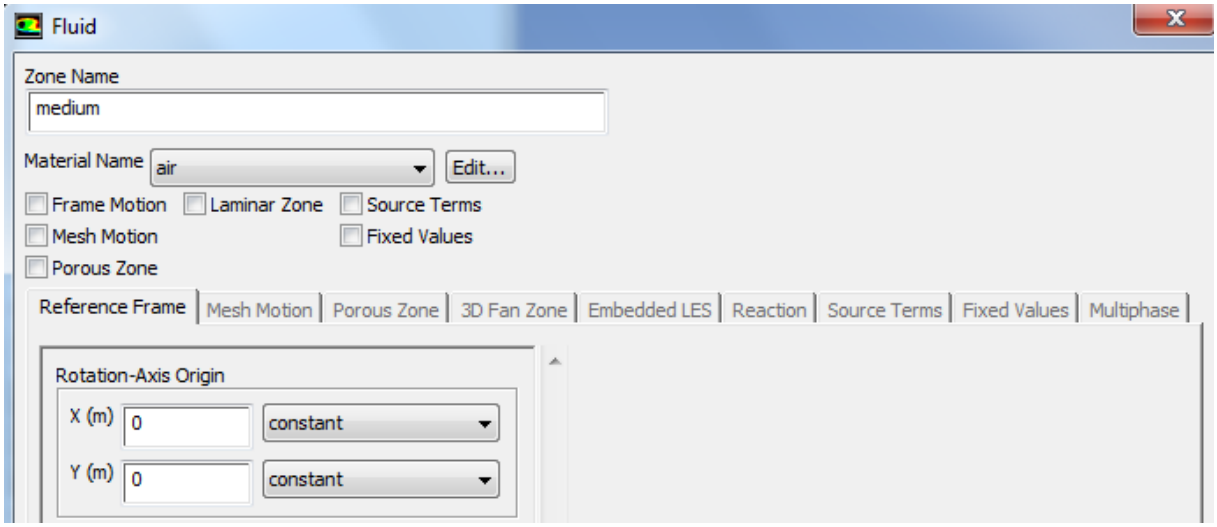

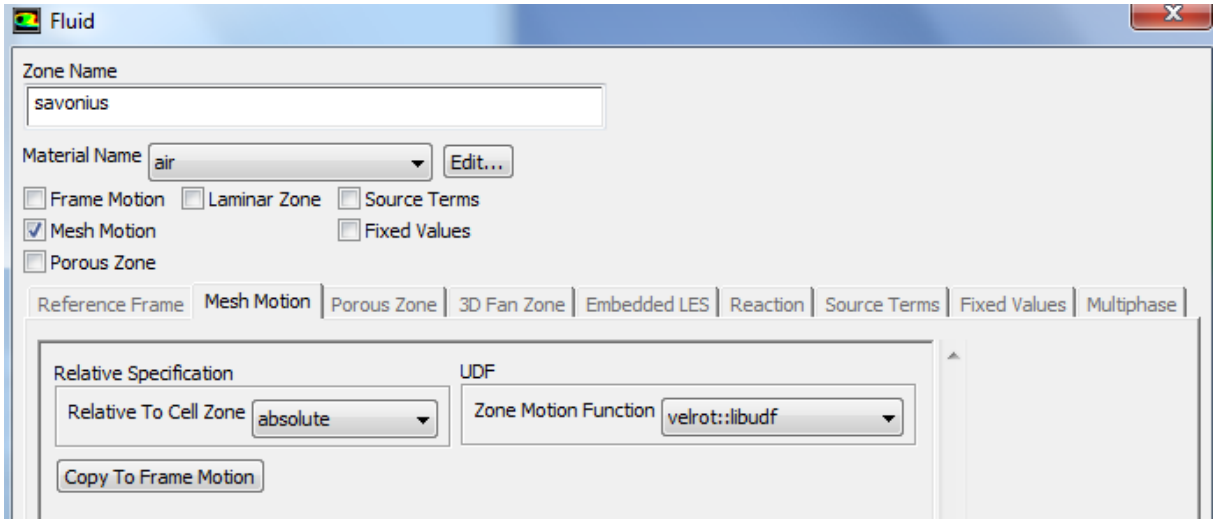

Cell zone conditions Settings

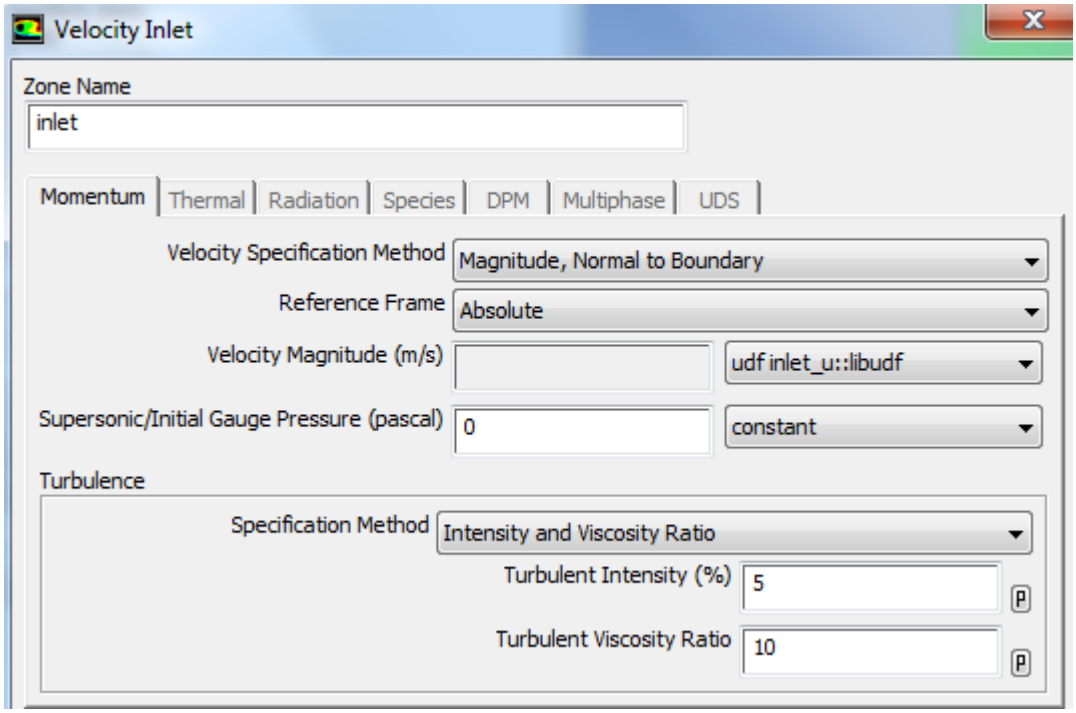
Velocity Inlet
Zone Name
inlet
Momentum
Thermal
Radiation
Species
DPM
Multiphase
UDS
Velocity Specification Method
Magnitude, Normal to Boundary
Reference Frame
Absolute
Velocity Magnitude (m/s)
udf inlet_u::libudf
Supersonic/Initial Gauge Pressure (pascal)
0
constant
Turbulence
Specification Method
Intensity and Viscosity Ratio
Turbulent Intensity (%)
5
Turbulent Viscosity Ratio
10

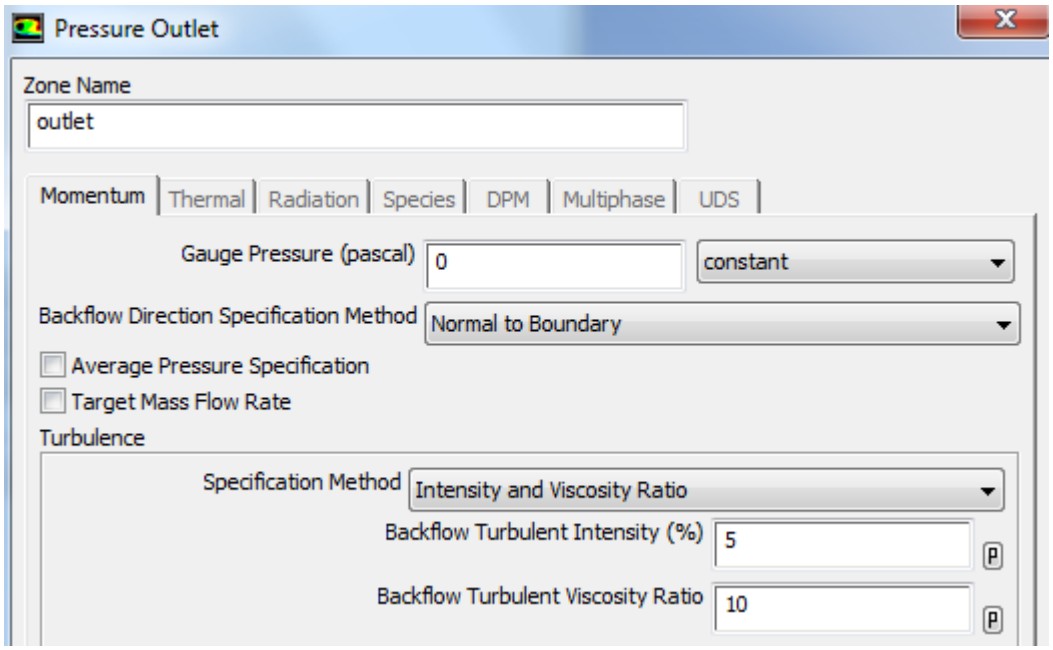
Pressure Outlet
Zone Name
outlet
Momentum
Thermal
Radiation
Species
DPM
Multiphase
UDS
Gauge Pressure (pascal)
0
constant
Backflow Direction Specification Method
Normal to Boundary
Average Pressure Specification
Target Mass Flow Rate
Turbulence
Specification Method
Intensity and Viscosity Ratio
Backflow Turbulent Intensity (%)
5
Backflow Turbulent Viscosity Ratio
10

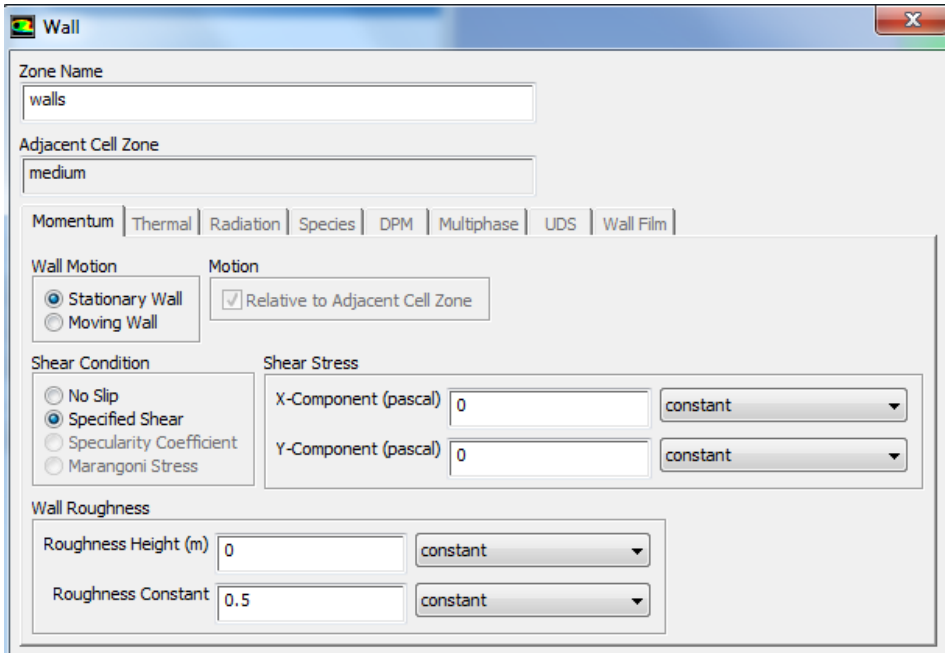

Boundary Conditions Settings

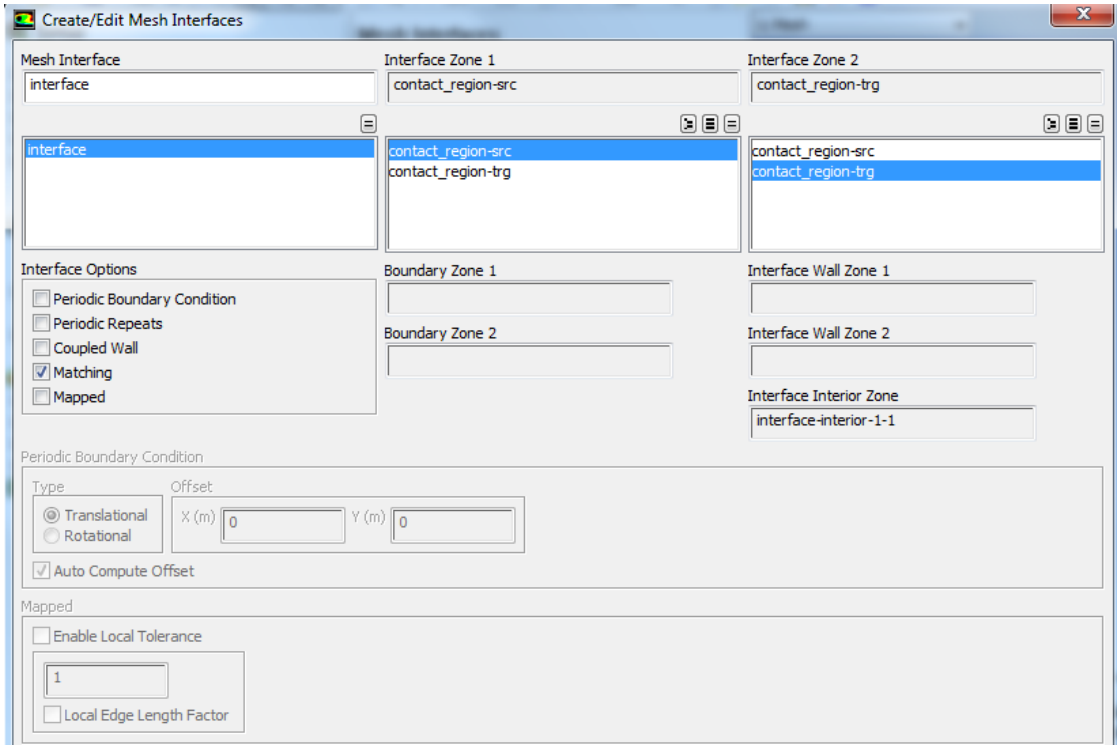

Inetrface Settings

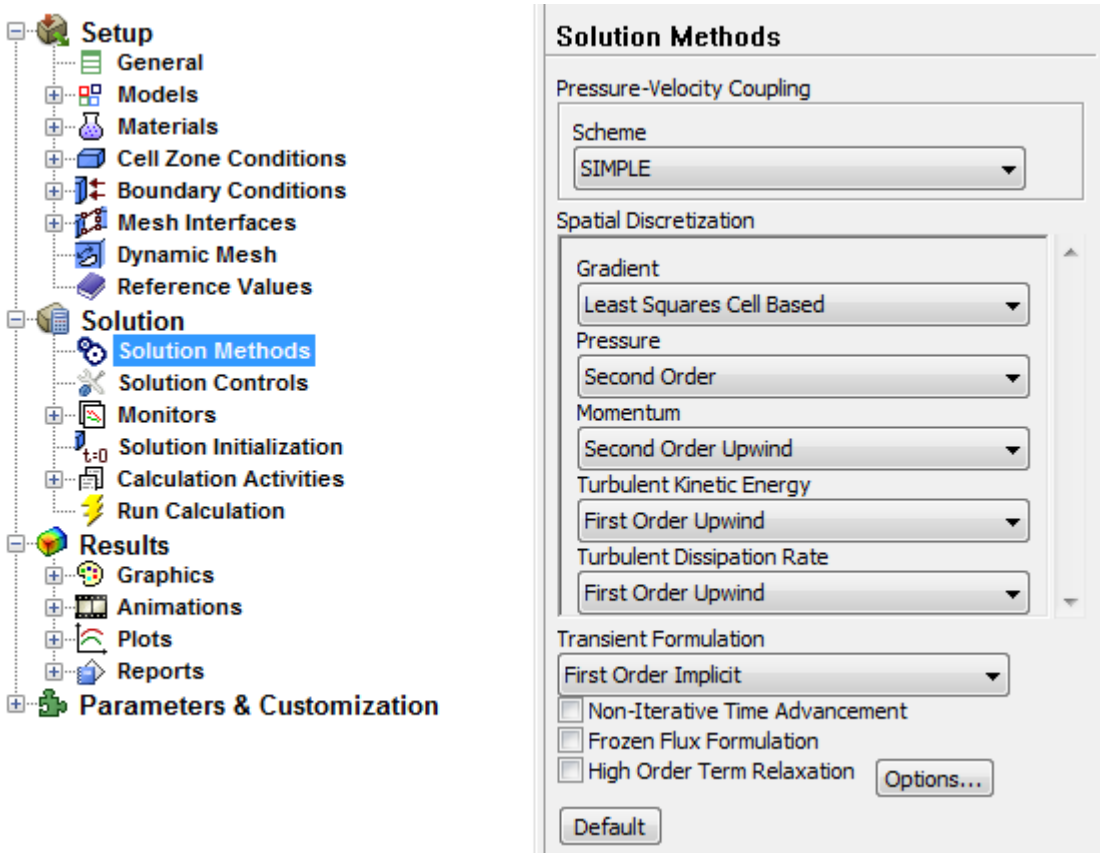

Solution Methods Settings

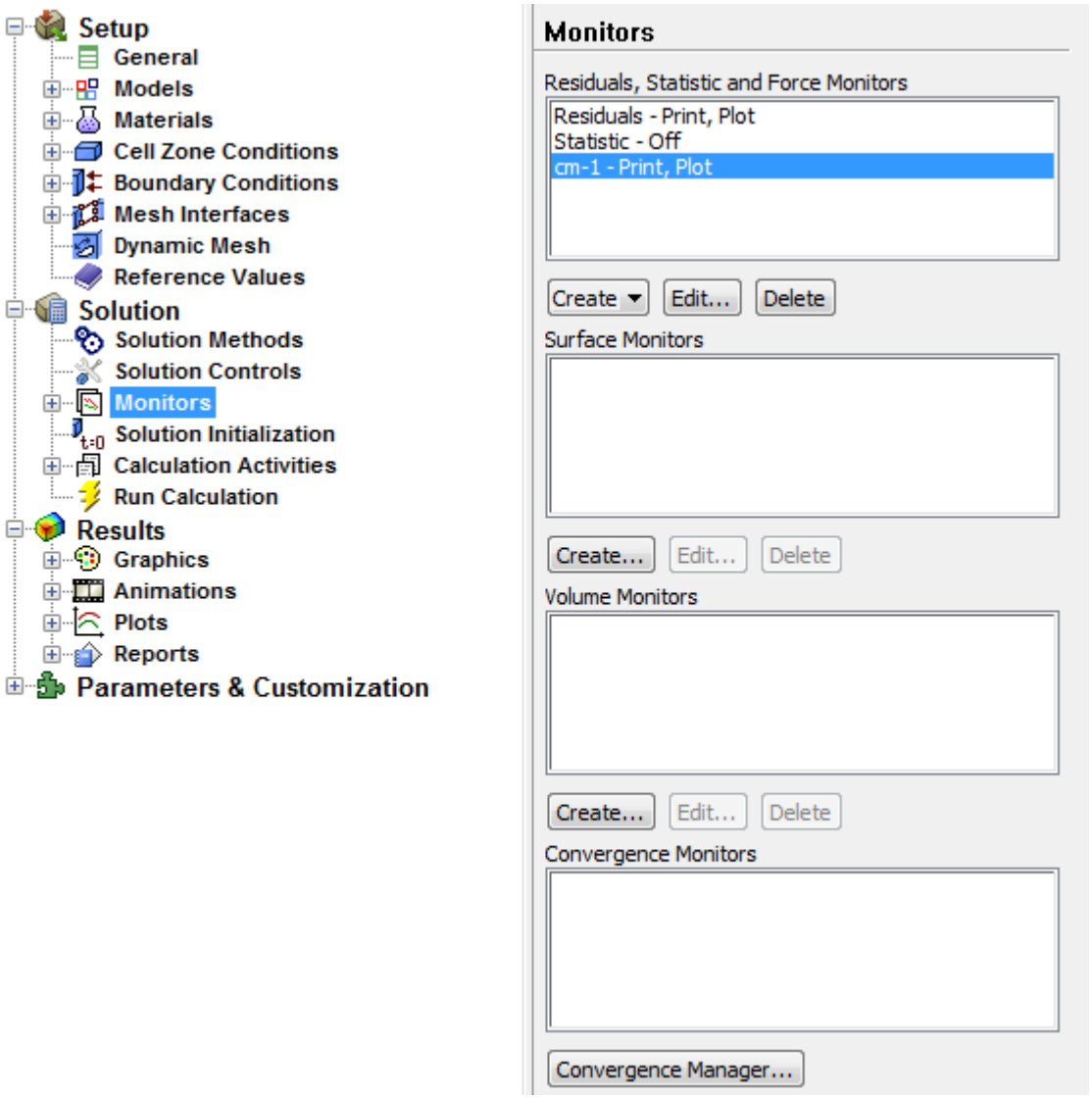

Monitors Settings

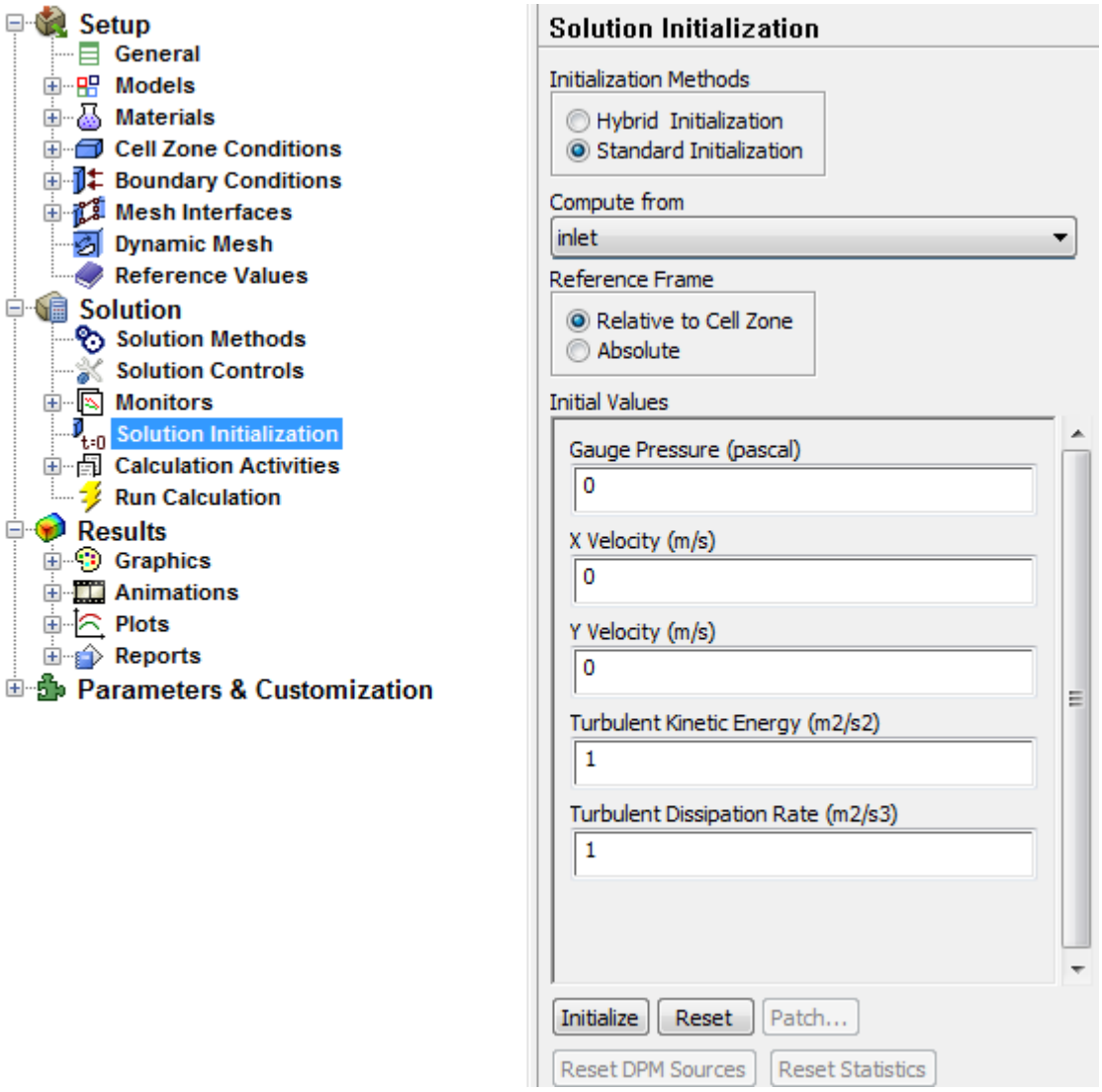

Solution Initialization Settings

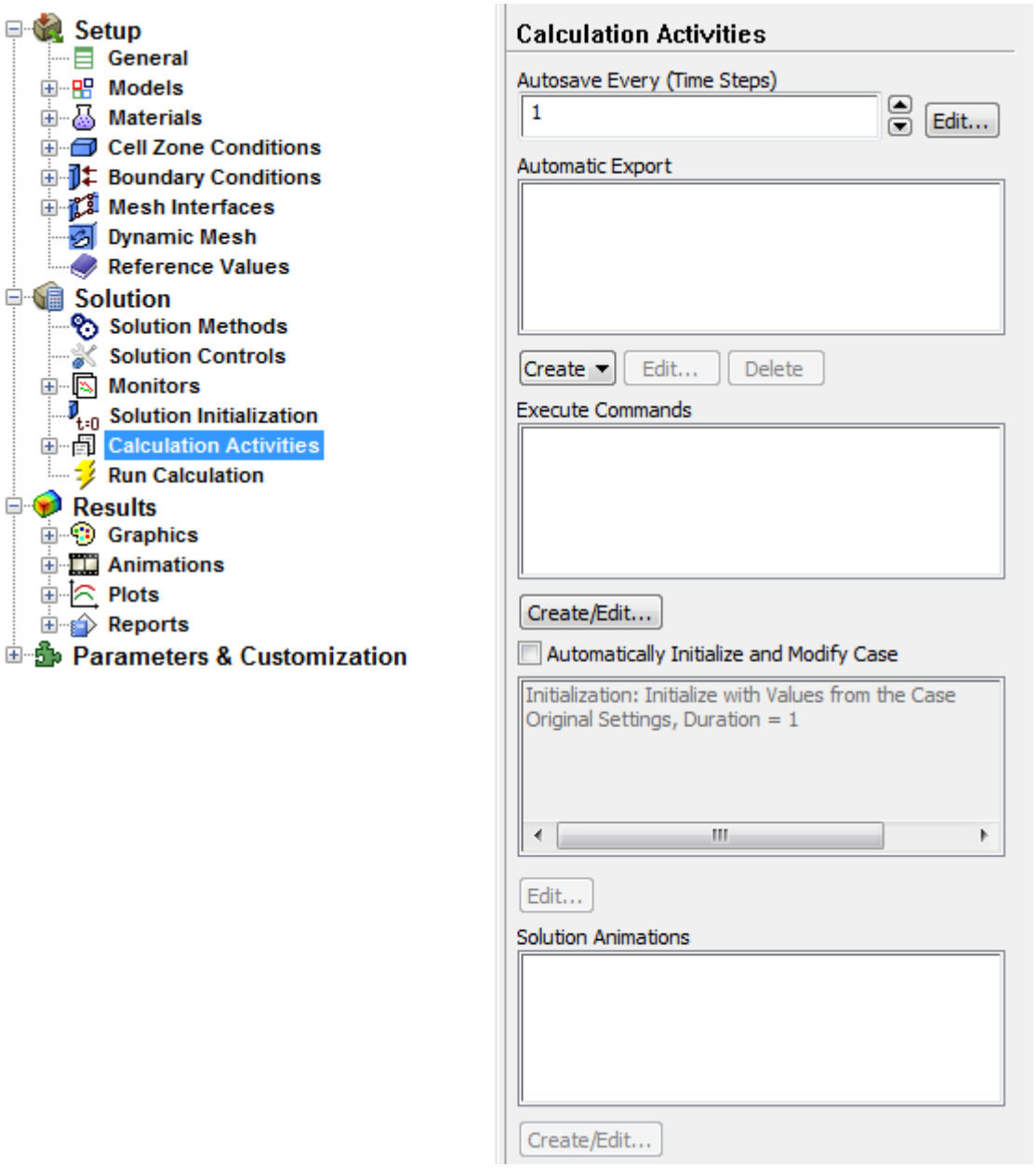

Calculation Activities Settings

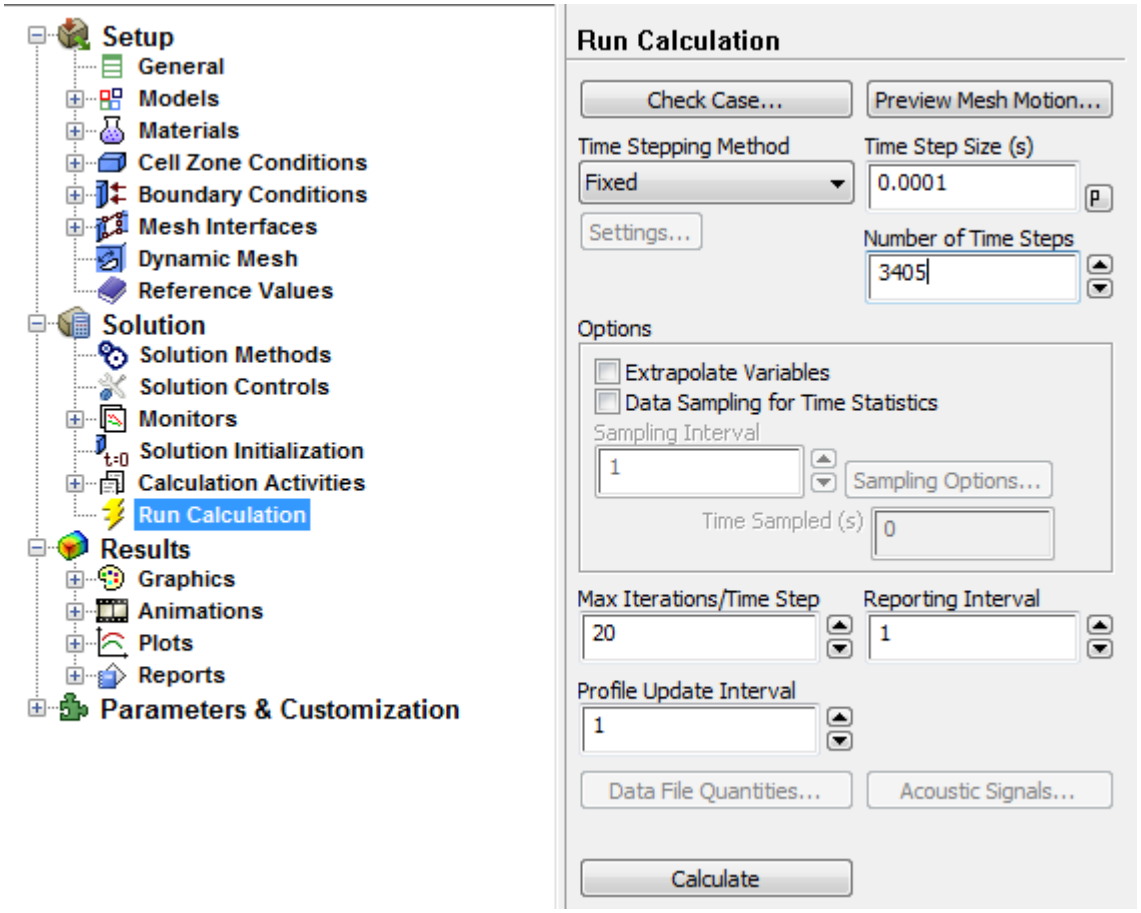

Calculation Settings

VII Mathematical Scheme Details, reference **[XVI]** :

Continuity equation in different coordinates systems:

Rectangular coordinates (x, y, z):

$$\frac{\partial \rho}{\partial t} + \frac{\partial}{\partial x}(\rho v_x) + \frac{\partial}{\partial y}(\rho v_y) + \frac{\partial}{\partial z}(\rho v_z) = 0$$

Cylindrical coordinates (r, ϴ, z):

$$\frac{\partial \rho}{\partial t} + \frac{1}{r}\frac{\partial}{\partial r}(\rho r v_r) + \frac{1}{r}\frac{\partial}{\partial \theta}(\rho v_\theta) + \frac{\partial}{\partial z}(\rho v_z) = 0$$

Spherical coordinates (r, ϴ, Φ):

$$\frac{\partial \rho}{\partial t} + \frac{1}{r^2}\frac{\partial}{\partial r}(\rho r^2 v_r) + \frac{1}{r\,sin\theta}\frac{\partial}{\partial \theta}(\rho v_\theta sin\theta) + \frac{1}{r\,sin\theta}\frac{\partial}{\partial \varphi}(\rho v_\varphi) = 0$$

The momentum equation in regular coordinates (x, y, z):

In terms of a velocity gradient for a Newtonian fluid with constants of ρ et η :

X-component:

$$\rho\left(\frac{\partial v_x}{\partial t} + v_x\frac{\partial v_x}{\partial x} + v_y\frac{\partial v_x}{\partial y} + v_z\frac{\partial v_x}{\partial z}\right) = -\frac{\partial P}{\partial x} + \eta\left(\frac{\partial^2 v_x}{\partial x^2} + \frac{\partial^2 v_x}{\partial y^2} + \frac{\partial^2 v_x}{\partial z^2}\right) + \rho g_x$$

Y-component:

$$\rho\left(\frac{\partial v_y}{\partial t} + v_x\frac{\partial v_y}{\partial x} + v_y\frac{\partial v_y}{\partial y} + v_z\frac{\partial v_y}{\partial z}\right) = -\frac{\partial P}{\partial y} + \eta\left(\frac{\partial^2 v_y}{\partial x^2} + \frac{\partial^2 v_y}{\partial y^2} + \frac{\partial^2 v_y}{\partial z^2}\right) + \rho g_y$$

Z-component:

$$\rho\left(\frac{\partial v_z}{\partial t}+v_x\frac{\partial v_z}{\partial x}+v_y\frac{\partial v_z}{\partial y}+v_z\frac{\partial v_z}{\partial z}\right)=-\frac{\partial P}{\partial z}+\eta\left(\frac{\partial^2 v_z}{\partial x^2}+\frac{\partial^2 v_z}{\partial y^2}+\frac{\partial^2 v_z}{\partial z^2}\right)+\rho g_z$$

In terms of τ:

X-component:

$$\rho\left(\frac{\partial v_x}{\partial t}+v_x\frac{\partial v_x}{\partial x}+v_y\frac{\partial v_x}{\partial y}+v_z\frac{\partial v_x}{\partial z}\right)=-\frac{\partial P}{\partial x}+\eta\left(\frac{\partial \tau_{xx}}{\partial x}+\frac{\partial \tau_{xy}}{\partial x}+\frac{\partial \tau_{xz}}{\partial x}\right)+\rho g_x$$

Y-component:

$$\rho\left(\frac{\partial v_y}{\partial t}+v_x\frac{\partial v_y}{\partial x}+v_y\frac{\partial v_y}{\partial y}+v_z\frac{\partial v_y}{\partial z}\right)=-\frac{\partial P}{\partial y}+\eta\left(\frac{\partial \tau_{yx}}{\partial x}+\frac{\partial \tau_{yy}}{\partial x}+\frac{\partial \tau_{yz}}{\partial x}\right)+\rho g_y$$

Z-component:

$$\rho\left(\frac{\partial v_z}{\partial t}+v_x\frac{\partial v_z}{\partial x}+v_y\frac{\partial v_z}{\partial y}+v_z\frac{\partial v_z}{\partial z}\right)=-\frac{\partial P}{\partial z}+\eta\left(\frac{\partial \tau_{zx}}{\partial x}+\frac{\partial \tau_{zy}}{\partial x}+\frac{\partial \tau_{zz}}{\partial x}\right)+\rho g_z$$